Utrecht University

Meteorology, Physical Oceanography and Climate

# Improvement of surface turbulent fluxes in the HARMONIE model

Nadia Bloemendaal

July 2016

Supervisors

Dr. A.B.C. Tijm (KNMI)

Prof. Dr. M.R. van den Broeke (Utrecht University)

Koninklijk Nederlands Meteorologisch Instituut
*Ministerie van Infrastructuur en Milieu*

Utrecht University

Cover photo: Hans Bloemendaal, “Kersenbloesem bij Ressen”, May 2013

# Abstract

In July 2015, the Netherlands experienced a heat wave with temperatures close to 38°C. However, HARMONIE version 36h1.4, the weather forecast model of KNMI, predicted temperatures exceeding 40°C. Model output revealed that this overestimation was caused by too low latent heat fluxes, in turn causing high (greater than 1) Bowen ratio values in large parts of the domain. Apart from temperatures, these too low latent heat fluxes also cause incorrect cloud formation and wind gusts forecasts. This research focuses on improving these surface turbulent fluxes in order to improve HARMONIE weather forecasts. Data analysis performed in this thesis demonstrates that high Bowen ratios occur more often in spring and summer in the HARMONIE domain. It turns out that the major cause for this is a significant drop in soil moisture in March. Due to this strong decrease, soil moisture levels remain low throughout spring and summer, causing too high temperature forecasts. This research shows that this decrease is initiated by a too early start of the growing season in the HARMONIE model; the leaf area index is too high in March in large parts of Europe, causing high evapotranspiration rates and thus a large drop in soil moisture levels. In addition, other problems regarding assumptions on this leaf area index are evaluated, such as the absence of a North - South gradient. Experiments performed in this research illustrate that a decrease in this leaf area index reduces evapotranspiration rates. This thesis proposes a new way of prescribing the leaf area index depending on soil temperatures and argues that by applying this method, more realistic leaf area index values are constructed. This way, model perfomances can improve.

# Acknowledgements

During this research, I met and worked with some people who made my stay here at the KNMI a pleasant experience. First of all, I want to thank Sander Tijm for being my supervisor at the KNMI. He introduced me to this topic but let me decide how I wanted to tackle this problem. He helped me retrieve datasets and fixing bugs whenever I did not know how to solve them. But above all, he has been a great sparring partner (and chit-chat company) whom without I would have never gotten this far in my research. I also want to thank Michiel van den Broeke, my supervisor at Utrecht University, for supervising me these past 8 months. The feedback and challenging remarks I got from him during our meetings or via email conversations improved my research and academic skills.

Secondly, my partners in crime Pleun Bonekamp and Rosalie Koen always enlightened my day. I will miss the many and diverse conversations during our lunches or coffee breaks, the critical comments, brainstorm sessions or occasional joking around during working hours.

Thirdly, I want to thank all my colleagues at the KNMI WKD department for the warm welcome I got, the interest they showed during my research and the great ambience they always created in the Meteorologenkamer. I learned a lot from you and I am grateful for that!

Lastly, without the support from my family and friends, I would not be where I am today. Thank you for always believing in me and my dreams of becoming a meteorologist.

# Contents

# List of Figures

# List of Tables

# 1 Introduction

In the summer of 2015, the Netherlands experienced a heat wave from 25 June up until 5 July. During this heat wave, temperatures of 38.2°C were recorded in Maastricht on 2 July, almost breaking the national record of 38.6°C, set in Warnsveld in 1944 (Sluijter, 2015). However, even higher temperatures were forecast by HARMONIE, a weather forecasting model used at KNMI (*Royal Netherlands Meteorological Institute*).

HARMONIE is short for *Hirlam Aladin Research On Mesoscale Operational Numerical Weather Prediction In Euromed*, and its operational version is version 36h1.4 (this will be abbreviated to HARMONIE36). Its forecast run at 2 July 2015 00:00 UTC for 2 July 2015 14:00 UTC is shown in figure 1:

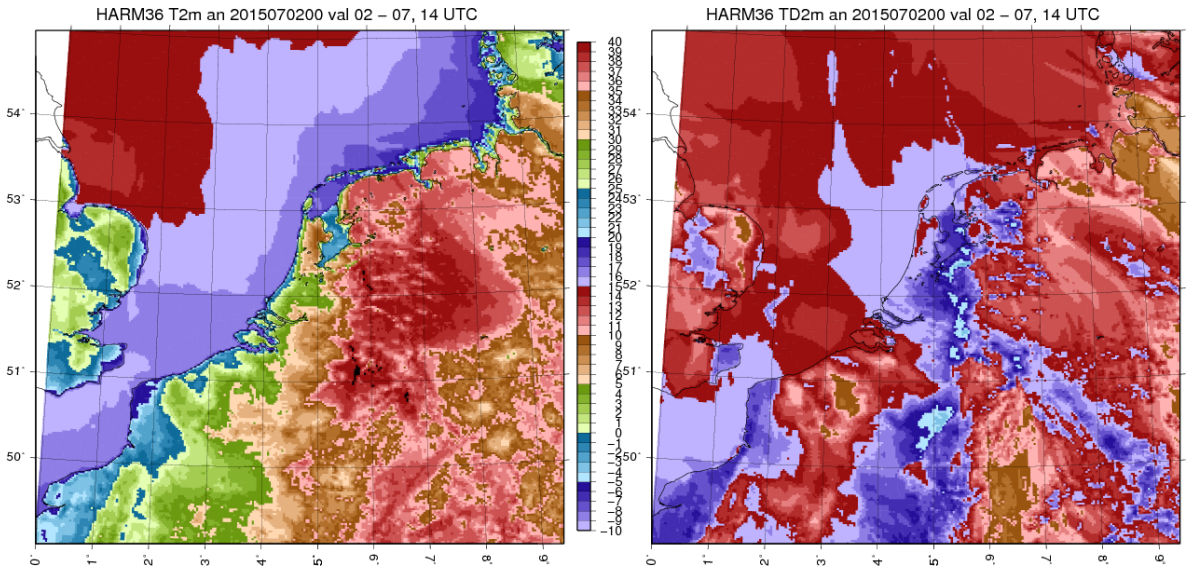


*Figure 1: HARMONIE36 model output of 2 meter temperature (left figure) and dew point temperature output on 2 July 2015 00:00 UTC, valid for 2 July 2015 14:00 UTC. From the HARMONIE36 database.*

The model output in figure 1 illustrates that temperatures exceeding 40°C were forecast in certain regions (dark areas in left figure), higher than the observed maximum temperature of 38.2°C. The same areas in the right panel of figure 1 show that the dew point temperatures there are relatively low. The National Oceanic and Atmospheric Administration (2009) defines the dew point temperature as the temperature to which air must be cooled in order to reach saturation (under constant air pressure and moisture content). Dew point temperatures are a measure of the amount of atmospheric moisture; a higher dew point temperature indicates a higher atmospheric moisture content, whilst a lower dew point temperature corresponds with low amounts of atmospheric moisture. This level of atmospheric moisture is directly influenced by the latent heat flux.

The amount of heat absorbed or released when water is evaporated from the surface or condensed on the surface, is called the latent heat flux (in $\mathrm{Wm}^{-2}$). The latent heat flux (LHF) serves as a measure of evapotranspiration and, consequently, as a measure of atmospheric humidity. In HARMONIE36, fluxes are defined positive when directed towards the surface. From now on, a high LHF is defined as a large (and thus, in this case, negative) flux from the surface to the atmosphere, and a low LHF as a small (close to zero or even positive) flux.

On 2 July, the LHF was forecast as illustrated in figure 2. Values close to 0 $\mathrm{Wm}^{-2}$ imply that

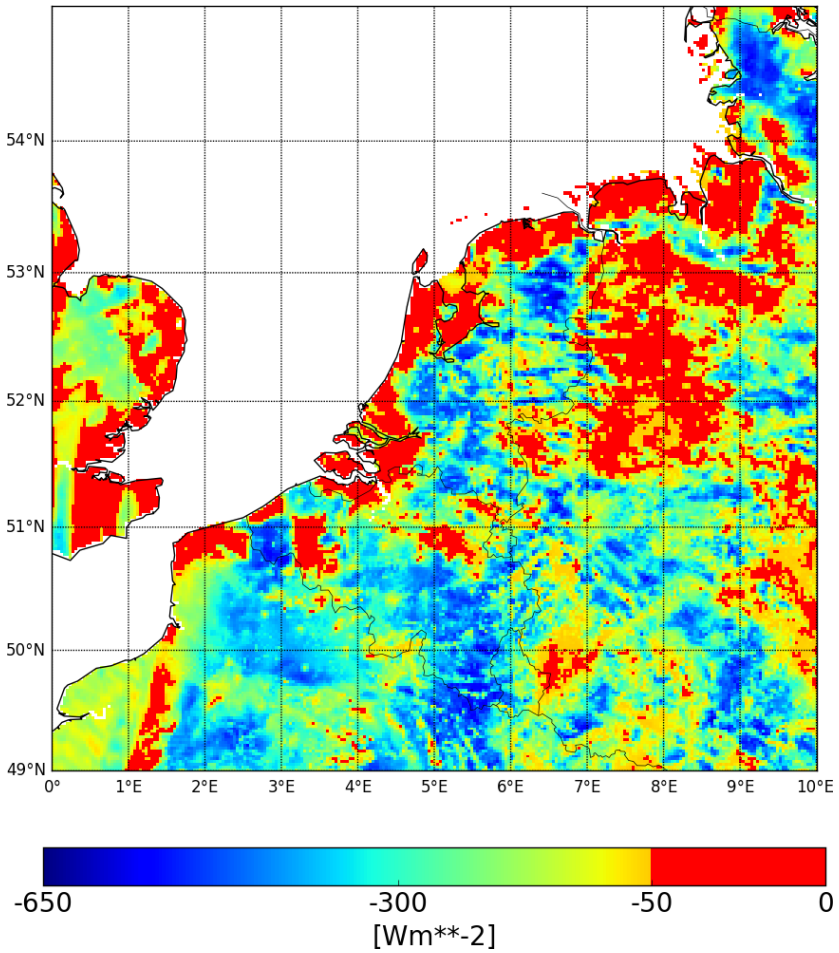


*Figure 2: LHF on 2 July 2015 in the Netherlands. The flux is given as the average flux between 11:00 UTC and 12:00 UTC, forecast at 2 July 0:00 UTC.*

almost no evapotranspiration is taking place, indicated in red. This day was sunny, so LHF should be large. Note the high resemblance between regions where the LHF is close to zero and the regions with low forecast dew point temperatures in figure 1. In these regions, values for $T_d$ range between 8-15°C. This is due to low amounts of atmospheric moisture, caused by low LHF values. In areas where the incoming solar radiation is not used for evapotranspiration, the energy is converted to heating the soil, hereby increasing surface temperatures. In turn, this causes temperature differences between the surface and the atmosphere. Therefore heat transfer will increase and atmospheric temperatures will rise. This heat transfer is represented by the sensible heat flux (SHF). The SHF is defined as the heat transport (flux) between the surface and the atmosphere (in $\mathrm{Wm}^{-2}$). This increase in energy conversion to heat transfer is also visible in figure 1 and 2: in places where the LHF is low, 2 meter temperatures are high and dew point temperatures low. It has a double effect on the relative humidity: a LHF decrease causes a decrease in the dew point temperature and thus a decrease in relative humidity. In addition, an increase in the SHF initiates a 2 meter temperature increase and thus a decrease in relative humidity as well.

Apart from the effect on temperature and dew point temperature forecasts, low atmospheric moisture contents also affect other meteorological phenomena. First of all, cloud formation relies on enough atmospheric moisture being available. This influences model performance directly; if the model

miscalculates cloud formation, fluxes can be calculated incorrectly and even convective showers and thunderstorms can be picked up (too) late by the model. Moreover, fog can be forecast wrong because it heavily depends on atmospheric moisture content. On the other hand, it is also possible that low latent heat fluxes cause thunderstorm formation in the model, though they are not observed in reality. An example of this are the isolated thunderstorms forecast over Gelderland, the Netherlands on 7 June 2016. On this day, HARMONIE36 overestimated temperatures in central Netherlands. The model output is given in figures 3 and 4:

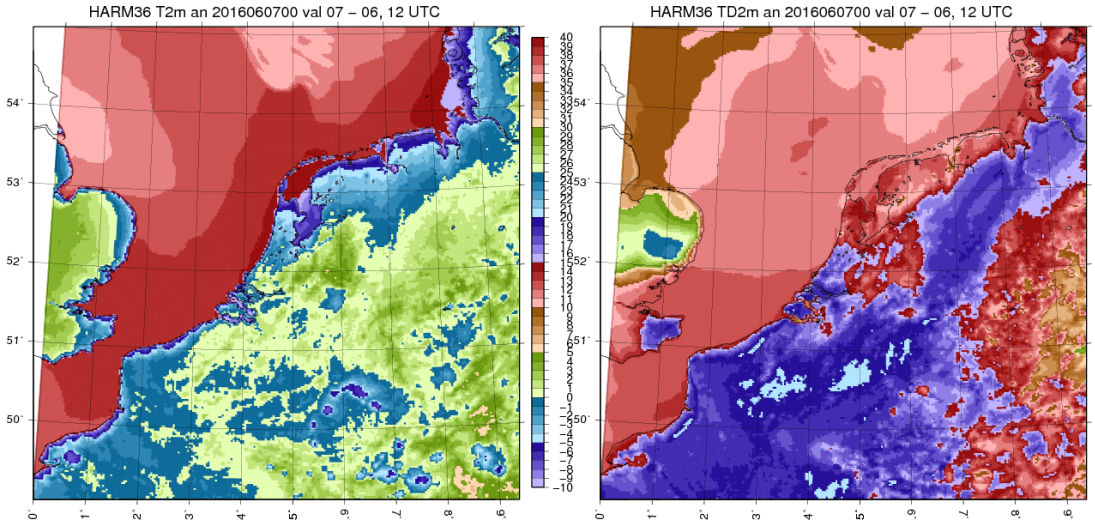


*Figure 3: HARMONIE36 model output of 2 meter temperature (left panel) and dew point temperature output on 7 June 2016 00:00 UTC, valid for 7 June 2016 12:00 UTC. From the HARMONIE36 database.*

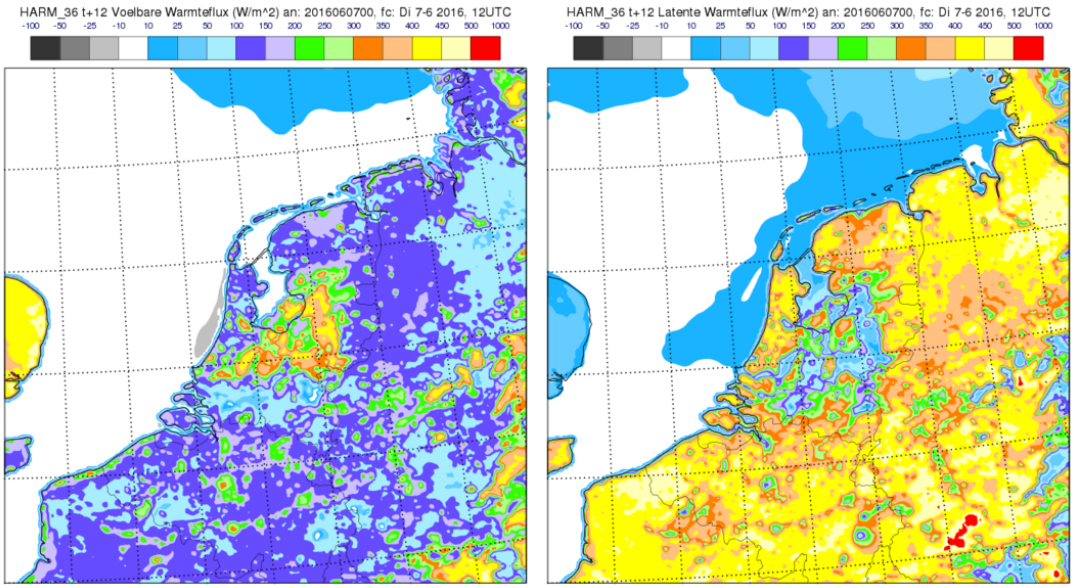


*Figure 4: HARMONIE36 model output of LHF (left panel) and SHF on 7 June 2016 00:00 UTC, valid for 7 June 12:00 UTC. From the HARMONIE36 database.*

At the Veluwe, HARMONIE36 forecast temperatures of around 30°C, whilst temperatures of around 26°C were observed. Over the same area, latent heat fluxes were low, see figure 4. Under these conditions, i.e. high temperatures and low relative humidity due to low LHF values, (thunder)storms can develop. This was also forecast by HARMONIE36, as is shown in figure 5. Note the high resemblance between the 'hook' -like shape in the same area over the Veluwe in figures 3, 4 and 5. However, these storms were not observed at all. On 7 June 2016, strong thunderstorms did develop in Belgium and Germany, close to the Dutch border (the showers to the south-east of the erroneously predicted ones).

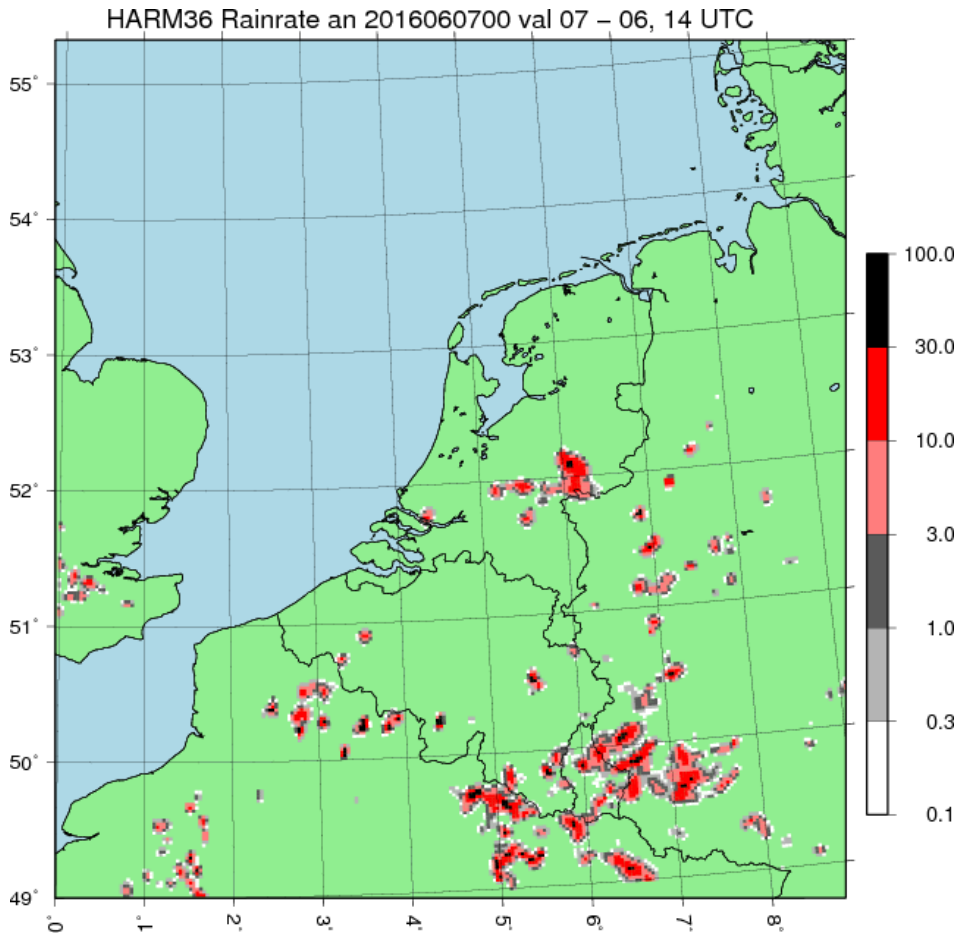


*Figure 5: HARMONIE36 model output of rainrate on 7 June 2016 00:00 UTC, valid for 7 June 2016 14:00 UTC. From the HARMONIE36 database.*

Apart from this (thunder)storm development, low latent heat fluxes can also influence wind gusts. Large temperature differences can initiate strong wind gusts during active showers, even up to "apocalyptic" values of 100 knots or 185 km/h, values more commonly found in (strong) hurricanes. It should be clear that these wind gusts are extremely rare in the Netherlands and the model output has to be discarded in this case. In addition, these strong wind gusts can also occur during showers in a too dry boundary layer. This too dry air causes precipitation to be evaporated before it reaches the ground, hereby increasing air density. This more moist air will then be heavier than its surroundings, and due to gravity effects, downbursts and thus wind gusts will be stronger than actually observed.

Temperature and dew point temperature misforecasting can thus have major effects on other

meteorological phenomena. In addition, at high temperatures, precautions have to be taken for vulnerable people as these temperatures can seriously affect their well-being. Because different (health) organisations are involved in executing these precautions, good temperature forecasting is essential. Moreover, strong thunderstorms can cause heavy precipitation and flooding, and KNMI has to issue a warning in that case. If these thunderstorms are forecast and warned for but not observed in reality, this might harm KNMI's credibility.

As stated before, these problems are mainly caused by too low LHF. Another way to evaluate turbulent surface fluxes is via the Bowen ratio. This Bowen ratio is defined as the ratio between the SHF and the LHF and is dimensionless. The Bowen ratio differs for different surface types. Over moist areas (wetlands), the LHF will be (much) larger than the SHF, causing the Bowen ratio to be smaller than 1. On the contrary, the Bowen ratio will be greater than 1 over semi-arid landscapes and deserts, since there is a large heat transport (large SHF) and a small evaporation flux, due to the absence of soil moisture and/or vegetation. In table 1, typical values for different surface types are listed.

*Table 1: Typical Bowen ratio values for different ecosystem types. From Chapin III et al. (2011), data from Jarvis (1976), Oke (1987) and Eugster et al. (2000).*

| Surface type | Bowen ratio |
|---|---|
| Desert | >10 |
| Semi-arid landscape | 2-6 |
| Arctic tundra | 0.3-2.0 |
| Temperate forest and grassland | 0.4-0.8 |
| Boreal forest | 0.5-1.5 |
| Forest, wet canopy | -0.7 - 0.4 |
| Water-stressed crops | 1.0-1.6 |
| Irrigated crops | -0.5 - 0.5 |
| Tropical wet forest | 0.1 -0.3 |
| Tropical ocean | <0.1 |

In the Netherlands, mostly temperate forests and crops/grasslands can be found. Hence, typical values of the Bowen ratio lie around 0.5. Only during long periods with warm and dry conditions, soil moisture may be depleted to the point that vegetation starts to limit evapotranspiration. In this case, the Bowen ratio will be greater than 0.5 - 1.0. However, these situations are quite rare. Whenever the Bowen ratio is greater than 1, the situation is uncommon for the Netherlands and the model is malperforming. This situation will be referred to as 'a high Bowen ratio'. One exception has to be made: over urbanised areas, the Bowen ratio is expected to exceed 1. This is due to little vegetation coverage in these areas, causing low evapotranspiration rates. Vegetation consists of a root zone, where soil moisture can be stored and accessed for evapotranspiration via the leaves of the vegetation in question. In addition, in summer, the SHF will be large in these urbanised areas since roads and buildings convert all solar energy to SHF.

Figure 6 shows the average Bowen ratio on 2 July between 11:00 UTC and 12:00 UTC, forecast at 2 July 00:00 UTC. As stated before, urbanised regions are expected to have high Bowen ratio values. Yet, the majority of these red areas are rural areas, with an expected Bowen ratio of around 0.5. This thus demonstrates that the Bowen ratio is too high in large parts of the HARMONIE domain.

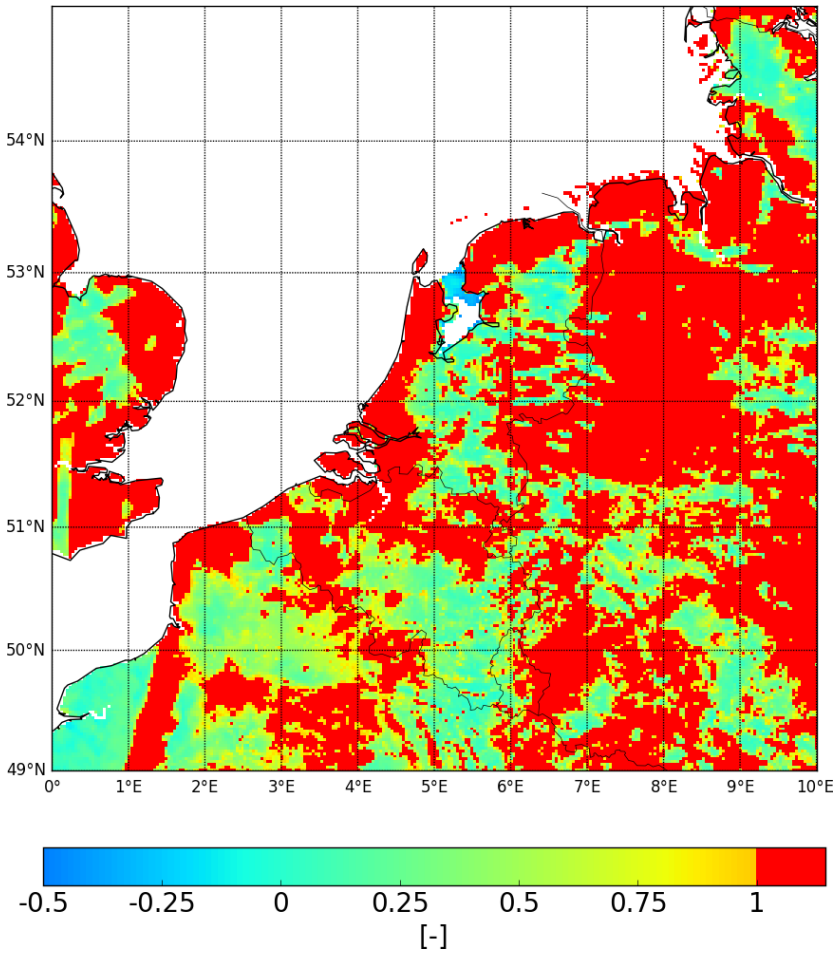


*Figure 6: The Bowen ratio on 2 July 2015, taken as the average value between 11:00 UTC and 12:00 UTC, forecast at 2 July 0:00 UTC.*

In this Master's thesis, we will investigate why the Bowen ratio is larger than 1 in large parts of the Netherlands. The influence of vegetation, its characteristics and the temporal variability of soil moisture will be analysed for both HARMONIE36 and HARMONIE38 (the successor of version 36), and a diagnosis will be made. Experiments will be constructed and executed in order to improve the LHF so that temperature forecasts will be more realistic. Finally, a conclusion will be drawn, and a discussion and recommendations for further research and development will be given.

# 2 HARMONIE

As was stated in the introduction, the weather forecasting model HARMONIE version 36h1.4 is used at KNMI. HARMONIE36 has a relatively high resolution of 2.5 km. Its post-processed data is generated on a regular latitude-longitude grid of 300x300 points, a sub-domain of the 789x789 model grid. This 300x300 grid covers the Netherlands, as well as parts of Belgium, Germany and Great Britain. However, it is not possible to execute experiments in HARMONIE36 anymore. This is why HARMONIE version 38h1.2 (HARMONIE38 hereafter), the updated version of HARMONIE36, will be used. HARMONIE38's datasets are not archived on the 300x300 grid, so the soil and flux data are retrieved from the original 789x789 grid. This grid covers central Europe and has the same spatial resolution. Because experiments will be performed and the next operational version of HARMONIE will be closest to HARMONIE38, both HARMONIE36 and HARMONIE38 will be discussed and evaluated simultaneously hereafter.

## 2.1 SURFEX and ISBA

In both HARMONIE36 and HARMONIE38, different types of surface cover are modelled using SURFEX (*Surface Externalisée*) (Le Moigne et al., 2012). SURFEX describes different types of surfaces: soil, urban environments, sea and inland water bodies. The first surface type is of interest here, because the problem sketched in the introduction focuses on processes occurring over land.
For soil modelling, ISBA (*Interactions Soil Biosphere Atmosphere*) is implemented in SURFEX. ISBA manages energy and water exchanges between the surface and the atmosphere (Le Moigne et al., 2012).

There are numerous equations used in ISBA to model the surface-atmosphere interaction. The relevant ones will be discussed here.

In ISBA, surface temperature is modelled according to the force-restore method proposed by Bhumralkar (1975) and Blackadar (1976):

$$\frac{\partial T_s}{\partial t} = C_T(R_n - H - LE) - \frac{2\pi}{\tau}(T_s - T_2) \tag{1}$$

$$\frac{\partial T_2}{\partial t} = \frac{1}{\tau}(T_s - T_2) \tag{2}$$

Here, $T_s$ is the surface temperature ($K$), $T_2$ the mean temperature ($K$) over one day $\tau$. $H$ and $LE$ are the sensible and latent heat fluxes ($Wm^{-2}$), and $R_n$ is the net radiation at the surface ($Wm^{-2}$) (Le Moigne et al., 2012). The first term on the right-hand side of equation 1 represents diurnal forcing by the heat flux $G$ (calculated as $G = R_n - H - LE$). The second term is a restoring term towards $T_2$. From equation 1, a low LHF (LE) causes a $T_s$ increase. Therefore the soil-atmosphere temperature gradient will increase, initiating a larger SHF (H). As a consequence, atmospheric temperatures will rise.

HARMONIE uses the three-layer version of ISBA. In this version, the soil is divided into three layers: the surface layer with a normalized depth $d_1$ of 1 cm and soil moisture content $w_g$ ($m^3m^{-3}$), the root layer with depth $d_2$ ($m$) and soil moisture content $w_2$ ($m^3m^{-3}$), and the deep layer with depth $d_3 - d_2$ (here, $d_3$ is the total soil depth in $m$) and soil moisture content $w_3$ ($m^3m^{-3}$). $d_2$ and $d_3$ are vegetation dependent constants, and $w_g$, $w_2$ and $w_3$ are modelled as follows (from Deardorff (1997) and Boone et al. (1999)):

$$\frac{\partial w_g}{\partial t} = \frac{C_1}{\rho_w d_1}\left(P_g - E_g\right) - \frac{C_2}{\tau}\left(w_g - w_{geq}\right); \quad 0 \leq w_g \leq w_{sat} \tag{3}$$

$$\frac{\partial w_2}{\partial t} = \frac{1}{\rho_w d_2}\left(P_g - E_g - E_{tr}\right) - \frac{C_3}{d_2\tau}\max[0,(w_2 - w_{fc})] - \frac{C_4}{\tau}\left(w_2 - w_3\right) \tag{4}$$

$$\frac{\partial w_3}{\partial t} = \frac{d_2}{(d_3 - d_2)}\left\{\frac{C_3}{d_2\tau}\max[0,(w_2 - w_{fc})] + \frac{C_4}{\tau}\left(w_2 - w_3\right)\right\} - \frac{C_3}{(d_3 - d_2)\tau}\max[0,(w_3 - w_{fc})]; \quad 0 \leq w_3 \leq w_{sat} \tag{5}$$

In equation 3, the first term on the right-hand side describes the increase or decrease in $w_g$ via precipitation/melting ($P_g$) and direct evaporation $E_g$. Both $P_g$ and $E_g$ are in $kgm^{-2}h^{-1}$. The water density is represented via $\rho_w$ ($kgm^{-3}$). The second term consists of the equilibrium surface volumetric moisture $w_{geq}$ and represents drainage.
In equation 4, changes in $w_2$ due to precipitation/melting, direct evaporation and evapotranspiration ($E_{tr}$) are described in the first term on the right-hand side. The second and third term cover drainage due to runoff (when $w_2$ exceeds the field capacity $w_{fc}$) and a soil moisture gradient, respectively. Note that in both equations 3 and 4, the term $P_g - E_g$ is present. Its influence is distributed over these layers via the dependence on $d_1$ and $d_2$ respectively.
$w_3$ in the last equation, equation 5, is mainly influenced by the root layer. The first term describes the influx from the root layer (by drainage and a soil moisture gradient), and the second term represents runoff in the deep layer. All excess soil moisture (when $w_3 > w_{fc}$) is removed from the system. $w_{sat}$ is the volumetric moisture content at saturation.
$C_1$, $C_2$, $C_3$ and $C_4$ are coefficients depending on the soil moisture content, sand and clay contents. $C_3$ is in $m$, $C_1$, $C_2$ and $C_4$ are dimensionless. For the exact definition, see Le Moigne et al. (2012).

## 2.2 ECOCLIMAP

Vegetation specifications like root zone depth are listed in ECOCLIMAP, a vegetation database provided by CNRM France. Its resolution is 1 km, and classifies global vegetation coverage. In HARMONIE36, ECOCLIMAP-I is used, whilst its successor ECOCLIMAP-II is operational in HARMONIE38. Both ECOCLIMAP-I and II use so-called tiles to describe different cover types. There are four tiles: Town, Nature, Water and Sea. The Nature tile is specified by 12 patches, which are used to describe different vegetation types. Every vegetation type is classified by a combination of these tiles and patches. The patch classification is as in table 2.

### 2.2.1 ECOCLIMAP-I (HARMONIE36)

ECOCLIMAP-I consists of 215 unique vegetation types, each labelled as a cover type number. Over Europe, CORINE (*Coordination of Information on Environment*) is used to classify each of these 215 vegetation types (Masson et al., 2003). Every vegetation type consists of characteristics like patch fraction, root zone depth and leaf area index (LAI). Root zone depths and patch fractions are constant and have to be determined once, whilst the LAI is variable in time due to sprouting and shedding of leaves.

SURFEX defines the LAI as the ratio of the total upper leaf (or needle) surface of vegetation divided by the surface area of the land on which the vegetation grows (Le Moigne et al., 2012).

*Table 2: ECOCLIMAP grouping of patches and tiles, from Faroux et al. (2014) and Le Moigne et al. (2012).*

| Tile name | Patch name |
|---|---|
| Town | |
| Nature | No vegetation (bare soil) |
| | Bare rock |
| | Permanent snow and ice |
| | Deciduous broadleaved forest |
| | Evergreen broadleaved trees |
| | Needle-leaf (coniferous) forest |
| | C3 crops |
| | C4 crops |
| | Irrigated crops |
| | C3 herbaceous (temperate grassland) |
| | C4 herbaceous (tropical grassland) |
| | Wetlands |
| Water (Lakes and rivers) | |
| Sea | |

In ECOCLIMAP-I, LAI values are calculated using lookup tables containing the annual LAI cycle, derived from *Advanced Very High Resolution Radiometer* (AVHRR). The resulting LAI is evaluated against in-situ observations, the ISLSPC-II (*International Satellite Land Surface Climatology Project*) LAI database and POLDER (*Polarization and Directionality of the Earth's Reflectance*) satellite LAI values (Centre Nationale de Recherches Météorologiques, 2015). Yet, contrary to these datasets, the LAI is not computed for each pixel in the domain, but is estimated per vegetation type (Masson et al., 2003). The LAI is calculated as:

$$LAI = LAI_{min} + (LAI_{max} - LAI_{min}) \frac{NDVI - NDVI_{min}}{NDVI_{max} - NDVI_{min}} \tag{6}$$

$LAI_{max}$ and $LAI_{min}$ are derived from in-situ measurements or empirically from ISBA simulations (Le Moigne et al., 2012). The *Normalized Difference Vegetation Index*, NDVI, is deduced from satellite normalised reflectances. Because it has been demonstrated that a correlation exists between NDVI values and the photosynthesis activity by vegetation, the NDVI is considered in the LAI determination.

The LAI is updated roughly every 10 days. These periods are defined as the 1st from the 10th; the 11th to the 20th and the 21th to the end of each month (Faroux et al., 2014).

### 2.2.2 ECOCLIMAP-II (HARMONIE38)

ECOCLIMAP-II describes 273 different vegetation types. The vegetation types itself are also re-defined, except for vegetation types related to urban environments (151-160 in ECOCLIMAP-I); these

vegetation types are adapted directly from the previous version. ECOCLIMAP-II takes the existing cover maps Global Land Cover2000 (GLC2000) and Corine Land Cover2000 (CLC2000) into account, and splits existing classes into new classes that possess a better regional character (Centre Nationale de Recherches Météorologiques (2015),Le Moigne et al. (2012)). NDVI is taken from SPOT/Vegetation. Patch definitions are the same as in ECOCLIMAP-I, but two patches are excluded in ECOCLIMAP-II: patches 5 and 11 (evergreen broad-leaved forest and C4 herbaceous) (Faroux et al., 2014).

In ECOCLIMAP-I, the LAI was represented as a list, depending on the patch and vegetation type, and has been monitored during one year. In ECOCLIMAP-II, the LAI is again patch and vegetation type dependent, however there are multiple LAI datasets one can choose from. Individual LAI datasets are available for (experimental) runs performed in the time interval 2002-2006. For years outside of this interval, the climatological LAI is taken, calculated as the average LAI over this 2002-2006 interval. This is beneficial since, contrary to ECOCLIMAP-I, small anomalies are now filtered out. However, large anomalies may still be present. The summer of 2003 is ranked one of the hottest summers on record (Sluijter, 2003). In addition, July 2006 was very hot and dry, whilst August 2006 was characterised by many rainy days (Sluijter, 2006). By considering the time interval 2002-2006, these extremes are included in the climatological LAI.

# 3 Problem diagnosis

## 3.1 Bowen ratio in 2015

In the introduction, we have seen the model output for 2 July 2015, where Bowen ratios were high in large parts of the domain. Next, it is of interest to see how the model is performing throughout the year 2015 in order to determine whether these high Bowen ratio values are only present under extreme conditions, as was the case on 2 July, or whether they occur more often. For 2015, the available HARMONIE36 data set ranges from 6 January until 30 August 2015, excluding 17 August and 19 August. This data set consists of the +11h and +12h surface turbulent flux forecast of the 00:00 UTC run. This data set is sufficient since the complete spring and summer periods are present. In these periods, the combination of high solar radiation and vegetation activeness should cause large latent heat fluxes. The surface fluxes are initially given as accumulated fluxes, but are converted to an average flux between 11:00 UTC and 12:00 UTC. The Bowen ratio is thus an average value between 11:00 - 12:00 UTC.

One way to analyse the Bowen ratio spatial pattern throughout the time interval is by plotting and examining the Bowen ratio for every single day. However, this way 235 figures have to be analysed, and it might not be clear whether there are specific regions with a frequent occurrence of a high Bowen ratio. This is of interest since these specific regions might portray a consistent error and can influence neighbouring grid points, hereby initiating a snowball effect. This is why the number of days where the Bowen ratio is high will be plotted. This plot provides a quick overview of regions with a high count, i.e. where latent heat fluxes are low relatively often, and a low count.

Figure 7 shows this plot for HARMONIE36. One can see that grid points with an orange-reddish colour are points where the Bowen ratio is high relatively often. The majority of the isolated locations with these colours are urbanised regions; one can recognise large cities in the Netherlands like Amsterdam and Rotterdam, cities in Belgium, the Ruhr area and the city of London. It has been explained in the introduction why Bowen ratios can get high over these areas. As this situation is explainable and expectable, we will not examine these areas more in detail.
Another area with relatively high Bowen ratio counts is the east coast of Great Britain. Here, low latent heat fluxes (and thus high Bowen ratios) are likely caused by the advection of moist sea air. This moist sea air causes the soil-atmosphere gradient to be small, resulting in a low LHF. Nevertheless, it is questionable whether this effect should be visible so far inland.

Yet, there are also sub-urban and rural areas with high Bowen ratio counts. This cannot be due to little vegetation presence, as was the case in urban areas. Furthermore, because these locations lie further inland, advection of moist sea air should not play a role here. From looking at figure 7, a few questions arise:

1. Is there enough soil moisture available in these areas for the plants to evapotranspire? If there is not enough soil moisture present in the system at all, latent heat fluxes will be small.

2. Are there distinct vegetation types causing these high Bowen ratio counts? It is plausible that there are certain vegetation types with corresponding characteristics that cause low latent heat fluxes. For instance a small root zone depth $d_2$, a vegetation dependent parameter, causes little soil moisture being able to be stored in the root zone, so that the root zone can dry out quickly and evapotranspiration rates decrease.

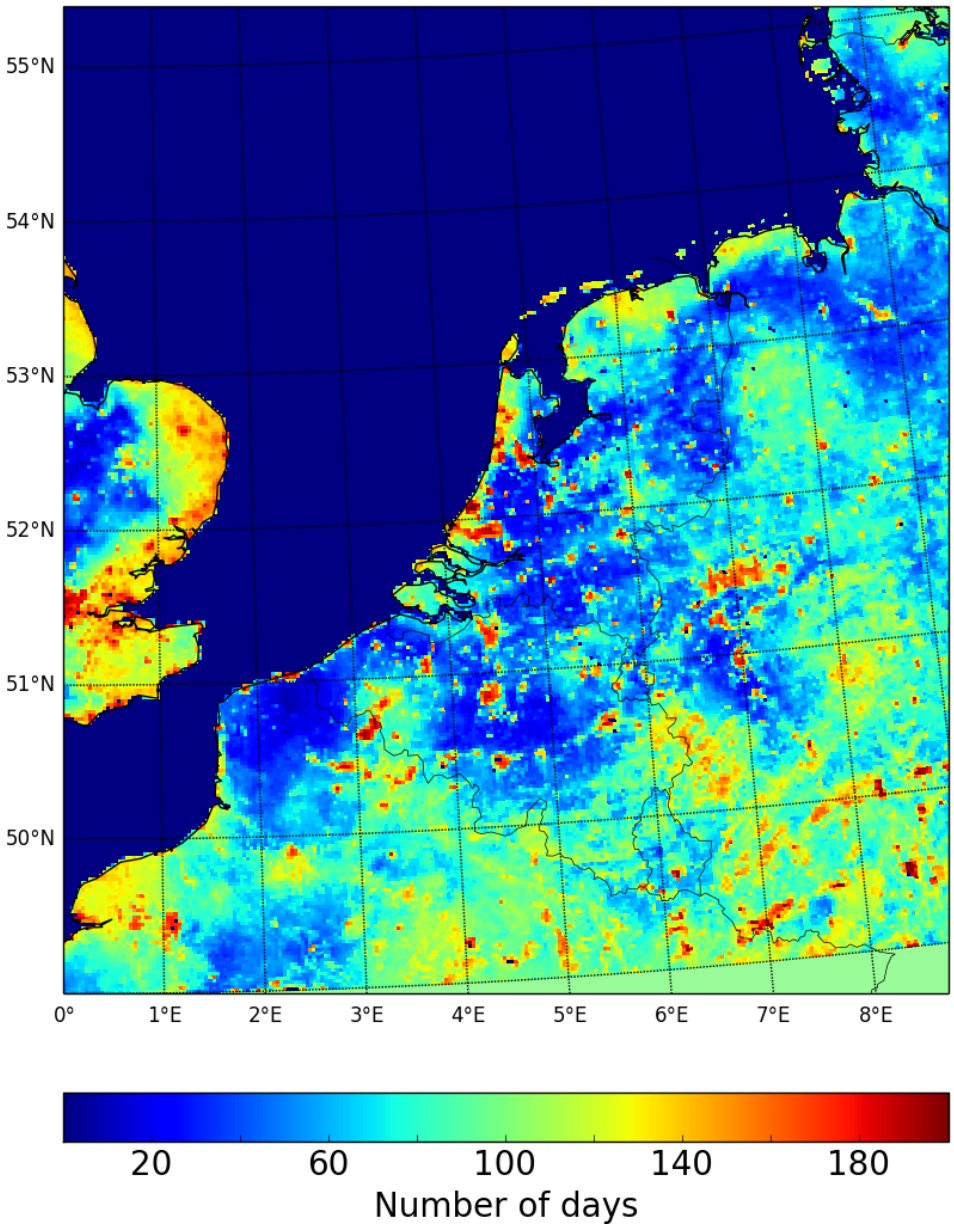


*Figure 7: Number of days where the Bowen ratio is greater than 1 for HARMONIE36. The time interval is 6 January - 30 August 2015 (total of 235 days).*

HARMONIE38's time series ranges from 10 February till 31 August 2015. This is slightly shorter than for HARMONIE36 (201 versus 235 days), however spring and summer are still within this time interval. As was stated in section 2, HARMONIE38's domain covers central Europe. Because there are no large differences in vegetation type coverage throughout Europe, a Bowen ratio greater than 1 is still uncommon.

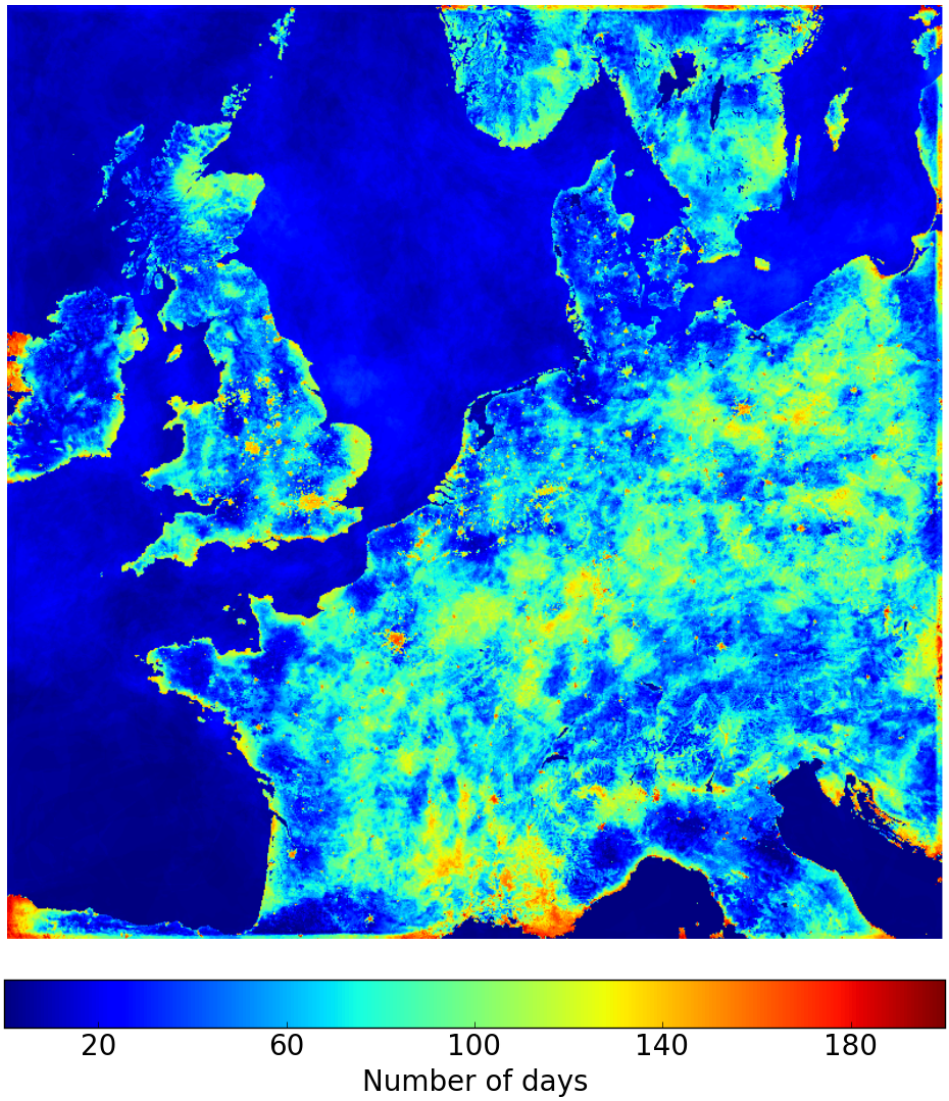


*Figure 8: Number of days where the Bowen ratio is greater than 1 for HARMONIE38. The time interval is 10 February - 31 August 2015 (total of 201 days).*

Figure 8 shows the number of days where the Bowen ratio is high. Again, urbanised areas like Paris and London have a high Bowen ratio count. Furthermore, boundary conditions also cause high Bowen ratio counts, as is visible in the western part of Ireland, Spain and Portugal. Moreover, almost all coastal regions regularly experience a high Bowen ratio, something likely due to the advection of moist air originating over sea.
In central Europe, a wide band with a high count is visible. These areas are not influenced by either urban areas, boundary conditions or advection of moist sea air. Therefore, other options like vegetation influence or soil moisture absence need to be considered here.
On the other hand, there are also areas that have improved significantly compared to HARMONIE36. The biggest change is visible in the northern part of the Netherlands (Friesland and Groningen), where almost no high Bowen ratio are registered anymore, compared to over 100 days in HARMONIE36. Still, Bowen ratios are too high in large parts of both the HARMONIE36 and HARMONIE38 domain.

## 3.2 Vegetation coverage in the HARMONIE domain

In order to test for correlation between vegetation types and high Bowen ratio counts, vegetation cover distribution has to be evaluated.
In HARMONIE36, ECOCLIMAP-I is used (see paragraph 2.2.1), consisting of 215 vegetation types. Because multiple vegetation types can be present at one grid point, it will be confusing to plot all vegetation types together with their fractions per grid point. Instead, so-called dominant vegetation types are considered. Here, a vegetation type is said to be dominant at a certain grid point when at least 70% of this grid point is covered by this vegetation type. If there is no dominant vegetation type, the grid point is said to be covered by vegetation type 'Mix'. This vegetation type is not part of the original ECOCLIMAP coverage scheme, but has been added manually for diagnostic purposes. Note that it is possible that some grid points are now classified as 'Mix' due to interpolation methods caused by the conversion from Lambert projection (the 789x789 grid) to the regular lat-lon grid (300x300 grid). However, this way of interpolating is not of interest here, and will therefore not be discussed any further.
Applying this filter yields 30 dominant vegetation types (including 'Mix'). In figure 9, the distribution of dominant vegetation types and vegetation type 'Mix' in HARMONIE36 is shown. Comparing figure 9 with figure 7 shows that there is no conclusive outcome as to which vegetation type is responsible for high frequency counts. In the northern part of the Netherlands, pastures can be found in regions with a high Bowen ratio count, but in other regions with this same dominant vegetation type, the Bowen ratio count is lower. Apart from this, also temperate crops and forests seem to have a high frequency count in one place, but a low count in other places. Moreover, our manually added vegetation type 'Mix', of which the composition per grid point is unknown at this point, seems to show the same amount of influence.

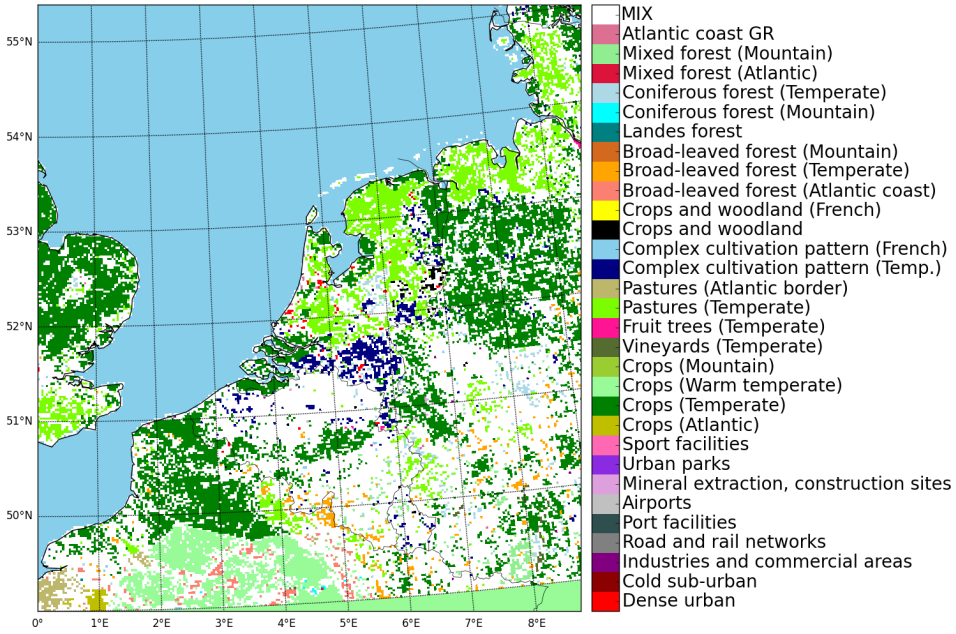


*Figure 9: Distribution of dominant vegetation types and vegetation type 'Mix' over land in ECOCLIMAP-I (HARMONIE36).*

In ECOCLIMAP-II, implemented in HARMONIE38, there are 273 defined classes. Only considering the dominant vegetation types leaves 128 vegetation types, 129 if vegetation type 'Mix' is included. This huge amount of dominant vegetation types is rather difficult to visualise clearly. Therefore, we

would like to refer to figure 7 of Faroux et al. (2014) for an overview of the dominant patterns. Comparing this figure to figure 8 also shows no distinct relationship between (several) dominant vegetation type(s) and a high frequency count in HARMONIE38. This leads to the conclusion that this hypothesis can be discarded for both HARMONIE36 and HARMONIE38.

## 3.3 Available water for transpiration

Another possible cause of low LHF values is soil moisture scarcity, as was proposed in subsection 3.1. Because soil moisture is important for both vegetation viability and atmospheric moisture contents (and, consequently, dew point temperatures), it is crucial to have a sufficient amount of soil moisture. Whether there can be soil moisture stored in the root zone at all depends on two factors: first, the soil type (clay, sand or loam) determines the storage capability of the soil. A clay ground can hold more soil moisture than a sandy ground. Second, the root zone depth $d_2$ (in $m$) also influences the amount of soil moisture available for evapotranspiration. For the same soil type, a small $d_2$ obviously allows for less soil moisture storage than a large $d_2$.

The influence of the soil type on vegetation viability can be illustrated via the wilting point $w_{wilt}$ ($m^3m^{-3}$). $w_{wilt}$ is amount of soil moisture retained by the soil, but unavailable for the vegetation. If the root zone soil moisture $w_2$ ($m^3m^{-3}$) drops below $w_{wilt}$, the plant is wilting and stops transpiring (becomes completely inactive). At this point, the LHF will be close to zero. $w_{wilt}$ depends on the amount of clay in the soil (in %) and is calculated in SURFEX as (Le Moigne et al., 2012):

$$w_{wilt} = 37.1342 \cdot 10^{-3}(\text{clay})^{0.5} \tag{7}$$

In order to introduce $d_2$ dependency, let us define the available water for transpiration as the amount of water available for the plant to transpire. The available water $AW$ (in mm) at a certain grid point is then:

$$AW(t) = (w_2(t) - w_{wilt}) \cdot d_2 \cdot 1000 \tag{8}$$

with $w_2(t)$ the root liquid volume water content (in $m^3m^{-3}$) and $t$ the time (according to the temporal resolution of $w_2$). Whenever $AW < 0$, the plant is wilting.

$w_2$, and hereby thus also $AW$, might change due to two processes: because of effects described in equation 4, of which precipitation and evapotranspiration are of greatest influence, and due to data assimilation. Data assimilation is the feedback mechanism between the observations and the model output; by analysing the observations and possibly adjusting the model parameters, a new input data set is generated for the next model run. The relevant parameters checked during this feedback session are 2 meter temperatures and dew point temperatures. The important effect here is that $w_2$ is increased when temperatures are too high and dew point temperatures too low, hereby converting more solar energy to evapotranspiration (LHF) than surface heating and thus heat transfer (SHF), therewith decreasing 2 meter temperatures and increasing dew point temperatures. Consequently, $w_2$ is decreased when temperatures are too low and dew point temperatures too high, so that less water is available for evapotranspiration and 2 meter temperatures thus increase and dew point temperatures decrease. In HARMONIE, this data assimilation is performed every 3 hours. This topic will be discussed in more detail in subsection 3.6.

Apart from the wilting point, the saturation point can also be calculated. Whenever the root zone reaches saturation, the ground is saturated and any more water cannot be stored in the soil; runoff occurs. The saturation point $w_{sat}$ is determined in SURFEX as (Le Moigne et al., 2012)

$$w_{sat} = (-1.08 \cdot \text{sand} + 494.305) \cdot 10^{-3} \tag{9}$$

$w_{sat}$ is thus a function of the amount of sand in the soil (in %).

The maximum amount of available water $AW_{max}$ (in mm) (or, following Le Moigne et al. (2012), the maximum deficit $D_0$), is now

$$AW_{max} = D_0 = (w_{sat} - w_{wilt}) \cdot d_2 \cdot 1000 \tag{10}$$

If $AW > AW_{max}$, runoff occurs. Note that $AW_{max}$ is constant in time.

Under a certain level $AW_{crit}$, the vegetation will experience water stress. At this point, the plant will not evapotranspire freely (as is the case when $AW_{crit} < AW < AW_{max}$), but will adjust its evapotranspiration rate according to the available water. This critical level $AW_{crit}$ (in mm) is constant and is determined as

$$AW_{crit} = (w_{fc} - w_{wilt}) \cdot d_2 \cdot 1000 \tag{11}$$

where $w_{fc}$ (in $m^3 m^{-3}$) is the field capacity depending on the percentage clay, defined by Le Moigne et al. (2012) as

$$w_{fc} = 89.0467 \cdot 10^{-3} \cdot (\text{clay})^{0.3496} \tag{12}$$

## 3.4 Available water in HARMONIE

### 3.4.1 Spatial distribution

It is of crucial importance to check whether there is enough soil moisture available for transpiration in the system. If this level is not sufficient, e.g. AW is (close to) zero, vegetation will experience water stress and eventually start wilting. At that point, no evapotranspiration is taking place, so that the LHF will be low and the Bowen ratio high.
To start off with, we will analyse the available water, defined as in equation 8, at two selected days in 2015: 5 March and 2 July 2015. $AW_{max}$ and $AW_{crit}$ are calculated as in equations 10 and 11, respectively. Information on sand and clay fractions in the HARMONIE domain can be found in Appendix A.1.

For HARMONIE36, the maximum available water $AW_{max}$, the critical level $AW_{crit}$ and the available water at 5 March 12:00 UTC and 2 July 2015 12:00 UTC (forecast at 00:00 UTC) are plotted in figure 10. It shows that there is a significant difference between available water levels at 5 March and 2 July 2015. In figure 10c, available water levels are still sufficient for vegetation to evapotranspire, and these levels mostly lie above the critical level $AW_{crit}$. There are some regions where little water is available, but these areas are mostly urbanised and therefore these low levels are to be expected here. However, on 2 July large areas in the domain suffer from severe available water scarcity or are even below wilting point. These areas are indicated in white over land. These low levels have a devastating effect on the vegetation; most vegetation would be dead or close to dying. Evapotranspiration rates will be low and almost all solar radiation will be converted to heating of the soil. Most importantly, available water levels seem to be sufficient in March, but have dropped drastically in July. The question thus is: what happens between March and July that causes this large drop in available water?

Figure 11 shows the spatial distribution of the (forecast) available water in HARMONIE38 on 5 March 2015 12:00 UTC and 2 July 2015 12:00 UTC, both calculated at 00:00 UTC. Again a distinct difference between 5 March and 2 July 2015 is visible. There appears to be enough water available in most parts of Europe in March, see figure 11c. Low available water levels are to be expected in mountainous areas like the Scottish Highlands and the Alps, since there is little vegetation (and more

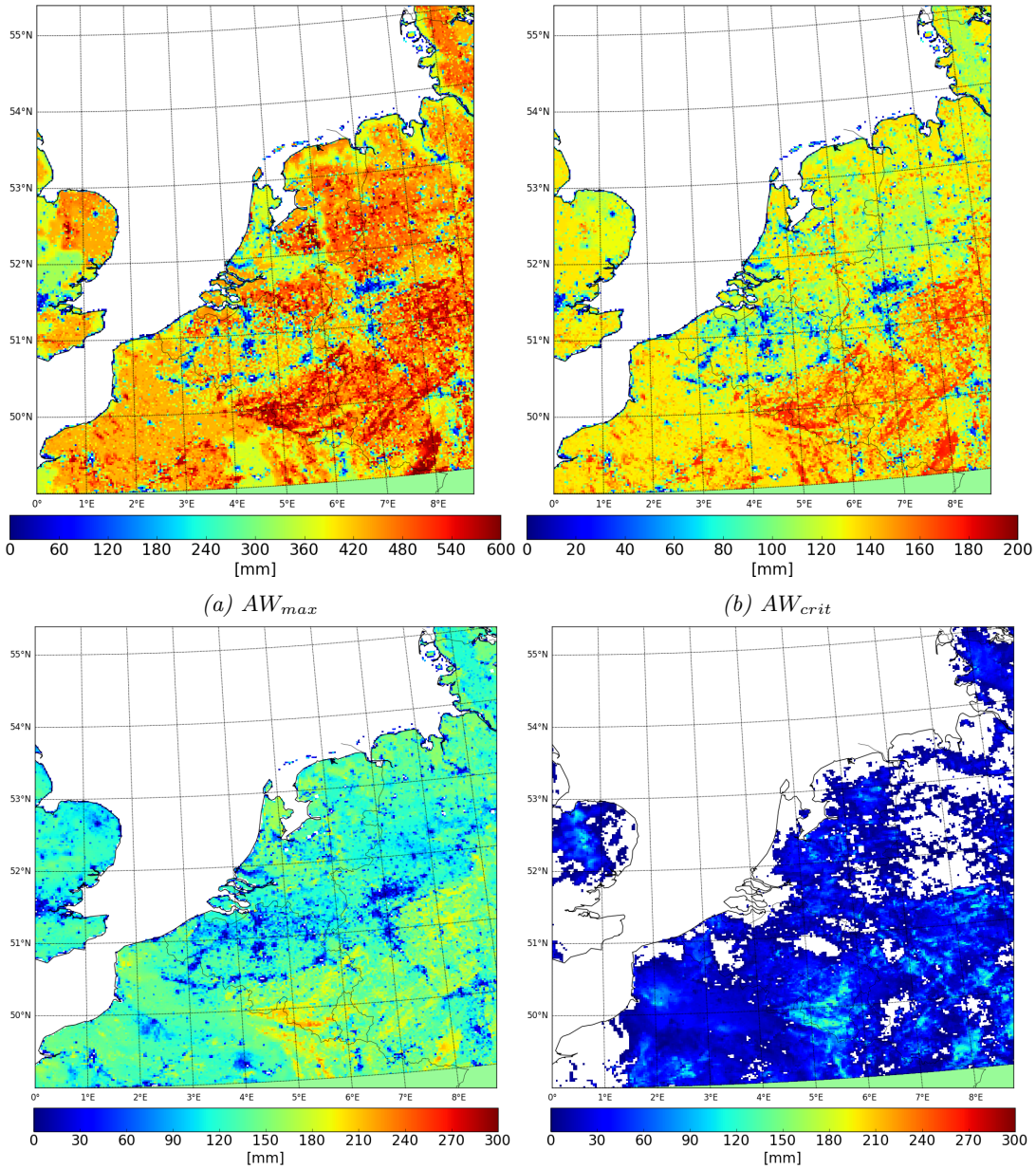


*(a) $AW_{max}$* *(b) $AW_{crit}$*

*(c) AW 5 March 2015* *(d) AW 2 July 2015*

*Figure 10: $AW_{max}$, $AW_{crit}$ and available water levels on 5 March and 2 July 2015 12:00 UTC (forecast at 0:00 UTC) in the HARMONIE36 domain. Note the scale differences between the figures.*

bare rock) at higher altitudes. However in central France, these low levels are unexpected and might lead to serious water stress.

Figure 11d illustrates that available water levels are (close to) zero almost everywhere in the domain, indicating that the ground is (almost) too dry for vegetation to survive. Under these circumstances, almost no evapotranspiration will take place and temperatures will rise quickly. In reality, there should be enough moisture in the root zone, since vegetation only wilts under extreme circumstances, with high temperatures and no precipitation for a long period of time. Although large parts of Europe

experienced a heat wave in that week, there was still enough soil moisture available for the vegetation; most vegetation types survived this heat wave.

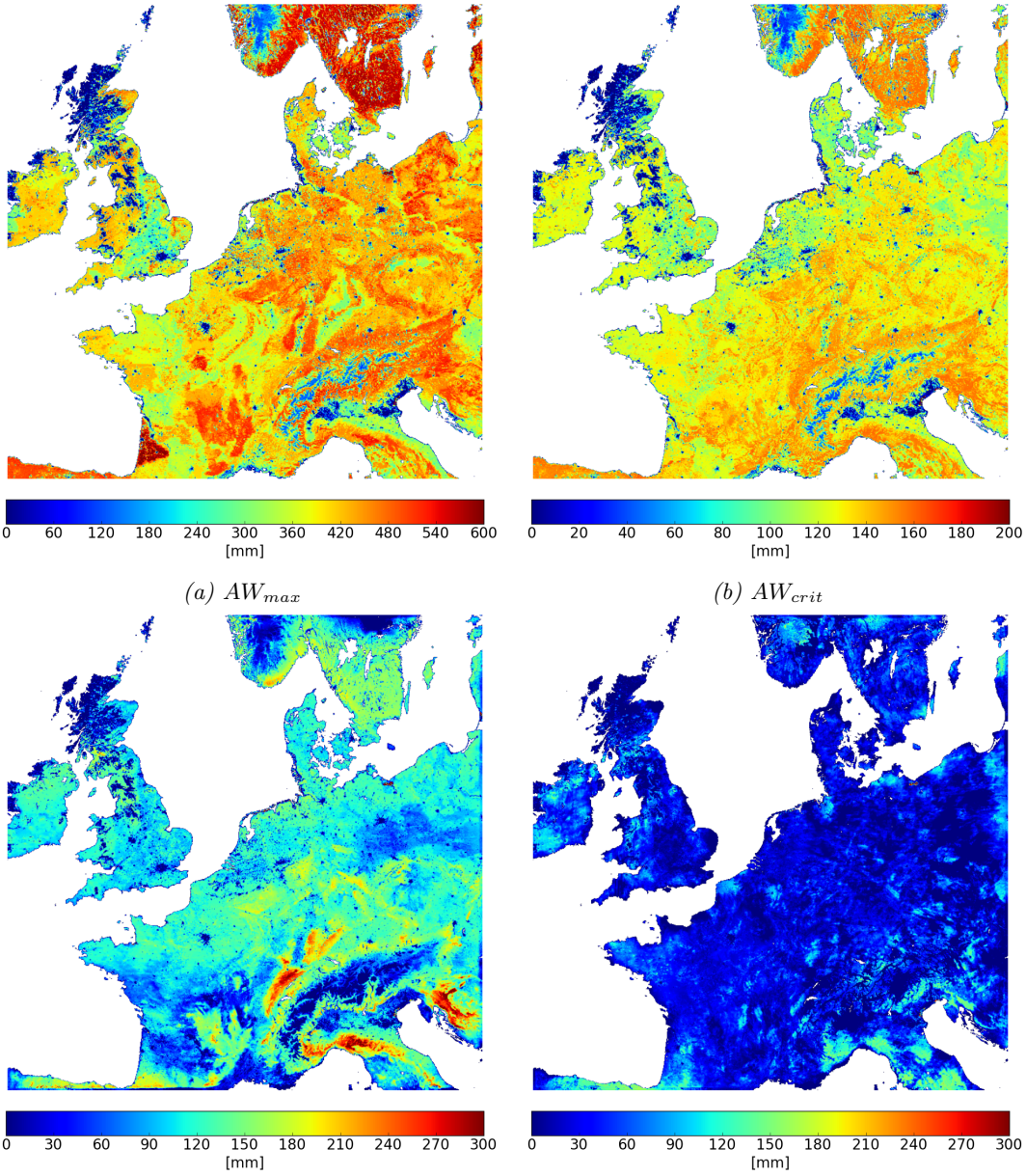


*(a)* $AW_{max}$ *(b)* $AW_{crit}$

*(c) AW 5 March 2015* *(d) AW 2 July 2015*

*Figure 11:* $AW_{max}$, $AW_{crit}$ *and available water levels on 5 March and 2 July 2015 12:00 UTC (forecast at 0:00 UTC) in the HARMONIE38 domain. Note the scale differences between the figures.*

### 3.4.2 Temporal profiles

No specific vegetation type can be held accountable for the high Bowen ratio occurrences (see subsections 3.1 and 3.2). This might imply that these high Bowen ratios are location related, which

was the case at the boundaries of the domain and at coastal areas but seemed rather uncorrelated in central Europe, instead of vegetation related. Local differences would then be caused by local characteristics like clay or sand fractions instead of differences in vegetation cover. In order to assess these local differences, we have to select specific locations satisfying the following: the same dominant vegetation type can be found at two distinct locations. The first location is defined as a location where the Bowen ratio is greater than 1 for less than 20% of the days in the time interval (this grid point is called B20). The other location is chosen such that Bowen ratio values are greater than 1 for more than 60% of the days (B60 hereafter). This way, the same vegetation characteristics are shared between both locations, but the locations themselves differ in high Bowen ratio occurrences. If different reasons exist for this available water reduction between both locations, it is clear that not a common denominator (like a certain vegetation characteristic) is influencing this decrease, but also local differences drive this drop.

For HARMONIE36, 7 vegetation types satisfy these criteria. These vegetation types, together with their relative occurrence (as a percentage of the total number of land grid points) are listed in table 3. Because our manually added vegetation type 'Mix' is a composition of multiple vegetation types and this composition differs per grid point, this vegetation type is not selected on purpose. However, in order to put the frequencies of the other vegetation types into perspective, it will be included in table 3.
For HARMONIE38, a sub-domain of the 789x789 grid is selected so that the number of vegetation types to be analysed is reduced. Therefore a new domain is defined, covering the Netherlands and parts of Belgium and Germany. In this domain, there are 19 vegetation types that satisfy the criteria set previously. These vegetation types are listed in table 4. Both tables show that these 7 and 19 vegetation types in HARMONIE36 and HARMONIE38 respectively cover a relatively large part of the domain. If it turns out that high Bowen ratios are caused by vegetation type characteristics, adjusting this vegetation type could mean a significant (positive) impact on the model performance in the domain.

*Table 3: Relative frequency of occurrence and number of grid points covered by the 7 dominant vegetation types in question in HARMONIE36 plus vegetation type 'Mix'. There are a total of 31 dominant vegetation types, and 53176 land points.*

| Vegetation type | Rel. freq. of occ. (%) | Number of grid points | Vegetation type | Rel. freq. of occ.(%) | Number of grid points |
|---|---|---|---|---|---|
| Crops (Temperate) | 26.5 | 14116 | Broad-leaved forest (Temperate) | 1.3 | 684 |
| Crops (Warm temperate) | 3.2 | 1702 | Coniferous forest (Temperate) | 1.5 | 778 |
| Pastures (Temperate) | 6.9 | 3646 | Mixed forest (Mountain) | 0.7 | 379 |
| Complex cultivation pattern (Temperate) | 1.6 | 843 | 'Mix' (not included in further analysis) | 56 | 29967 |

Plotting the time series at the selected locations will clarify whether this decrease in available water is due to vegetation type characteristics (same temporal profile) or location differences, or possibly a combination of the two. The available water temporal profile of the 7 vegetation types in HARMONIE36 is given in figure 12. One clear aspect pops up in every single plot of figure 12; available water levels drop significantly at the beginning of March. This sharp decrease affects the amount of available water throughout the remaining of spring and summer, because the model appears to not recover from this decrease. On average, the soil loses about 100 mm of moisture in a matter of days, or

*Table 4: Relative frequency of occurrence of and number of grid points covered by the 19 dominant vegetation types in question in HARMONIE38. There are a total of 54 dominant vegetation types, and 56958 land points.*

| Vegetation type | Rel. freq. of occ. (%) | Number of grid points | Vegetation type | Rel. freq. of occ.(%) | Number of grid points |
|---|---|---|---|---|---|
| Temperate BF1 | 2 | 1143 | Bene black sea crops1 | 3.4 | 1912 |
| Temperate complex1 | 0.1 | 54 | North Atlantic crops1 | 0.2 | 112 |
| Temp herbaceous CF1 | 3.1 | 1767 | Pole crops1 | 0.1 | 54 |
| Atlantic coast BF1 | 0.1 | 82 | Cent EU sparse crops1 | 0.9 | 499 |
| Temperate complex2 | 0.7 | 421 | German crops1 | 1.6 | 888 |
| Atlantic complex3 | 1.7 | 976 | Beauce crops1 | 2.8 | 1607 |
| Atlantic complex4 | 0.5 | 312 | Neu Atl sparse crops1 | 1.3 | 719 |
| Fr med sparse crops1 | 0.3 | 175 | Channel crops1 | 2.1 | 1221 |
| Fr med sparse crops2 | 0.3 | 143 | Channel crops2 | 2.3 | 1307 |
| Atl med sparse crops1 | 0.2 | 92 | 'Mix' (not included in further analysis) | 71 | 40334 |

around 10 mm a day, whilst the actual average amount of evapotranspiration during this time of year is around 1-2 mm a day. Only favourable conditions (dry air, high temperatures) will cause maximum evapotranspiration rates of 8 mm a day. This drop is observed for both B20 and B60 at the same time of year, indicating the influence of a common denominator like vegetation characteristics. Note that this gradient differs for both locations: B20 seems to show a smaller gradient than B60, although this gradient is still larger than 1-2 mm a day. This difference is likely caused by local effects. This will be discussed later.

For HARMONIE38, the available water temporal profiles for 5 of the 19 vegetation types are plotted in figure 13. The profiles for the other vegetation types show a similar pattern and can be found in Appendix A.2. In HARMONIE38 (figure 13), the same time series characteristics are visible as in HARMONIE36 (figure 12). There is a distinct decrease in March for almost all locations, but B20, indicated in red, appears to have more soil moisture available throughout summer than B60. This could explain why high Bowen ratios occur more often at B60 than at B20. The sharp peaks observed throughout the time series of both HARMONIE36 and HARMONIE38 are caused by data assimilation. The effect of data assimilation will be analysed more in detail in section 3.6.

Possible causes of differences between the B20 and B60 available water levels are local effects like ground composition (sand, clay, loam), vegetation coverage and the influence of atmospheric processes. If ground compositions differ significantly, e.g. there is a higher percentage of clay present at B20 than at B60, the latter will be able to store less soil moisture. In order to test this, we will check clay fractions and $w_{wilt}$ values at both locations, see table 5.

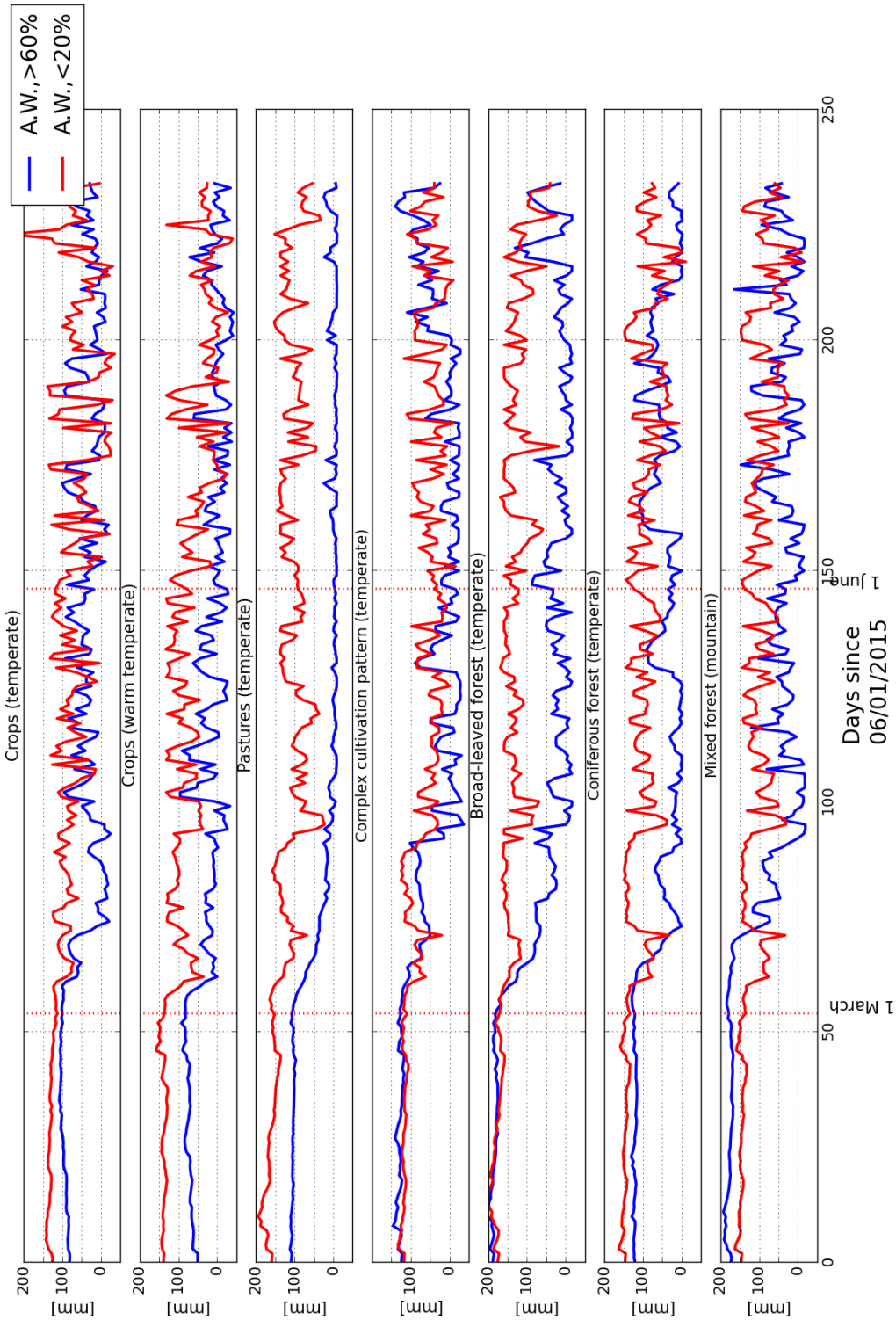


*Figure 12: Available water (in mm, as defined in equation 8) for the 7 vegetation types in HARMONIE36. The red line corresponds with the time profile of the location where less than 20% of the days, the Bowen ratio is high (B20). The blue line represents the time profile of the location where more than 60% of the days, the Bowen ratio is high (B60). The time interval is 6 January (set as day 0) - 30 August 2015.*

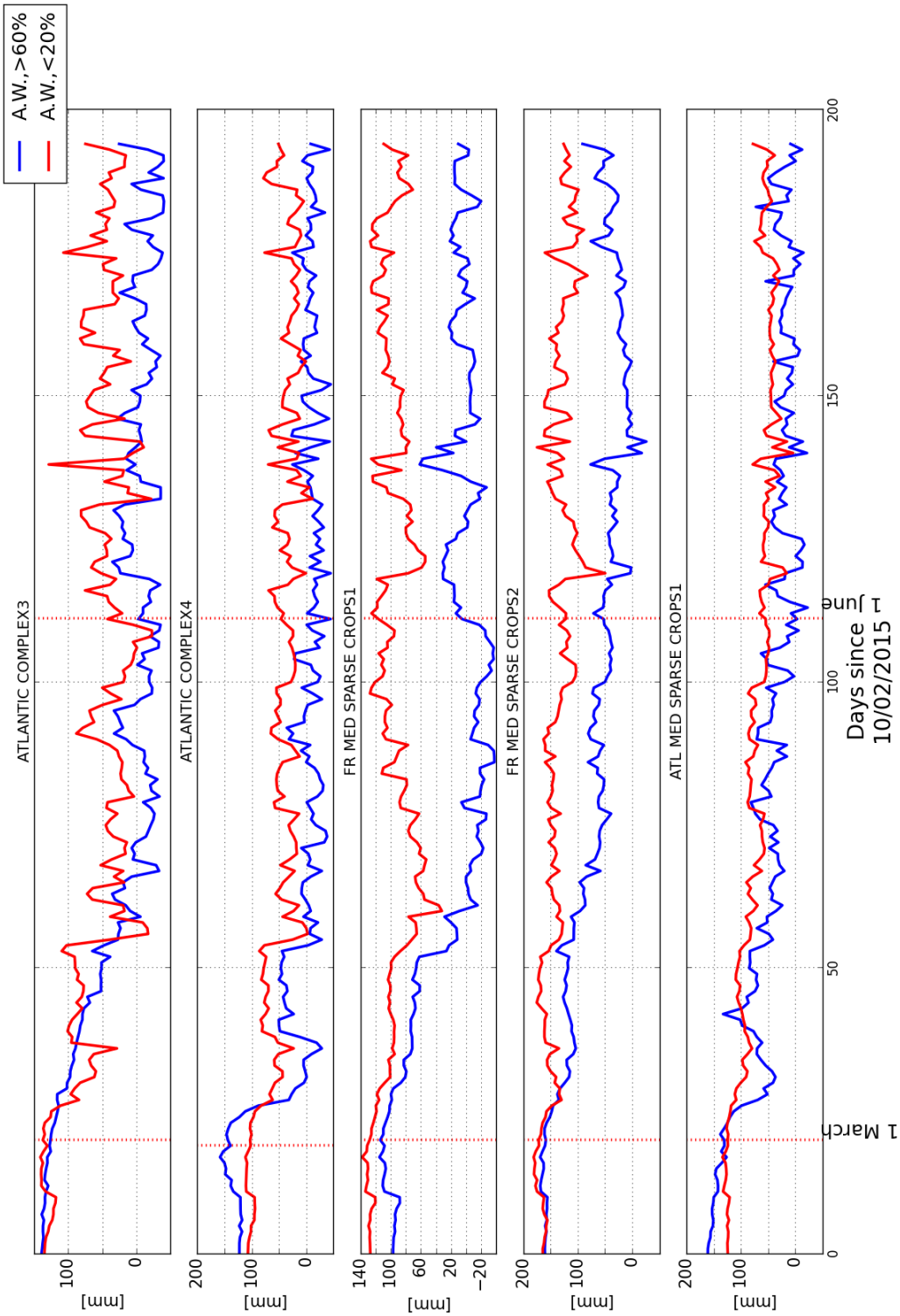


*Figure 13: Available water (in mm, as defined in equation 8) for 5 of the 19 vegetation types in HARMONIE38. The red line corresponds with the time profile of the location where less than 20% of the days, the Bowen ratio is high (B20). The blue line represents the time profile of the location where more than 60% of the days, the Bowen ratio is high (B60). The time interval is 10 February - 31 August 2015.*

*Table 5: Clay fractions and $w_{wilt}$ values at B20 and B60 for the 7 vegetation types in HARMONIE36.*

| Vegetation type | Fraction clay | | $w_{wilt}$ | |
|---|---|---|---|---|
| | B20 | B60 | B20 | B60 |
| Crops (Temperate) | 0.198 | 0.187 | 0.165 | 0.160 |
| Crops (Warm temperate) | 0.190 | 0.190 | 0.162 | 0.162 |
| Pastures (Temperate) | 0.324 | 0.141 | 0.211 | 0.140 |
| Complex cultivation pattern (Temperate) | 0.056 | 0.118 | 0.088 | 0.128 |
| Broad-leaved forest (Temperate) | 0.290 | 0.190 | 0.200 | 0.162 |
| Coniferous forest (Temperate) | 0.061 | 0.062 | 0.092 | 0.093 |
| Mixed forest (Mountain) | 0.062 | 0.177 | 0.091 | 0.156 |

For HARMONIE36, table 5 shows that only vegetation types 'Pastures (Temperate)', 'Complex cultivation pattern (Temperate)', 'Broad-leaved forest (Temperate)' and 'Mixed forest (Mountain)' show some difference in clay fractions and $w_{wilt}$ values. However, in general there appears no clear relationship between B20 and low $w_{wilt}$ values.
For HARMONIE38, the results are displayed in table 6. Apart from vegetation types 'Atlantic complex4' and 'North Atlantic crops1', there are no significant differences in clay fractions and wilting point values at the other locations. In general, local differences in clay fraction are unlikely the cause of differences in available water levels between B20 and B60 in summer.

*Table 6: Clay fractions and $w_{wilt}$ values at B20 and B60 for the 19 vegetation types in HARMONIE38.*

| Vegetation type | Fraction clay | | $w_{wilt}$ | |
|---|---|---|---|---|
| | B20 | B60 | B20 | B60 |
| Temperate BF1 | 0.180 | 0.174 | 0.157 | 0.155 |
| Temperate complex1 | 0.174 | 0.174 | 0.155 | 0.155 |
| Temp herbaceous CF1 | 0.327 | 0.288 | 0.212 | 0.200 |
| Atlantic coast BF1 | 0.235 | 0.272 | 0.180 | 0.193 |
| Temperate complex2 | 0.062 | 0.174 | 0.092 | 0.155 |
| Atlantic complex3 | 0.327 | 0.414 | 0.212 | 0.242 |
| Atlantic complex4 | 0.062 | 0.283 | 0.09 | 0.197 |
| Fr med sparse crops1 | 0.175 | 0.11 | 0.155 | 0.123 |
| Fr med sparse crops2 | 0.19 | 0.174 | 0.162 | 0.155 |
| Atl med sparse crops1 | 0.046 | 0.179 | 0.080 | 0.157 |
| Bene black sea crops1 | 0.062 | 0.11 | 0.092 | 0.123 |
| North Atlantic crops1 | 0.379 | 0.142 | 0.229 | 0.140 |
| Pole crops1 | 0.19 | 0.19 | 0.162 | 0.162 |
| Cent EU sparse crops1 | 0.19 | 0.288 | 0.162 | 0.199 |
| German crops1 | 0.19 | 0.174 | 0.162 | 0.155 |
| Beauce crops1 | 0.19 | 0.174 | 0.162 | 0.155 |
| Neu Atl sparse crops1 | 0.126 | 0.174 | 0.132 | 0.155 |
| Channel crops1 | 0.312 | 0.142 | 0.132 | 0.155 |
| Channel crops2 | 0.142 | 0.142 | 0.140 | 0.140 |

Due to the definition of dominant vegetation types, 30% of the grid point might be covered by other vegetation types. If the composition of the other vegetation types differ at the two locations, it is possible that its characteristics cause a difference in available water levels. However, since the

fraction of the grid point covered by another vegetation type is at most 30%, it is likely that this will have a limited effect.
Apart from clay fractions, atmospheric processes also cause local differences. If the local atmosphere at B20 is more moist (higher relative humidity) than at B60, LHF values at B20 will be lower than at 60 and more evapotranspiration will take place at B60 due to a larger soil-atmosphere moisture gradient. These differences in relative humidity can be caused by e.g. moist air advection caused by high evapotranspiration rates at a nearby location or the presence of open water. This is thus a plausible explanation for differences between B20 and B60.

## 3.5 The influence of vegetation characteristics: LAI

Because the drop in available water observed in figures 12 and 13 occurred for all vegetation types at both locations, the effect of spatial differences can be ruled out as a possible cause for this. This leaves us at having a closer look at vegetation characteristics. There are various characteristics that define a certain vegetation type. Apart from patch distribution, which by itself does not influence available water levels and evapotranspiration, one can think of root zone depth and leaf area index (LAI) as vegetation dependent characteristics that influence evapotranspiration levels. Root zone depth, however, is constant in time and therefore cannot influence this temporal fluctuation in available water. On the other hand, the LAI is variable in time and plays an important role in evapotranspiration: a higher LAI implies a larger leaf surface from which evapotranspiration can take place. The way in which LAI is determined in ECOCLIMAP-I and ECOCLIMAP-II has been explained in paragraphs 2.2.1 and 2.2.2.

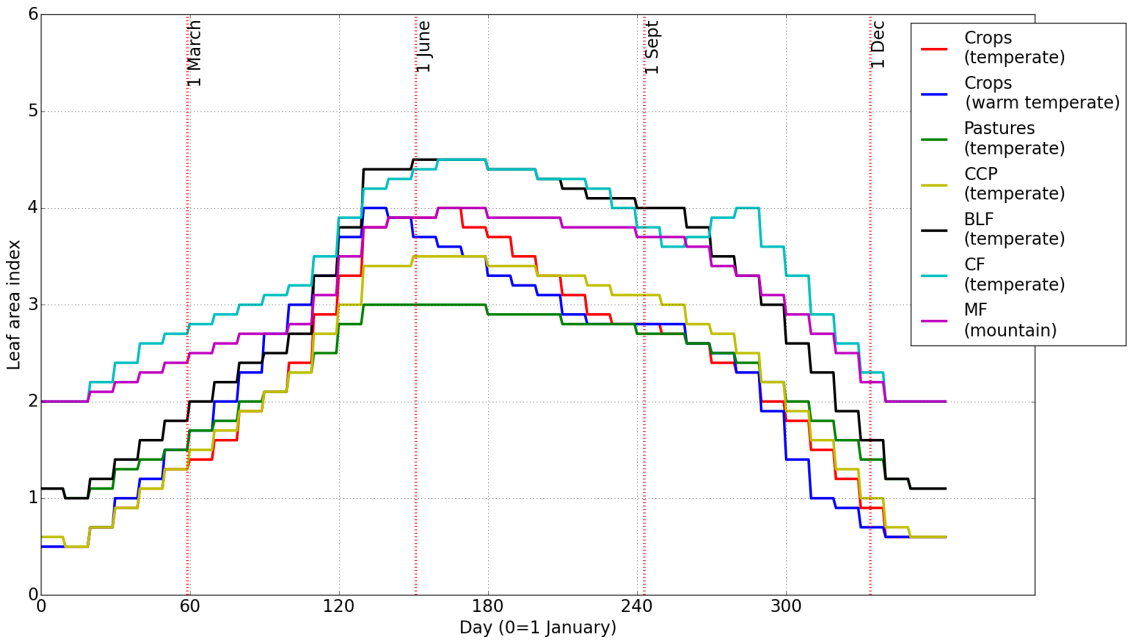


*Figure 14: LAI temporal profile for the 7 vegetation types in HARMONIE36.*

Figures 14 and 15 show the LAI curves for the 7 and 19 vegetation types, respectively. Both LAI profiles show a clear start and end of the growing season, with a peak around June/July. Because of the way $LAI_{max}$ is determined (i.e. via satellite and in-situ measurements, see paragraphs 2.2.1 and 2.2.2), the maximum LAI values are plausible. Therefore, we rather focus on LAI values at the start of the growing season, that appears to be off here; in the Netherlands, temperate vegetation

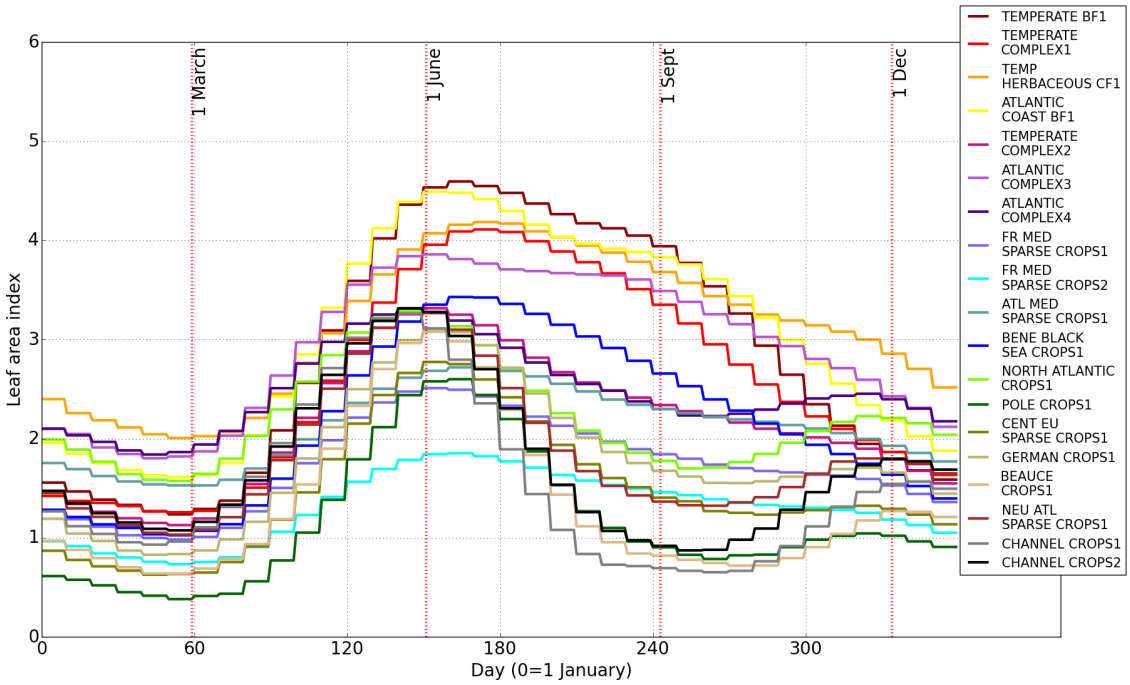


*Figure 15: LAI temporal profile for the 19 vegetation types in HARMONIE38.*

usually starts sprouting leaves in April, but the LAI profiles in figure 14 imply that the growing season commences at the end of January. Apart from being unrealistic, this early start of the growing season also initiates another problem: a too high LAI in spring causes high evapotranspiration rates due to a large leaf surface. Recall that this pattern is also observed in figures 12 and 13. The significant drop of around 100 mm in the first weeks of March is most likely caused by this high LAI. It is more realistic when temperate vegetation in the Netherlands has a LAI between 0-1 before the start of the growing season, and then would slowly increase until te maximum is reached in June/July.
In addition, vegetation type 'Coniferous forest (Temperate)' seems to have an unrealistic LAI curve. To start with, coniferous trees do not shed their needles and do not have such a distinct growing season. Furthermore, the LAI is not expected to increase again in October. It is possible that the latter is caused by a perturbation, since there exists no clear physical explanation for this increase.

HARMONIE38 comes with an updated version of ECOCLIMAP, where vegetation types themselves have also been redefined. For all vegetation types in figure 15, it still holds that the LAI needs to be reduced in early spring. Under the current conditions, evapotranspiration rates are too high in March due to this large LAI. This is also seen in figure 13. We will conduct some experiments to test this statement.

Lastly, some general remarks on the LAI database in ECOCLIMAP. First of all, since only climatological values are available (for 2015) in both ECOCLIMAP versions, there exists no annual variation and the LAI curve is the same every year. This implies that the start and duration of the growing season as well as the LAI increments are the same every year: annual variations like an early or late start of the growing season are filtered out. Secondly, this LAI curve is applied to the same vegetation types found in different regions in Europe. This means that the same vegetation in southern France and northern Sweden will sprout its leaves at the same day in both versions of HARMONIE, despite the large temperature difference between both locations. We will analyse these shortcomings in more detail in section 5.

## 3.6 Measuring model improvements via data assimilation

In this research, we aim to improve surface turbulent fluxes in the whole HARMONIE domain. However, there are only a few measurement stations registering these fluxes. Therefore, comparing these observations with the model output would imply that improvements in HARMONIE's output can be registered on a few grid points instead of in the whole domain. Moreover, if the model is already performing sufficiently on these grid points, this evaluation could lead to distorted conclusions. This is why model output will not be compared to flux measurements, but we will measure model improvement via the effect of data assimilation.

There are two possible causes for large data assimilation effects. If atmospheric temperatures are too low and dew point temperatures too high, data assimilation will extract $w_2$ in order to generate a smaller LHF, higher surface temperatures and thus a larger SHF. If atmospheric temperatures are too high and dew point temperatures too low, soil moisture will be added to the root zone in order to increase the LHF, decrease surface temperatures and therewith decrease the SHF. This will decrease 2 meter temperatures and increase dew point temperatures. However, if too much soil moisture is added or removed, atmospheric temperatures and dew point temperatures will again deviate too much and soil moisture will be adjusted the next cycle, hereby causing the spiky profiles observed in figures 12 and 13. Data assimilation thus affects $w_2$ levels and is therefore of significant importance in this research. Hence, data assimilation serves as a measure of how well the model is performing; if the magnitude of the data assimilation is high, model output deviates (too) much from observations. Consequently, if adjustments in the model cause this magnitude to decrease compared to the reference model, this is an indication that the model has improved and the output corresponds better to the observations. Apart from its direct effect on the LHF, $w_2$ can also be adjusted to regulate heat conduction in the soil. If $w_2$ is decreased, heat conduction decreases and surface temperatures will increase.

In order to analyse the effects of data assimilation, two time intervals are selected in both models: 1-19 March and 25 June - 5 July 2015 for HARMONIE36, and 5-14 March and 27 June - 5 July 2015 for HARMONIE38. These intervals cover the significant drop in March and the heat wave in July, plus there was little precipitation in both HARMONIE domains during these intervals. For these time periods, HARMONIE's 3-hourly output is considered. At every new cycle, data assimilation is performed. This implies that over the course of one day, data assimilation is executed 8 times a day. Data assimilation increments are calculated by taking the difference between available water levels at the +3h forecast run of the previous cycle $t-1$ (indicated by $AW^{+3h}(t-1)$) and the 0h run of the current cycle $t$ (indicated by $AW^{+0h}(t)$). The average height of these increments will be determined by calculating the absolute difference between these two cycles at a certain grid point, averaged over the number of days under consideration. This average absolute difference (AAD, in mm) is thus defined as:

$$AAD(t) = \frac{\sum_n \left| AW^{+0h}(t) - AW^{+3h}(t-1) \right|}{n} \tag{13}$$

With $n$ the number of days. The average absolute difference at 12:00 UTC is therefore the absolute difference of the available water of the 3h forecast run from the 9:00 UTC cycle and the 0h run of the 12:00 UTC cycle, averaged over all days. This way, it is clear during what time of day data assimilation effects are largest.

For HARMONIE36, vegetation type 'Crops (Temperate)' will be discussed here. The other vegetation types can be found in Appendix A.3.1. Note here that for HARMONIE36, the +3h forecast runs are not available. This is why the average absolute difference is here calculated as the difference between the 0h runs of the two cycles $t$ and $t-1$. This implies that the average absolute difference

now also consists of evapotranspiration and precipitation effects. However, it is not clear how big these contributions are, since these model values can only be calculated by using this +3h forecast. This is why we will consider estimated evapotranspiration rates for both time intervals.

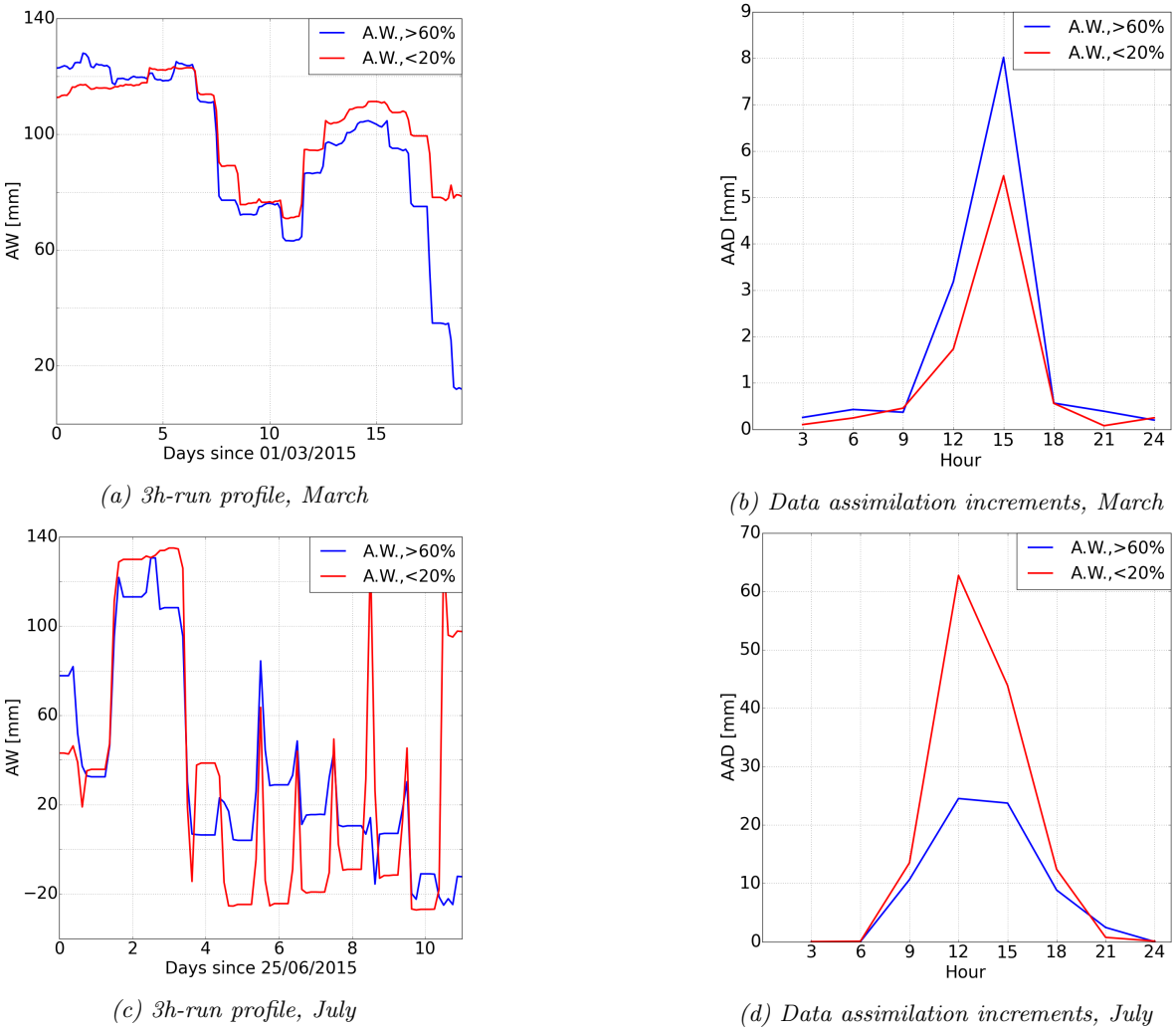


*(a) 3h-run profile, March*

*(b) Data assimilation increments, March*

*(c) 3h-run profile, July*

*(d) Data assimilation increments, July*

*Figure 16: 3h-run profiles of available water and data assimilation increments (average absolute difference) for vegetation type 'Crops (Temperate)' (HARMONIE36). Time intervals are 1 March - 19 March and 25 June - 5 July 2015. The red line represents B20, the blue line B60.*

In figure 16a, soil moisture levels decrease almost 100 mm in 19 days' time at B60. This decrease is caused by data assimilation, since evapotranspiration itself could never cause this amount to be extracted from the root zone in such a short time period. B20 is also subject to large adjustments via data assimilation. Large drops and increases are visible in figure 16a, but the vegetation at B20 is left with more than 4 times as much available water than the one at B60. As has been discussed previously, such drastic losses indicate that temperatures are too low in the model; a problem that is likely caused by the large LAI in this time of year.

Figure 16b clearly illustrates the large adjustments made by the data assimilation. Over the course of 19 days, an average of 13.4 mm of soil moisture a day is added or removed at B60. Because little precipitation fell in this time period at this location, this 13 mm a day is mostly a combination of data assimilation effects and evapotranspiration rates. Estimated evapotranspiration rates lie around

1-2 mm a day in this time of year, so this implies that on average 11-12 mm per day is being added or removed by the data assimilation. From figure 16a, it should be clear that this soil moisture is mostly being removed. These large adjustments emphasise that atmospheric temperatures are too low and dew point temperatures too high, due to too high evapotranspiration rates caused by to high LAI values.
In July, data assimilation impacts are even larger than in March. On multiple occasions, B60 varies from more than 100 mm to below wilting point ($AW < 0$) in a few hours' time. This overshooting is the sole effect of data assimilation. A sharp increase in soil moisture is being corrected for the cycle after, indicating that this adjustment was too drastic: atmospheric temperatures dropped too fast and dew point temperatures increased too much. This effect is also visible in figure 16d, which shows that an average of 133 mm a day is being added or removed. Again little precipitation fell in this time period, and since 8 mm a day will evapotranspire under extreme conditions, more than 125 mm a day is actually being adjusted by the data assimilation. Note that B60 is performing better than B20 in this case: this is likely caused by local effects.

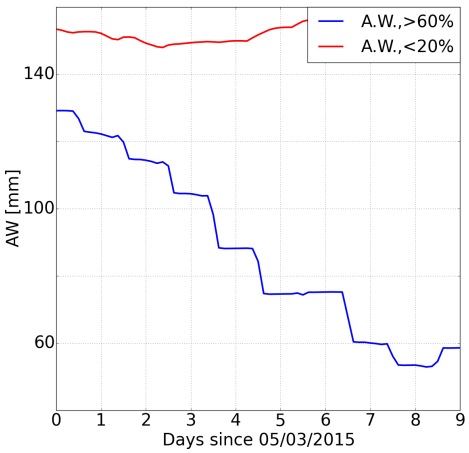


*(a) 3h run profile, March*

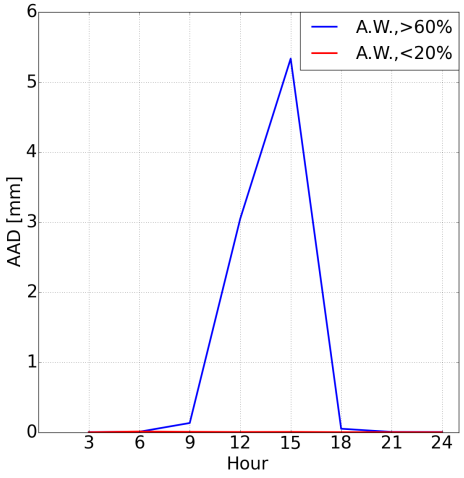


*(b) Data assimilation increments, March*

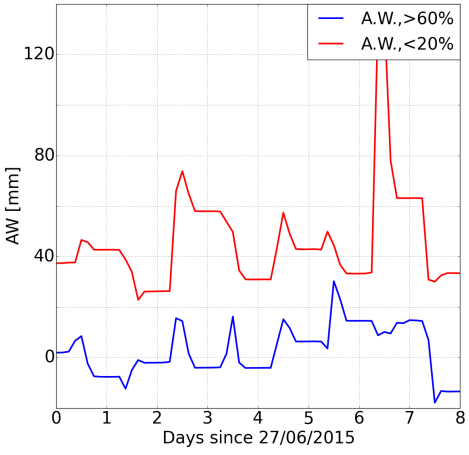


*(c) 3h run profile, July*

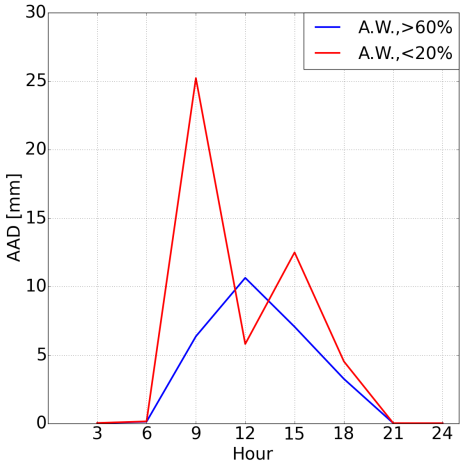


*(d) Data assimilation increments, July*

*Figure 17: 3h-run profile of available water and data assimilation increments (accumulated absolute difference) for vegetation type 'Temperate complex1' (HARMONIE38). Time intervals are 5 March - 14 March and 27 June - 5 July 2015. The red line corresponds with B20, the blue line with B60.*

For HARMONIE38, the same procedure is followed, with the exception that the +3h forecast runs are now available and being used. Here, vegetation type 'Temperate complex1' will be discussed. The outcomes for the other vegetation types can be found in Appendix A.3.2. Figure 17a shows that still a lot of soil moisture is removed from the system at the bad location. The model loses around 70 mm of available water in 9 days' time, largely caused by the data assimilation effects. This is also visible in figure 17b: around 9 mm a day is added or removed due to data assimilation effects. From figure 17a, it is clear that the majority of these effects cause a decrease in available water level. Note that B20 is actually performing well: data assimilation effects are almost 0. At this location, the increase in available water observed in figure 17a is caused by precipitation and melting processes. Local effects thus drive this difference between B20 and B60: evapotranspiration rates are lower at B20 than at B60 due to different meteorological conditions.
In July, again large adjustments are visible at both B20 and B60. On average 48 mm a day is being adjusted at B20, and 28 mm at B60. Although there is more water available at B20, data assimilation still needs to adjust model output. A relaxation of these data assimilation effects, in combination with higher available water levels and perhaps evapotranspiration reductions, is necessary in order to reduce these large average adjustments in both HARMONIE36 and HARMONIE38. This implies that evapotranspiration rates are too high and/or local effects are playing a role here. Note that vegetation is wilting ($AW < 0$) at B60 for long periods of time.

## 3.7 Conclusions

In this section, we have seen that Bowen ratios greater than 1 occurs more often in the HARMONIE domains throughout spring and summer. This is not due to a consistent available water scarcity: there is enough soil moisture available at the beginning of spring in both HARMONIE versions. Other possible causes of these high Bowen ratio values are local effects and vegetation influences. These factors have been examined by selecting dominant vegetation types found at both a location where less than 20% of all days, the Bowen ratio is greater than 1 and a location where this is the case for more than 60% of all days. Plotting the available water time series at these locations for each of these vegetation types yielded that the same phenomenon was occurring at all locations. A significant drop in March causes low available water levels throughout the rest of spring and summer, resulting in little soil moisture available for evapotranspiration in summer.
Because this drop occurred at all locations at the same time of year, it is likely that this decrease is initiated by certain vegetation characteristics. A plausible characteristic causing this drop is the leaf area index. Plotting the LAI turned out that LAI values are too high in the Netherlands in early spring. In order to test this hypothesis, experiments will be conducted where the LAI will be adjusted in order to better fit realistic values.
Local differences might also influence available water levels. There is no clear relationship between lower clay fractions and higher Bowen ratio counts. In addition, other vegetation types only play a minor role, since $> 70\%$ is covered by the same vegetation type at both locations. However, it is likely that meteorological effects drive this difference between B20 and B60.

Because little LHF observations are available, a different method of observing model improvements has to be found. We therefore propose to consider data assimilation increments. It turns out that this data assimilation initiates large variations in available water, indicating large mismatches between model output and observations. If these sharp transitions are reduced, this will indicate that the model's output is corresponding better to reality.

# 4 Experiments in HARMONIE38

In this section, experiments will be performed in order to test the hypothesis that LAI values are too high in the beginning of March, causing too strong soil moisture losses. Because experiments cannot be conducted in HARMONIE36 anymore, HARMONIE38 will be used here. Two experiments concerning the LAI will be set up in this section: dividing the LAI by 2 and by 4. Because it is likely that these LAI adjustments are unrealistic for July, we will also conduct experiments regarding another vegetation characteristic influencing evapotranspiration rates, namely stomatal resistance, $R_{stom}$. The experiments conducted here will consist of multiplying $R_{stom}$ by 2 and 10, respectively.
Two time intervals will be considered. The first one ranges from 5-14 March 2015, hereby covering the sharp drop in March observed in the available water plots. The second one is chosen from 27 June - 5 July 2015, covering the heat wave that struck large parts of the HARMONIE domain. The initial soil and atmospheric conditions used for both reference runs and experiments runs are retrieved from the ECMWF database. The output is generated every 3-hourly cycle, during which data assimilation is performed.

## 4.1 Reference run

In section 3, 19 vegetation types and corresponding locations for HARMONIE38 were selected. Because it is possible that local effects affect the data assimilation increments and available water levels, these locations will be evaluated in the reference run. Every vegetation type will be listed by its cover number. In table 7, these numbers and corresponding vegetation name are listed.

*Table 7: Cover numbers for each of the 19 vegetation types in HARMONIE38*

| Cover number | Vegetation type | Cover number | vegetation type |
|---|---|---|---|
| 322 | Temperate BF1 | 455 | Bene Black Sea Crops1 |
| 323 | Temperate Complex1 | 460 | North Atlantic Crops1 |
| 325 | Temperate Herbaceous CF1 | 481 | Pole Crops1 |
| 326 | Atlantic Coast BF1 | 484 | Cent EU Sparse Crops1 |
| 361 | Temperate Complex2 | 485 | German Crops1 |
| 362 | Atlantic Complex3 | 486 | Beauce Crops1 |
| 363 | Atlantic Complex4 | 489 | Neu Atl Sparse Crops1 |
| 452 | Fr Med Sparse Crops1 | 492 | Channel Crops1 |
| 453 | Fr Med Sparse Crops2 | 493 | Channel Crops2 |
| 454 | Atl Med Sparse Crops1 | | |

In March, we have seen that the amount of available water dropped significantly within 9 days' time. This caused little soil moisture being left in summer, causing low LHF values and thus high Bowen ratios. It is therefore desired to reduce the magnitude of this drop in March. This can be visualised by plotting the difference between the amount of available water at 5 March 00:00 UTC and 14 March 00:00 UTC. The larger marker represents B60, the smaller one B20.

All areas marked in solid green are regions where the difference in available water between 5 and 14 March lies between 0 and 20 mm, or around 1-2 mm a day. These amounts are plausible evapotranspiration rates in this time of year. However, there are only few areas inside the domain where this criterion is actually met. There are a lot of regions where this difference is larger; this indicates that major adjustments via data assimilation are taking place. Especially in large regions in France and southern Germany, over 150 mm is extracted from the soil in these 9 days. This is a clear

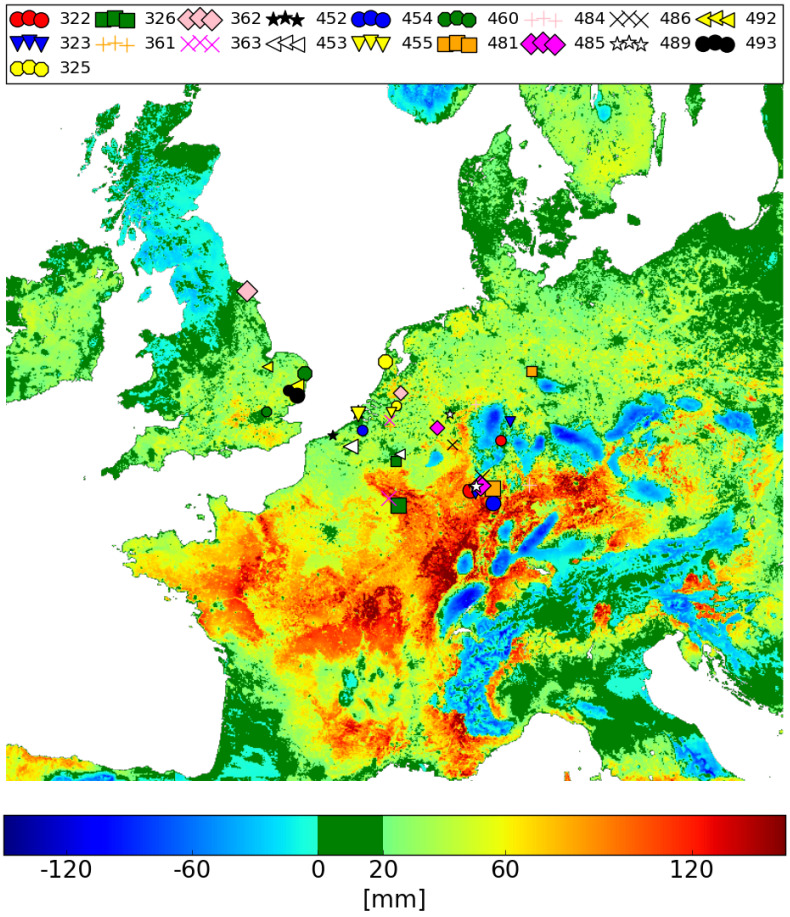


*Figure 18: Difference in available water between 5 March 00:00 UTC and 14 March 2015 00:00 UTC for the reference run. For locations with a difference greater than 0, there is a decrease in soil moisture. For locations where this value is smaller than 0, there is an increase in soil moisture. The solid green band represents a total amount of evapotranspiration between 0-20 mm over these 9 days.*

sign that model outputs differ from surface observations: 2 meter temperatures are too low for these areas, which is likely due to strong evapotranspiration in the model.
Average evapotranspiration rates (AER) per grid point per day, as forecast by the model, can be found in Appendix A.4.1.

Apart from a substantial soil moisture loss, there are also locations where root zone soil moisture levels increase over the time period. First of all, soil moisture may be added to the root zone due to precipitation. Figure 19a illustrates that in Norway, parts of Great Britain and at the Italian Adriatic coast, this accumulated precipitation (snow, graupel and rain) is greater than 80 mm in 9 days' time. These regions also show an increase in soil moisture in figure 18. Secondly, melting processes may also add soil moisture to the system. In order to test this, we need to check for frozen or near-frozen soil. This is done in figure 19b. Note the high resemblance between frozen ($T < 273$ K, indicated in navy) and near-frozen soil (here taken as $T < 278$ K, indicated in blue) and locations with a negative difference in figure 18. In these areas, melting processes cause an increase in liquid soil moisture content, and thus in available water. Lastly, it is also possible that due to data assimilation, moisture is added to the soil. This would be the case if model 2 meter temperatures are too high in combination

with too low dew point temperatures compared to observations. This is likely the case in southern France, since precipitation and frozen soil cannot explain this increase.

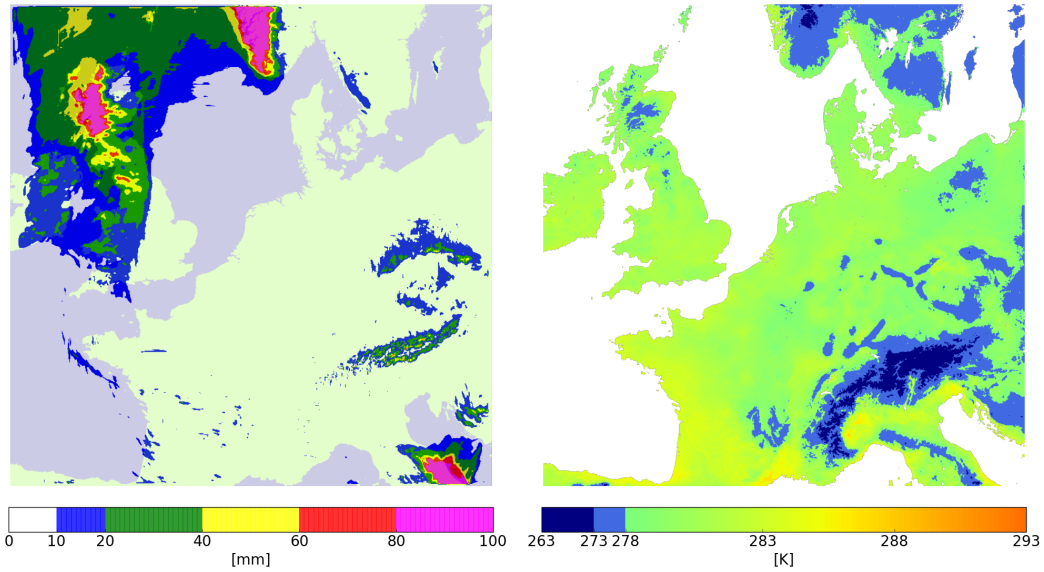


*(a) Accumulated precipitation (mm)* *(b) Average soil temperature (K)*

*Figure 19: Accumulated precipitation (in mm) and average soil temperature (in K) over the time period 5 March 00:00 UTC - 13 March 2015 21:00 UTC.*

Finally, we have to take a closer look at local differences between B20 and B60 in order to explain the differences in March observed in figures 12 and 13. Figure 18 highlights two patterns: first, some of the B60 (large marker) are located close to the shoreline. These locations are likely affected by moist sea air being advected over land. Second, other B60 points, located further inland, are mainly found in the reddish areas in France and Germany. Here, strong local effects from for instance vegetation play a major role. In these regions, large temperate and mixed forests are found. If the LAI of these trees in question is too high, too much evapotranspiration is taking place and hereby directly influence B60.
The majority of B20 are found in places where the difference in available water lies inside or close to the 0-20 mm interval.

A way to evaluate spatial patterns of data assimilation effects is considering the standard deviation. However, the standard deviation contour plots for March show roughly the same spatial distribution as the difference in available water. This is because in March, largest deviations from the mean are observed in locations where soil moisture loss gradients are largest. This is why we will solely analyse the difference in available water; the mean and standard deviation plots for March can be found in Appendix A.4. For July, we will discuss the mean and standard deviation since little information can be retrieved from the difference in available water: available water levels are already low and no significant drop occurred in the beginning of July (see figure 13).

Figure 20 shows us that large adjustments are made via data assimilation in central Europe, Sweden and Norway, whilst soil moisture levels are relatively low in most of these areas. However, average available water levels in Ireland, Sweden and Norway appear to be relatively high. This is possibly due to different vegetation characteristics or more precipitation in combination with less evapotranspiration. This will be discussed in section 7.
Figure 20a also illustrates that almost all B20 and B60 locations are found in areas undergoing severe

water stress. In addition, standard deviations are also relatively high at almost all B20 and B60 points. This explains the low available water levels and spiky profiles observed in figure 13. Because we are now interested in the model's performance throughout the whole domain, we will not discuss these B20 and B60 locations any further.

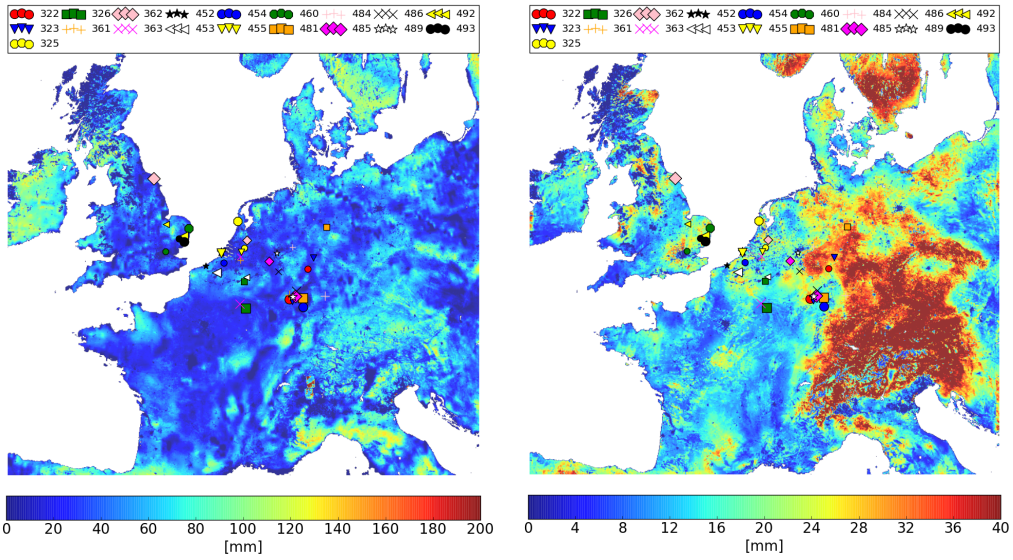


*(a) Mean* *(b) Standard deviation*

*Figure 20: Mean available water and standard deviation for the reference run. The time period is 27 June 00:00 UTC - 4 July 2015 21:00 UTC.*

## 4.2 LAI experiments

Two experiments will be conducted regarding the LAI: dividing the LAI by 2 and 4, respectively. In March, these divisions will simulate a later and/or slower start of the growing season, whereas adjusting the LAI in July will check whether the root zone can retain more soil moisture this way. Because best results are obtained for LAI/4, this experiment will be discussed here. The outcomes of the LAI/2 experiment are shown in Appendix A.5.

Figure 21 shows that large regions are now within the 0-20 mm interval compared to the reference run (figure 18). However, there are still regions where the difference in available water is more than 60 mm. For these regions, a more drastic LAI adjustment is necessary. For instance crop and deciduous forest vegetation types have a LAI close to 0 before the start of the growing season. Because a factor of 0.25 might still leave too high LAI values for these vegetation types, it is possible that a smaller factor is necessary here.
Apart from this, there are also areas where more soil moisture is added to the system compared to the reference run. Here, too low LAI values cause vegetation inactivation, and in order to initiate more evapotranspiration, soil moisture levels are increased. However, if available water levels are already above critical level ($AW_{crit}$), this soil moisture increase will have little effect since the plant is already evapotranspiring freely. So the LAI adjustment might be too drastic in these areas and higher LAI values are more realistic.

In July, average soil moisture levels have increased over large parts of the domain. Figure 22a shows that in central Europe, the amount of available water has increased from close to wilting point

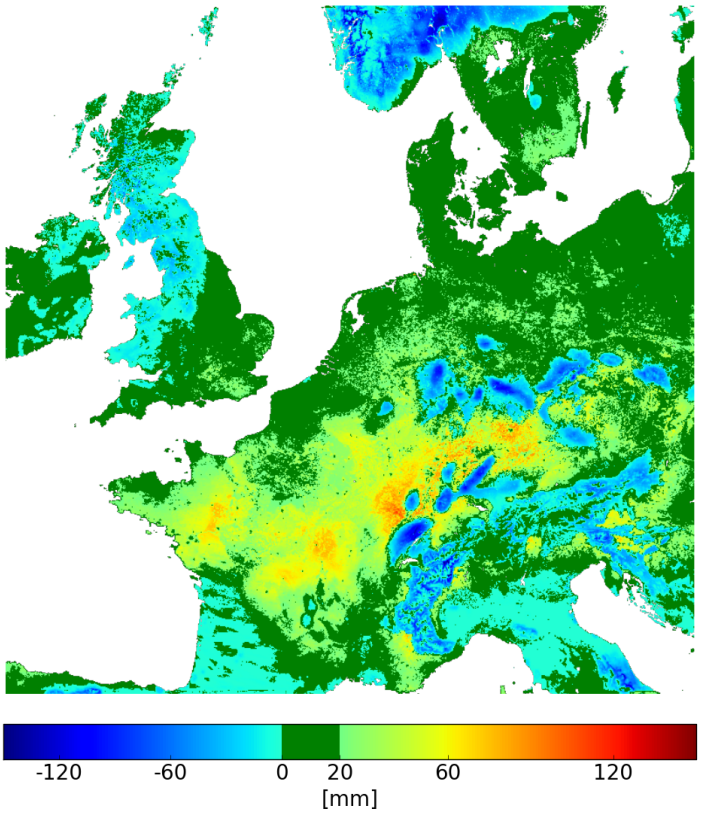


*Figure 21: Difference in available water between 5 March 00:00 UTC and 14 March 2015 00:00 UTC for experiment 2 - LAI/4.*

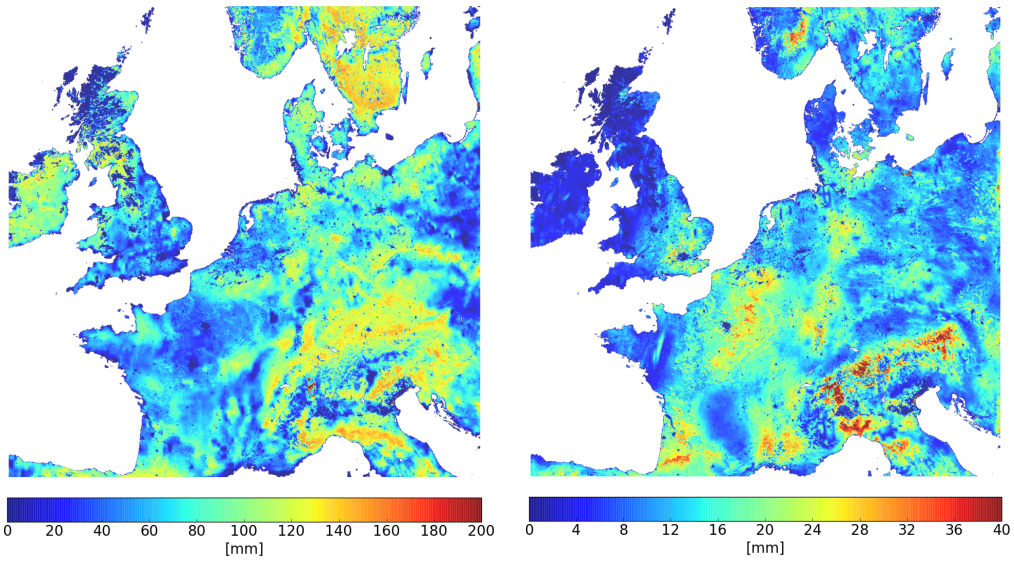


*(a) Mean* *(b) Standard deviation*

*Figure 22: Mean available water and standard deviation for experiment 2 - LAI/4 for July.*

to more sufficient levels. The data assimilation increments, illustrated via the standard deviation, has decreased compared to figure 20b. More soil moisture is thus retained this way.

## 4.3 Stomatal resistance experiments

Because a LAI/4 adjustment in July seems unrealistic, it is likely that other vegetation characteristics influencing evapotranspiration need to be adjusted in this time period, like stomatal resistance. Stomatal resistance regulates the rate at which water vapour is prevented from exiting the plant.

A higher stomatal resistance will imply lower evapotranspiration rates. In SURFEX, stomatal resistance is modelled as (Le Moigne et al., 2012)

$$R_{stom} = \frac{R_{smin}}{F_1 F_2 F_3 F_4 LAI} \tag{14}$$

$$\text{where} \quad F_1 = \frac{f + \frac{R_{smin}}{R_{smax}}}{1 + f} \tag{15}$$

$$F_2 = \frac{w_2 - w_{wilt}}{w_{fc} - w_{wilt}} \quad 0 \leq F_2 \leq 1 \tag{16}$$

$$F_3 = 1 - \gamma(q_{sat}(T_s) - q_a) \tag{17}$$

$$F_4 = 1 - 1.6 \times 10^{-3}(T_a - 298.15)^2 \tag{18}$$

$$f = 0.55 \frac{R_G}{R_{Gl}} \frac{2}{LAI} \tag{19}$$

$R_{smin}$ represents the minimum stomatal resistance (in $ms^{-1}$), and the maximum stomatal resistance $R_{smax}$ is arbitrarily set to 5000 $ms^{-1}$. $q_{sat}(T_s)$ is the saturated specific humidity in $kgkg^{-1}$ depending on the surface temperature $T_s$ in K, and $q_a$ the atmospheric specific humidity at the lowest atmospheric level (in $kgkg^{-1}$). $T_a$ represents the temperature at the lowest atmospheric level (in K). $\gamma$ is a species-dependent parameter from Jacquemin & Noilhan (1990). $R_G$ is the incoming photosynthetically active radiation on the foilage (in $Wm^2$) and $R_{Gl}$ is the maximum solar radiation usable in photosynthesis (in $Wm^2$), and is an assigned value.

Two experiments have been performed for the time interval in July, namely multiplying $R_{stom}$ by 2 and by 10. Figure 23 shows that for $2 \cdot R_{stom}$, standard deviations have decreased in central Europe. However, this adjustment is still performing worse than both LAI/2 and LAI/4 experiments. This is because a LAI adjustment, apart from the direct dependence, also affects other parameters influencing $R_{stom}$, like $w_2$, $q_{sat}$ (via $T_s$), $T_a$ and $f$. A LAI/2 adjustment thus means a more than a factor 2 multiplication of $R_{stom}$, and therefore this LAI/2 experiment shows more improvement than $2 \cdot R_{stom}$.
A factor 10 increase of $R_{stom}$, as is shown in figure 24, shows that data assimilation effects in Germany now have improved, whilst western Europe is now experiencing strong data assimilation effects. $R_{stom}$ is now thus too high, causing too low evapotranspiration rates and thus strong data assimilation interferences.

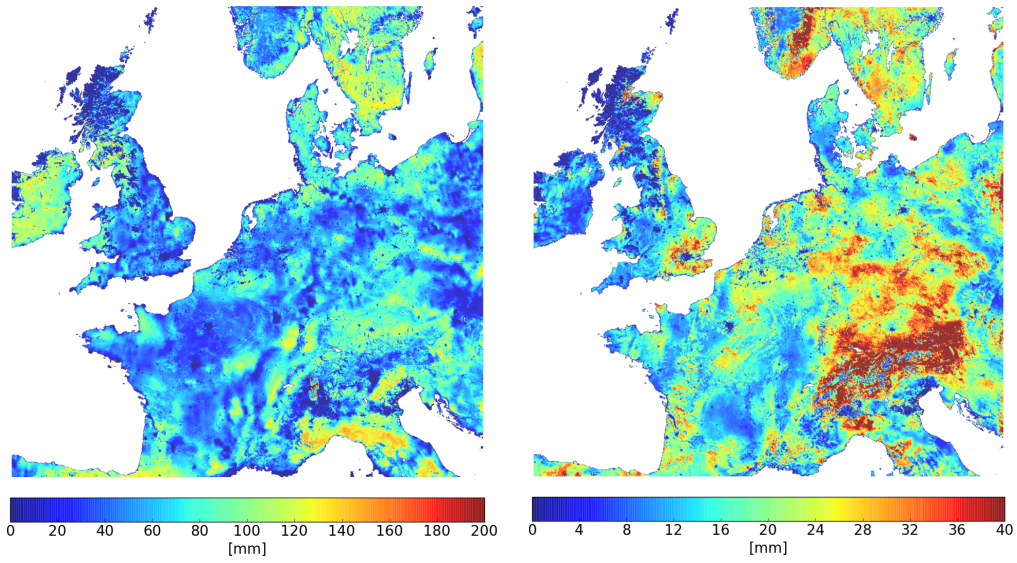


*(a) Mean* *(b) Standard deviation*

*Figure 23: Mean available water and standard deviation for* $2 \cdot R_{stom}$.

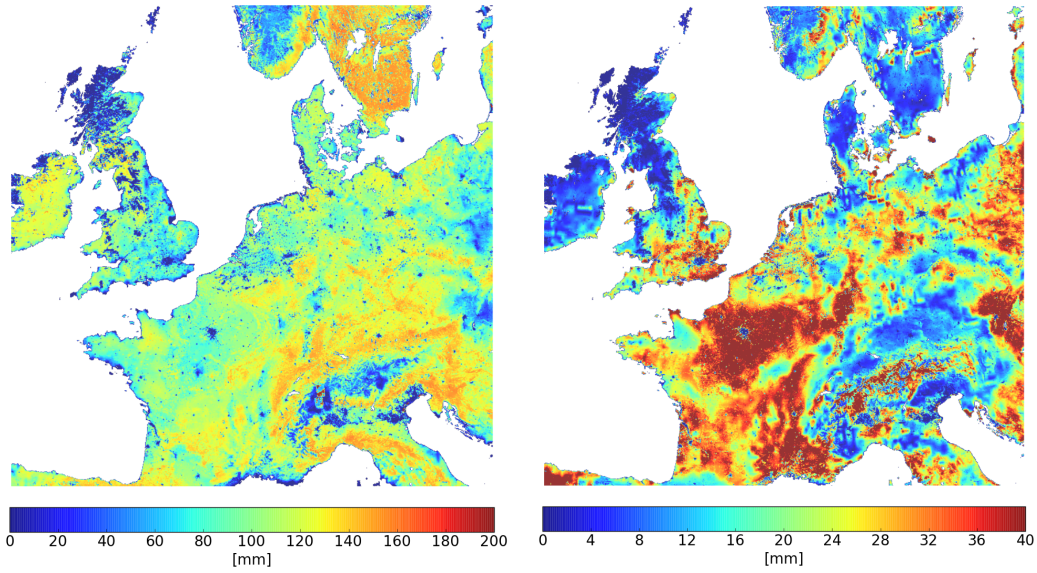


*(a) Mean* *(b) Standard deviation*

*Figure 24: Mean available water and standard deviation for* $10 \cdot R_{stom}$.

## 4.4 Average data assimilation increments

All in all, these experiments demonstrate that a reduction in LAI causes higher available water levels and lower standard deviations in most parts of Europe compared to the reference run. Lastly, we will test the model's performance by considering the data assimilation increments. Because the model's performance over the whole domain is considered, the average absolute difference discussed here is the absolute difference averaged over all land grid points and all days.

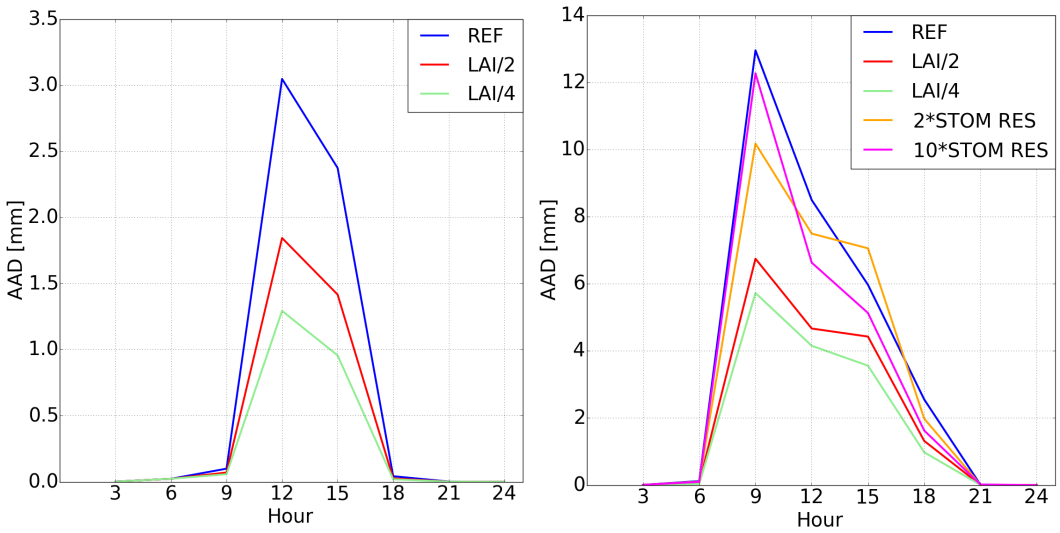


*(a) March* *(b) July*

*Figure 25: Average data assimilation increment per grid point per day for the reference and experimental runs for the time intervals in March and July.*

In March (figure 25a), a land grid point in the reference run undergoes on average soil moisture adjustments of 5.6 mm a day. This implies that over the course of 9 days, apart from actual evapotranspiration, an additional 50 mm is mostly being extracted from the soil. In the LAI/2 experiment, these data assimilation increments have reduced to around 3.4 mm a day per grid point, but best results are obtained in the LAI/4 experiment: 2.4 mm a day per grid point. However, in the last experiment, there were large areas observed where more soil moisture is being added compared to the reference run. These adjustments also account for the accumulated value of 3 mm a day - this value is a combination of added and extracted soil moisture, instead of merely extracted soil moisture as was the case in the reference run.
In July (figure 25b), again best results are obtained for the LAI/4 experiment: around 14.5 mm a day per grid point compared to 30 mm for the reference run. It is also clear that both the $2 \cdot R_{stom}$ and $10 \cdot R_{stom}$ experiments are initiating large data assimilation effects: 25.8 mm and 26.9 mm a day per grid point, respectively. As has been discussed previously, the reason both stomatal experiments are performing worse than the LAI experiments is that, in the case of $2 \cdot R_{stom}$, a LAI/2 adjustment has a larger than factor 2 effect on $R_{stom}$. In addition, $10 \cdot R_{stom}$ is proving to be a too drastic adjustment, causing large standard deviations in France due to too low evapotranspiration rates.

## 4.5 Conclusions

In this section, we have seen that LAI adjustments have proven to reduce soil moisture losses and data assimilation effects in both March and July time series. Best results were obtained for LAI/4, though it is questionable whether this adjustment is realistic for July. This is why we have performed 2 experiments regarding the stomatal resistance $R_{stom}$. From these experiments, it became clear that a LAI/2 adjustment has more effect than $2 \cdot R_{stom}$, as were to be expected. However, a $10 \cdot R_{stom}$ adjustment is too drastic and causes too large data assimilation increments in France due to too high temperatures.

# 5 A temperature-dependent LAI model

In section 4, some rough LAI adjustments were made in order to test their effects on evapotranspiration and data assimilation. Though these adjustments were homogeneously spread over Europe (e.g. not location dependent), major changes were noticeable in especially the height of the average data assimilation increments. However, this method does not capture any latitudinal differences in the start and length of the growing season. Moreover, in the original ECOCLIMAP-II version, one had to use climatological LAI values for runs outside of the 2002-2006 interval. This way there was no discrimination between different years and their growing seasons for a certain vegetation type; every year, the sprouting of leaves started at the exact same time. Applying a certain factor $f_{LAI}$ (depending on root zone temperatures) in the LAI model might cause latitudinal differences and therewith a discrimination in the start of the growing season. Furthermore, annual variations are now captured as well. Root zone temperatures themselves consist of a North-South gradient in early spring, and directly influence vegetation activity. After all, vegetation cannot grow as long as soil temperatures are below activation point. There are also other factors like Solar radiation and $CO_2$ (needed for photosynthesis) and (root zone) soil moisture availability that influence vegetation growth, but for the sake of simplicity, these factors will be left out.

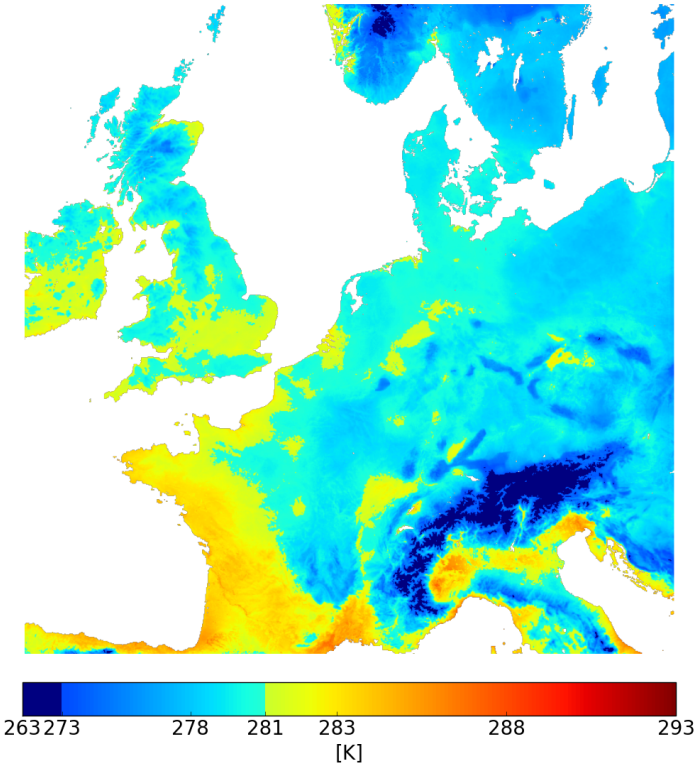


*Figure 26: Average soil temperature between 5 March 00:00 UTC and 14 March 2015 00:00 UTC (in K).*

Figure 26 demonstrates that soil temperatures are still below zero in certain regions in Europe, whereas in other regions temperatures are already high enough for vegetation to start growing. This threshold value lies on average around 8°C, but this will be analysed in more detail in subsection 5.1. Soil temperatures thus serve as a direct measure of the activeness of vegetation. Another benefit of taking soil temperatures is that, unlike air temperatures, small atmospheric temperature fluctuations

do not penetrate into the soil and affect $f_{LAI}$.

## 5.1 Method

### 5.1.1 Model construction

First, a rather simplistic shape of the rescaling model needs to be determined. Because the LAI is calculated via the patch fraction and patch LAI for every single vegetation type, it is logical to make the rescaling factor $f_{LAI}$ patch dependent as well.

Under a certain threshold temperature, vegetation is and cannot be active, simply because it is too cold. This threshold will be named the 'activation temperature', $T_{act}$, and is defined as the temperature at which the vegetation starts sprouting new leaves. This implies that for $T < T_{act}$, the rescaling factor will be constant, defined as $C_1$. Next, there is a certain optimal temperature $T_{opt}$ at which the leaves are optimally growing. In this case, $f_{LAI} = C_2$. Finally, the shape of the transition period between $T_{act}$ and $T_{opt}$ needs to be resolved. For simplicity reasons, we will assume that the transition between these two temperatures is linear, so that

$$f_{LAI} = \begin{cases} C_1 & T < T_{act} \\ (C_2 - C_1)\frac{T - T_{act}}{T_{opt} - T_{act}} + C_1 & T_{act} \leq T < T_{opt} \\ C_2 & T \geq T_{opt} \end{cases} \tag{20}$$

Here,$T$ is the soil temperature (in K). The adjusted LAI will now be calculated as

$$LAI = f_{LAI} \cdot LAI^* \tag{21}$$

where $LAI^*$ is the LAI value of a patch originally assigned by ECOCLIMAP-II. A few more remarks have to be made:

1. The model needs to 'remember' previous $f_{LAI}$ values. This will ensure that after a warm period with large vegetation activity (e.g. in spring), a colder period will not cause the rescaled LAI to decrease again, whilst $LAI^*$ was actually increasing. This situation is imaginable during spring, when a sequence of warm days usually causes quick leaf growth, yet a colder period afterwards will not cause the tree to shed its leaves, but will at most decelerate or delay the growing process. Using $f_{LAI}$ memory will prevent this effect. This memory will be modelled by adding the constraint $f_{LAI}(t) = \max[f_{LAI}(t), f_{LAI}(t-1)]$.
2. Because the $f_{LAI}$ will be multiplied with $LAI^*$, the original LAI-curve will be preserved, so shedding of leaves in late summer and autumn will still be modelled. However, it is uncertain whether this shedding is temperature dependent as well, i.e. whether shedding accelerates under certain temperatures. Because we are interested in reconstructing the start of the growing season, we will not incorporate this. We will come back to this in section 7.

### 5.1.2 Temperatures per patch

For every patch, values for $T_{act}$ and $T_{opt}$ will be assigned. There are a few nature patches with no vegetation, namely patch 1 (bare soil), patch 2 (bare rock) and patch 3 (permanent snow and

ice). These will not be discussed. Furthermore, in ECOCLIMAP-II, patch 5 (evergreen broad-leaved forest) has been removed from the classification, see Faroux et al. (2014). In addition, patch 11 (C4 herbaceous) has no longer been conserved in as well. This is why these patches will not be dealt with as well in this rescaling model.

Table 8 provides a short overview of the selected temperature threshold values.

*Table 8: Selected $T_{act}$ and $T_{opt}$ values for the different patches*

| Patch | $T_{act}$ (°C) | $T_{opt}$ (°C) | From |
|---|---|---|---|
| 1 - Bare soil | No LAI | | |
| 2 - Bare rock | No LAI | | |
| 3 - Permanent snow and ice | No LAI | | |
| 4 - Deciduous broad-leaved forest | 5 | 15 | Sykes & Colin Prentice (1996), Butt et al. (2014), Hänninen (2016), Hollinger et al. (1994) |
| 5 - Evergreen broad-leaved forest | Absent | | |
| 6 - Coniferous forest | 0 | 10 | Tanja et al. (2003), Jarvis & Linder (2000),National Aeronautics and Space Administration (2016) |
| 7 - C3 crops | 5 | 18 | Hatfield et al. (2008), Krug (1997), Rubatzky & Yamaguchi (1997), Hatfield & Prueger (2015) |
| 8 - C4 crops | 15 | 27 | Hatfield et al. (2008), Krug (1997),Rubatzky & Yamaguchi (1997), Hatfield & Prueger (2015) |
| 9 - Irrigated crops | 10 | 15 | the Food and Agriculture Organization of the United Nations (2015) |
| 10 - C3 herbaceous | 5 | 12 | Cornell University (2006) |
| 11 - C4 herbaceous | Absent | | |
| 12 - Wetlands | 5 | 20 | Williams (1992) |

## 5.2 Spatial distribution of the adjusted LAI values

As an first model construction to test for the presence of a LAI North-South gradient and a delay in the start of the growing season in higher latitudes, we will apply the temperature model sketched previously in the first semester of 2015. We will select $C_1 = 0.25$ and $C_2 = 1$ for all patches discussed in 5.1.2, with the exception of patch 6. Dividing the LAI by 4 for this patch might be a bit rigorous, since a needle-leaf tree has a merely constant LAI throughout the year. Therefore, $C_1$=0.5 and $C_2 = 1$ for patch 6. In figure 27, the LAI spatial distribution for two days around the start of the growing season is shown. The left panel represents the original ECOCLIMAP-II LAI, the right panel the adjusted, temperature-dependent one.

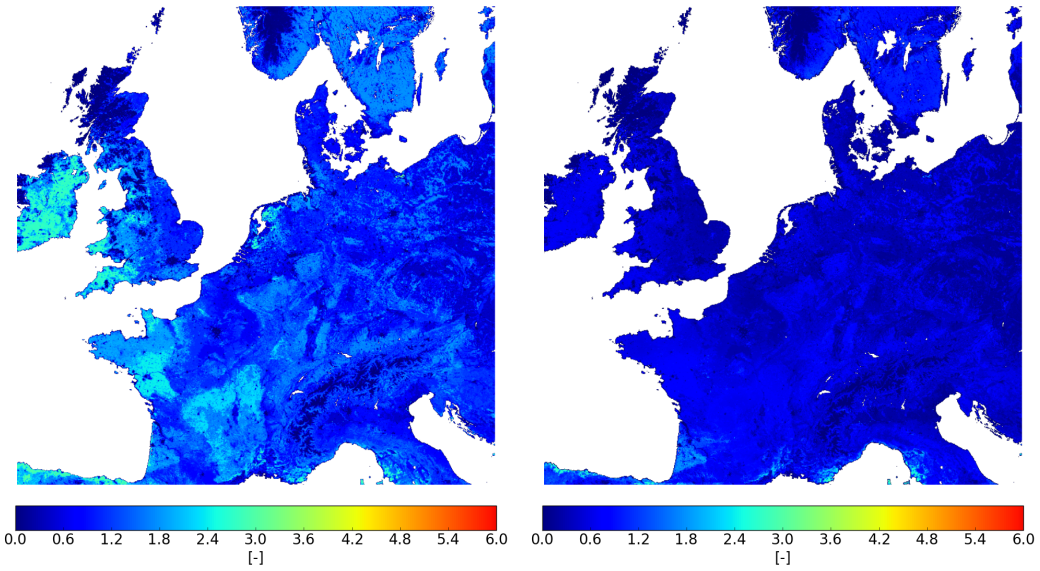


*(a) ECOCLIMAP-II 03-03-2015* *(b) Temperature model 03-03-2015*

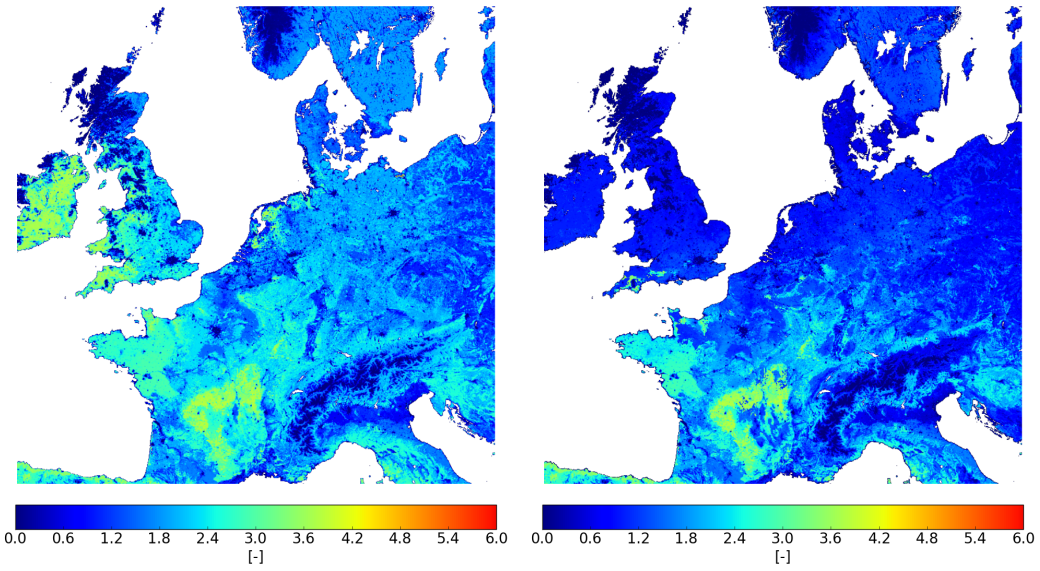


*(c) ECOCLIMAP-II 13-04-2015* *(d) Temperature model 13-04-2015*

*Figure 27: LAI spatial distribution in the HARMONIE38 domain for 3 March and 13 April 2015. The left panel represents the original, climatological LAI values coming from the ECOCLIMAP-II database. The right panel shows the adjusted, temperature-dependent LAI profile.*

Around 3 March 2015, soil temperatures are still too low in large parts of Europe for the vegetation to become active. However, the original ECOCLIMAP-II version (figure 27a) shows that in Ireland and parts of France, Great Britain and the Netherlands, LAI values are already close to 2-2.5. Under these circumstances, vegetation can start evapotranspiring and available water levels will drop fast, as was observed in sections 3 and 4. If soil temperature is taken into consideration, LAI values remain low, see figure 27b. Here, LAI values correspond more closely to reality, since vegetation is not active yet in large parts of Europe.

In figure 27d, a distinct North-South gradient is visible. In southern Europe, vegetation is active in large regions, whereas in other parts of Europe vegetation is just starting to sprout its leaves. This gradient was not distinct in the original ECOCLIMAP-II version, see figure 27c. Here, LAI values are relatively high almost everywhere, and vegetation is assumed to be active. In reality, there are barely any leaves yet from which evapotranspiration can take place.

## 5.3 Implementation in HARMONIE38

In order to test this temperature-dependent LAI model, it is implemented in the *isba.F90* subroutine in HARMONIE38. However, due to the complex structure of HARMONIE, $C_1$, $C_2$ and the $T_{act}$ and $T_{opt}$ threshold values have been set once and therefore the $f_{LAI}$ curve is homogeneous for all patches. Furthermore, the $f_{LAI}$ memory function is not implemented in these experiments, as to reduce model complexity. Two seperate experiments, each with a different $f_{LAI}$ curves, are conducted.

### 5.3.1 Model construction

In the first experiment (Temperature model 1 hereafter), we will select $C_1 = 0.25$ and $C_2 = 1$. For the second experiment (Temperature model 2 hereafter), $C_1 = 0.1$ and $C_2 = 0.5$. $T_{act} = 281$K and $T_{opt} = 288$K in both experiments.

### 5.3.2 Results

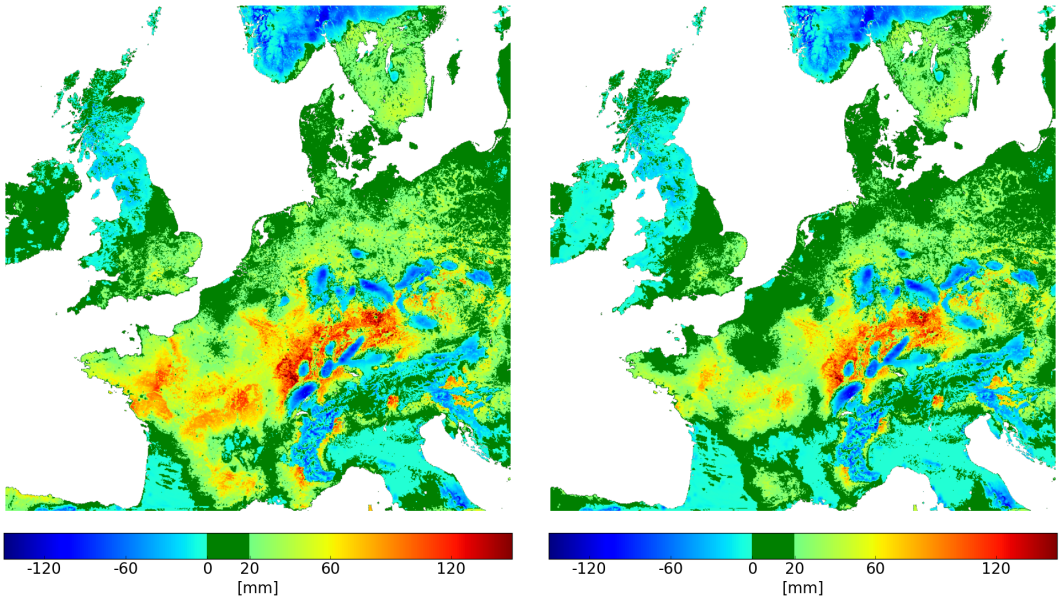


*(a) Temperature model 1* *(b) Temperature model 2*

*Figure 28: Difference in available water between 5 March 00:00 UTC and 14 March 2015 00:00 UTC for the two temperature models.*

**Difference in available water** From figure 28, it is clear that Temperature model 2 is performing better in central Europe compared to Temperature model 1. However, there are larger areas where soil moisture is being added in Temperature model 2 than in Temperature model 1: in Ireland, LAI values are too low in Temperature model 2, while Temperature model 1 is performing better in this area. In southern France and Italy, soil moisture is being added in both model versions. However, we have seen from the LAI experiments conducted in subsection 4.2 that even a factor 2 reduction is too drastic here: the reference run has been performing best in these regions.

**Average data assimilation increments** The effect of both temperature models is illustrated best in figure 29, where the average absolute difference (defined in subsection 3.6) averaged over all land grid points is plotted. It shows that all experiments are performing better than the reference run, yet both LAI/2 and LAI/4 adjustments have lower average data assimilation increments than either one of the temperature-dependent models: 4.5 mm (Temperature model 1) and 3.9 mm a day (Temperature model 2) is on average being adjusted by the data assimilation every day at a grid point, compared to 3.4 and 2.4 mm in the LAI/2 and LAI/4 experiments, respectively. The cause of this difference between the LAI models and the temperature-dependent models will be evaluated in more detail in subsection 5.4.

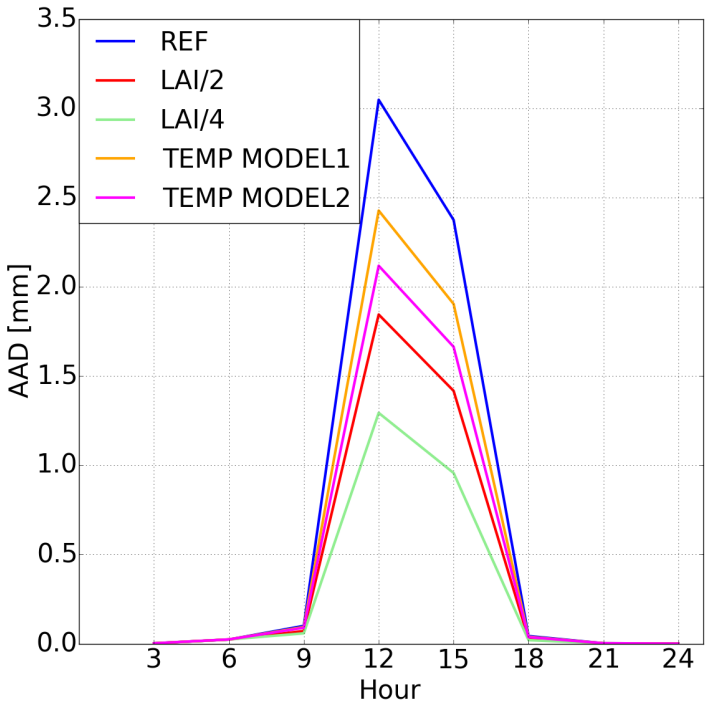


*Figure 29: Data assimilation effects of all March experiments.*

## 5.4 Recommendations for improving the temperature model

Every single experiment performs better on average than the reference run. However, the observed effect differs per region, causing different models to perform better in different areas. $f_{LAI}$ values from the 12:00 UTC cycle for both temperature models can be found in Appendix A.6. This value is of main interest here because highest evapotranspiration rates are recorded at 15:00 UTC (see figure A.36a,

which are influenced by the LAI value assigned at 12:00 UTC. The recommendations discussed in the following solely hold for the beginning of March. A different period might need different $C_1$ and $C_2$ values, but this has not been evaluated in this research.

In southern France and Italy, every model caused soil moisture to be added in certain regions compared to the reference run, implying that evapotranspiration rates are too low in these areas in every experiment. The reference run is performing best here and $C_1$ and $C_2$ should be 1 in order to follow the original ECOCLIMAP-II LAI curve.
In central Europe, our main focus lied on decreasing the large drop observed in the reference run. All experiments managed to reduce this drop, but best results are obtained in the LAI/4 experiment. However, in this experiment there are still areas where more than 60 mm is extracted from the root zone in these 10 days. In Temperature model 2, $f_{LAI}$ values here are higher than 0.25 on some days. This thus demonstrates that $f_{LAI}$ values of below 0.25 are essential to reduce evapotranspiration rates and data assimilation effects in these regions. Therefore $C_1 < 0.1$ and/or $C_2 < 0.5$.
In Great Britain and Ireland, both LAI/2 and Temperature model 1 have roughly the same effect, which is likely caused by Temperature model 1 generating LAI values close to 0.5. Still, these experiments do prove that a LAI adjustment close to/of LAI/2 is working better than the ECOCLIMAP-II values assigned currently. $C_1$ and $C_2$ likely lie close to 0.25 and 1, respectively.
In Scandinavia , northern Germany and Poland, LAI/4 is proving to initiate realistic soil moisture losses in the most areas. From figures A.44 and A.45, we see that both temperature models cause $f_{LAI}$ values of above 0.25. Readjusting $C_1$ and $C_2$ such that $C_1 < 0.1$ and/or $C_2 < 0.5$ will likely work best here.
In the Benelux, overall Temperature model 2 is performing best, but there are areas where soil moisture levels are now being increased. This is likely due to a too low LAI, since the same areas in the LAI/4 experiment do show soil moisture losses between 0-20 mm.

## 5.5 Conclusions

Both temperature-dependent LAI models introduced in this section capture annual variations as well as the possibility of having a North-South gradient. The average data assimilation increments showed that both models are performing better than the reference run, but they are still worse than the LAI experiments conducted in subsection 4.2. By looking at some qualitative differences throughout Europe, it showed that different regions in Europe perform best under different experiments. This illustrates that not one solution can be considered optimal. The two temperature models presented here are rather simple models applied throughout Europe. This might cause too low LAI values in southern regions, where perhaps different $T_{act}$ and $T_{opt}$ hold compared to higher latitude regions, something also illustrated by the fact that soil moisture levels were increasing in these areas for both temperature models. Furthermore, in both models too high LAI values are generated in areas like Scandinavia and central Europe, proven by the fact that the LAI/4 experiment is performing better in these regions. Therefore, a temperature dependent LAI model will have to be adjusted to local scale instead of one model being applied the same way throughout Europe. In addition, these HARMONIE38 implementations did not discriminate between different patches and there was no $f_{LAI}$ memory included. Using such a temperature model on a longer spatial scale should consist of these aspects as well.

# 6 Conclusions

In this Master's thesis, we investigated why low latent heat fluxes are forecast in summer in the HARMONIE model. From analysing the Bowen ratios throughout 2015, it showed that high Bowen ratios (i.e. greater than 1) occur relatively often in sub-urban and rural areas in both the HARMONIE36 and HARMONIE38 domain. By considering dominant vegetation types (see subsection 3.2 for the exact definition), it became clear these areas with high Bowen ratio occurrences are not covered by specific vegetation types.

In order to analyse soil moisture availability, we defined the available water for transpiration (see equation 8). The available water spatial distribution at 5 March and 2 July 2015 revealed sufficient water levels in March, but severe water scarcity in July throughout the domain. Because different effects might cause this drop in available water, we plotted the time series at selected locations covered by the same dominant vegetation type. These time series showed a significant decrease in available water levels in March, which the model never recovers from. Since this drop occurred at almost all locations, this proved the influence of a common denominator: vegetation characteristics. Local effects like differences in atmospheric conditions likely have a minor influence on available water levels. The leaf area index (LAI) is such a vegetation characteristic that is variable in time and directly influences evapotranspiration rates. By plotting the LAI curves for the dominant vegetation types under consideration illustrated a too early start of the growing season, causing too high LAI values in early March. This provides enough leaf surface to cause too high evapotranspiration rates, therewith too low 2 meter temperatures and too high dew point temperatures. Moreover, the process of data assimilation will then extract more soil moisture from the root zone, in order to decrease LHF and thus increase 2 meter temperatures and decrease dew point temperatures again. This leads to soil moisture decreases of over 100 mm between 5 and 14 March 2015 in various regions of both HARMONIE domains.

Experiments regarding these LAI values were conducted in order to prove their influence on this drop in March. It turns out both LAI/2 and LAI/4 experiments reduce this gradient in large parts of the domain. Yet, since the LAI ECOCLIMAP-II database currently does not consist of annual variations as well as spatial differences, two temperature dependent LAI models were constructed (see section 5) in order to allow for this. Although local improvements were observed in both models in the same time period, the overall performance did not improve compared to the LAI/2 and LAI/4 experiments. This is caused by LAI values still being too high in both temperature models in these areas. Still we recommend using the temperature-dependent model, but $C_1$ and $C_2$ values have to be adjusted such that $f_{LAI} \leq 0.25$ in central and northern Europe before the start of the growing season.

In July, again both LAI/2 and LAI/4 models perform better than the reference run. However, it is debatable whether LAI adjustments in July are realistic. We therefore focussed on stomatal resistance ($R_{stom}$) as well. In order to test its effects, both a factor 2 and factor 10 increase of $R_{stom}$ have been evaluated. Again both versions proved to improve model output compared to the reference run, yet their effects are smaller than for the LAI/2 and LAI/4 experiments. This is due to the fact that a LAI adjustment also affects $R_{stom}$, and that this effect is larger than a factor 2 or 4 increase in $R_{stom}$, respectively. Furthermore, a factor 10 increase in $R_{stom}$ is too rigorous since vegetation is now too inactive, hereby causing data assimilation to adjust root zone soil moisture contents more than in the case of LAI/2 or LAI/4.

# 7 Discussion

## 7.1 Assumptions and simplifications made in this research

During the course of this research, we made various assumptions and simplifications in order to construct a problem diagnosis and perform the experiments. To begin with, we defined the amount of available water for transpiration via the root zone depth. For all dominant vegetation types in section 3.4, we used the prescribed root zone depth. However, this is a rough estimation of the actual root zone depth at both B20 and B60. The actual root zone depth may vary between these two locations due to the presence of other vegetation types, since these dominant vegetation types cover more than 70% of a grid point, but seldom the whole grid point. Taking the weighted average (as has been done in figures 10 and 11) could result in a different value for the root zone depth. However, this remaining 30% will only have a minor influence on the average root zone depth. Moreover, because of the linear dependence on root zone depth, a slightly different root zone depth would not affect the actual characteristics of the available water curve like the significant drop in early March or the low values in July. Therefore the conclusions drawn regarding these available water profiles would still hold if one takes the actual weighted averaged root zone depths instead of the root zone depth of the dominant vegetation type.
Besides, this root zone depth is a prescribed value per vegetation type in ECOCLIMAP. This also means that local differences are not taken into account: everywhere in the domain, the same vegetation type has the same root zone depth. It would be more realistic if these local differences are actually modelled as well.

We also saw that adjusting the LAI and/or $R_{stom}$ improves the model. However, we did not analyse the effect of these adjustments on other parameters. In SURFEX, the height of herbaceous vegetation is calculated as $h = LAI/6$ (Masson et al., 2003). This height might influence small-scale turbulence and eddy transport, but this has not been studied in this thesis. Nonetheless, the decrease in data assimilation increments shows that the model as a whole improves when LAI and $R_{stom}$ values are decreased. Further research might clarify whether the proposed adjustments have a (negative) side effect on other parameters.

For the temperature-dependent LAI model, we solely considered soil temperature as an indicator of vegetation growth. Although it improved HARMONIE's start of the growing season, there are also other parameters that can be taken into account like solar radiation, available water and the presence of $CO_2$ for photosynthesis. Including these will make the model more realistic, yet it will improve the model slightly compared to including soil temperatures.
Next, $T_{act}$ and $T_{opt}$, the activation and optimal temperatures respectively, are taken as averages from atmospheric and soil temperatures found in literature. Though these temperatures are not solely soil temperatures, it is sufficient for now to use these in the temperature-dependent model to analyse their effects on $f_{LAI}$.
In addition, more temperature thresholds can be considered apart from $T_{act}$ and $T_{opt}$. Vegetation growth is optimal between a certain temperature range. $T_{opt}$ has been taken as the minimum of this range, but a maximum can be implemented as well. Because we were interested in reconstructing a more realistic growth season and a more distinct North-South gradient in spring, this maximum $T_{opt}$ value was not of interest since temperatures are usually too low for this threshold value. However, if one wants to make this model suitable for all seasons, one should also incorporate this maximum $T_{opt}$. Furthermore, there is also a temperature threshold value after which vegetation dies because it is too hot. If desired, this could also be included in the model.
Lastly, we introduced a'memory function', so that LAI values could not decrease anymore as soon as the growing season had started in spring. Yet, after summer, the shedding of leaves should also be modelled, i.e. the LAI should decrease again. Because the maximum constraint can cause a

LAI increase during this shedding period, one should incorporate a minimum constraint of the form $f_{LAI}(t) = \min[f_{LAI}(t), f_{LAI}(t-1)]$. This way, LAI values will not increase during a warmer period in autumn. In addition, although this shedding is incorporated in the LAI curve, we did not consider any temperature dependence - it is possible that this shedding of leaves accelerates when temperatures drop below a certain threshold. This effect was not analysed because we were only interested in the start of the growing season. Further research will clarify this effect.

Both temperature models, as well as the LAI and $R_{stom}$ experiments, demonstrated that not one model is performing best on every location in Europe. Since the temperature-dependent models do consist of the necessary characteristics like annual variations and spatial differences, we do recommend to implement such a model in a future HARMONIE version. Such a temperature-dependent model will have to be adjusted to local scale by applying different $C_1$ and $C_2$ values and therewith different $f_{LAI}$ curves for different regions in Europe. It is very likely that this $f_{LAI}$ will also have to be seasonal dependent, in order to exclude the possibility of too low LAI values in summer. In addition to implementing this temperature model, it is likely that $R_{stom}$ will also need to be readjusted in this new HARMONIE version.

## 7.2 ECOCLIMAP

Apart from assumptions made in this thesis, we also have to look at ECOCLIMAP's assumptions. To start with, there are now 273 vegetation types defined in ECOCLIMAP-II. This should improve the model compared to ECOCLIMAP-I (where 214 vegetation types had been distinguished). However, it is still discussable whether ECOCLIMAP-II's classification process is close to optimal. It still occurs that vegetation characteristics are indifferent of location. Distinguishing and classifying more vegetation types will make the model more realistic.
Furthermore, Garrigues et al. (2008) concludes that, compared to GOBCARBON, CYCLOPES and MODIS, ECOCLIMAP is performing worst when it comes to annual LAI values. We discussed previously that due to the lack of an annual variation and the absence of a North-South gradient, ECOCLIMAP's LAI database is poorly reconstructing the actual growing season. It is therefore plausible that incorporating a different vegetation database will improve HARMONIE's performance as well.

In addition, we want to point out the model output over Ireland and Scandinavia. In these regions, LAI values are already relatively high in early spring (around 5 in large parts of Ireland). However, looking at figure 20 depicts still relatively high average available water values, and low standard deviations. This is contradictory to our findings that high LAI values cause low soil moisture levels in summer. However, it is plausible that due to local weather conditions (e.g. frequent cloudiness, high precipitation), soil moisture levels are able to remain high throughout spring and summer.

# 8 Recommendations and remarks for further research

**Temperature dependent model** In section 5, we constructed a rather simplistic model to adjust LAI values according to soil temperatures. This model proved to capture a more distinct North-South gradient, as well as the possibility of annual variations in the LAI curve. However, this simplistic model could be extended with some more constraints in order to make it more realistic. A few suggestions are listed below:

1. Apart from soil temperature alone, other parameters like solar radiation, $CO_2$ and available water levels can also be incorporated.
2. We have used a rather simplistic shape for $f_{LAI}$, where $f_{LAI}$ increases linearly for $T_{act} < T < T_{opt}$, and $LAI = f_{LAI} \cdot LAI^*$. Because this linear dependence of $f_{LAI}$ on soil temperatures has merely been constructed as a first attempt, further research could help define this relationship better.
3. Other combinations of $C_1$ and $C_2$ values than the ones discussed in this thesis also have to be evaluated. These $C_1$ and $C_2$ values are location-dependent: higher $C_1$ and $C_2$ values should be implemented for southerly regions. Furthermore, it is likely that $C_1$ and $C_2$ also vary on a temporal scale, with lower $C_1$ and $C_2$ values in winter and higher values in summer.
4. For now, only $T_{act}$ and $T_{opt}$ have been used in calculating $f_{LAI}$. These values have been determined using the average of values found in existing literature. However, more research on this might help determine the exact values for $T_{act}$ and $T_{opt}$ per patch or even per vegetation type. In addition, there also exists a temperature threshold after which the vegetation dies because temperatures are too high. This threshold has been left out of this model but could perhaps be incorporated in future modelling.
5. $f_{LAI}$ is updated in spring and summer in such a way that its value is never lower than the previous update (e.g. $f_{LAI}(t) = \max[f_{LAI}(t), f_{LAI}(t-1)]$). However, after summer, trees will shed their leaves, i.e. the LAI will decrease again. Because we do not want LAI values to increase again during autumn, we should incorporate a $f_{LAI}$ minimum constraint like $f_{LAI}(t) = \min[f_{LAI}(t), f_{LAI}(t-1)]$, and should hold as soon as LAI values start to decrease. Because we were interested in reconstructing the start of the growing season, we did not look at this minimum constraint, but it should be included when one is going to run on a yearly timescale. Furthermore, it is uncertain whether this shedding accelerates under certain temperatures. Further research on this could help determine if this hypothesis is true, and if so what these threshold values will be.

Lastly, in order to test its performance, this model should be run for a complete spring and summer period. By doing so, one can test whether available water is retained better and if a (quick) drying out of the soil is prevented this way.

**Stomatal resistance** Other $R_{stom}$ adjustments have to be evaluated as well. In this research, we have varied and tested $R_{stom}$ in the July time series to compensate for LAI adjustments which are rather unrealistic in summer. I Because these $R_{stom}$ adjustments did improve the model's performance, it is also possible that $R_{stom}$ needs to be adjusted at the start of the growing season.

**Vegetation cover classification** In ECOCLIMAP-II, 273 vegetation types have been classified by using a combination of different satellite data. However, since the same vegetation type with the same

characteristics can be found in different places in Europe, it is desirable to update ECOCLIMAP-II with more vegetation types, incorporate a local discriminator per vegetation type and/or utilize a different vegetation database, like has been proposed in Garrigues et al. (2008).

**Data assimilation** Data assimilation is useful whenever the model's output deviates too much from observations. However, the magnitude of the increments is debatable. Especially during the heat wave in the first week of July, data assimilation caused large jumps in the amount of available water, adjusting soil moisture levels by over 50 mm in a few hours' time. The fact that these jumps had to be corrected again the cycle after shows that the magnitude of these data assimilation adjustments are too large in the first place. Because the way data assimilation is performed was outside the scope of this Master's thesis, we suggest that different methods reducing these large increments should be analysed. In order to ensure no severe water scarcity ($AW < 0$), we propose let these increments be a fraction of actual available water levels. This way, large adjustments in July are reduced.

**Influence on other parameters** In this thesis, we have evaluated the influence of LAI decrements and $R_{stom}$ increments on soil moisture levels. However, we have not considered the effect of such adjustments on other parameters like roughness length or vegetation fraction, and the complications this might have on other meteorological phenomena like eddy transport. Since the model improved as a whole (from looking at the data assimilation), these effects likely do not play a major role. Further research will clarify this statement.

# A Figures

## A.1 Clay and sand spatial distribution

In figures A.1-A.4, the fractions of clay and sand are plotted. These fractions were retrieved from the HARMONIE36 and HARMONIE38 database.

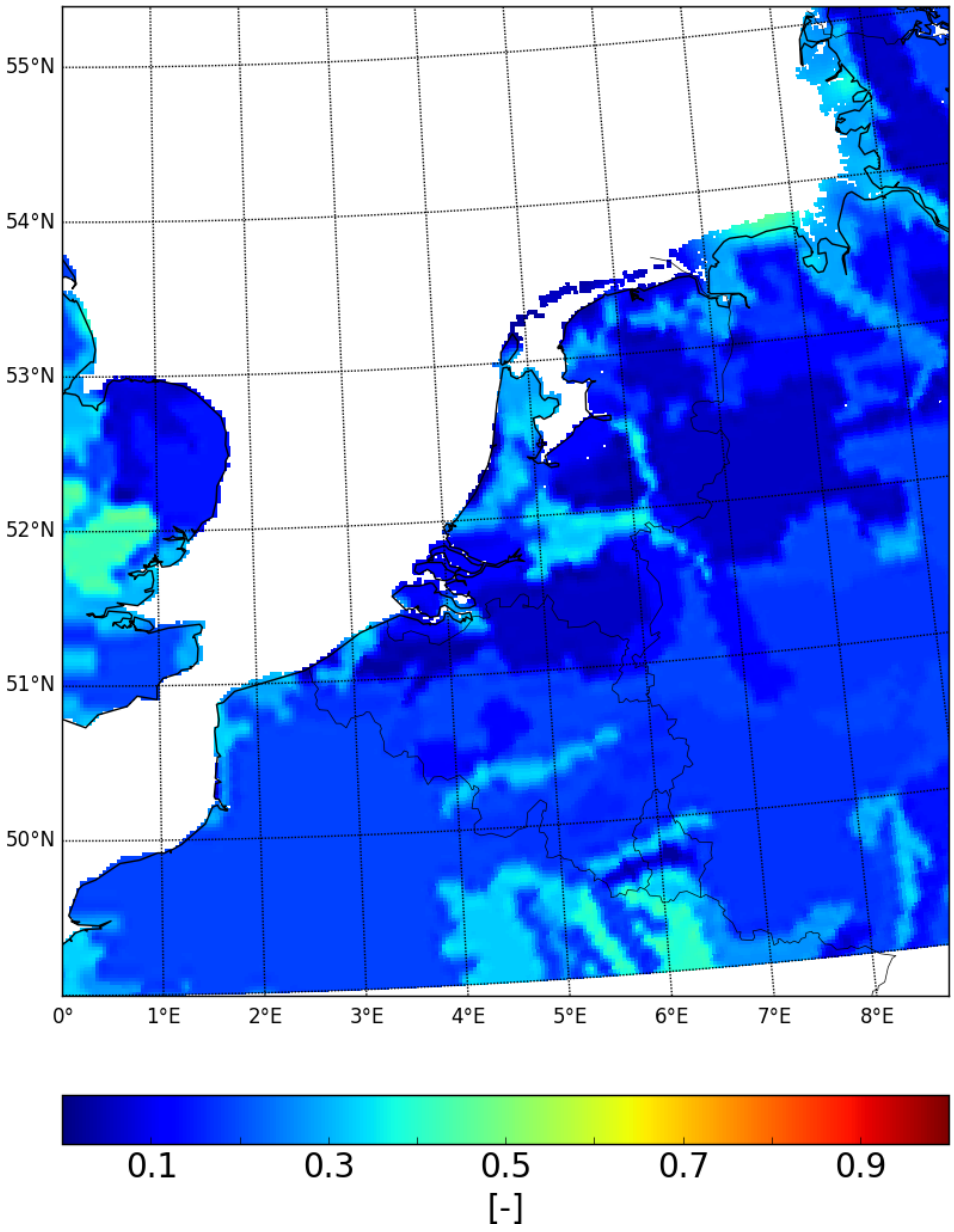


*Figure A.1: Spatial distribution of the fraction of clay for HARMONIE36.*

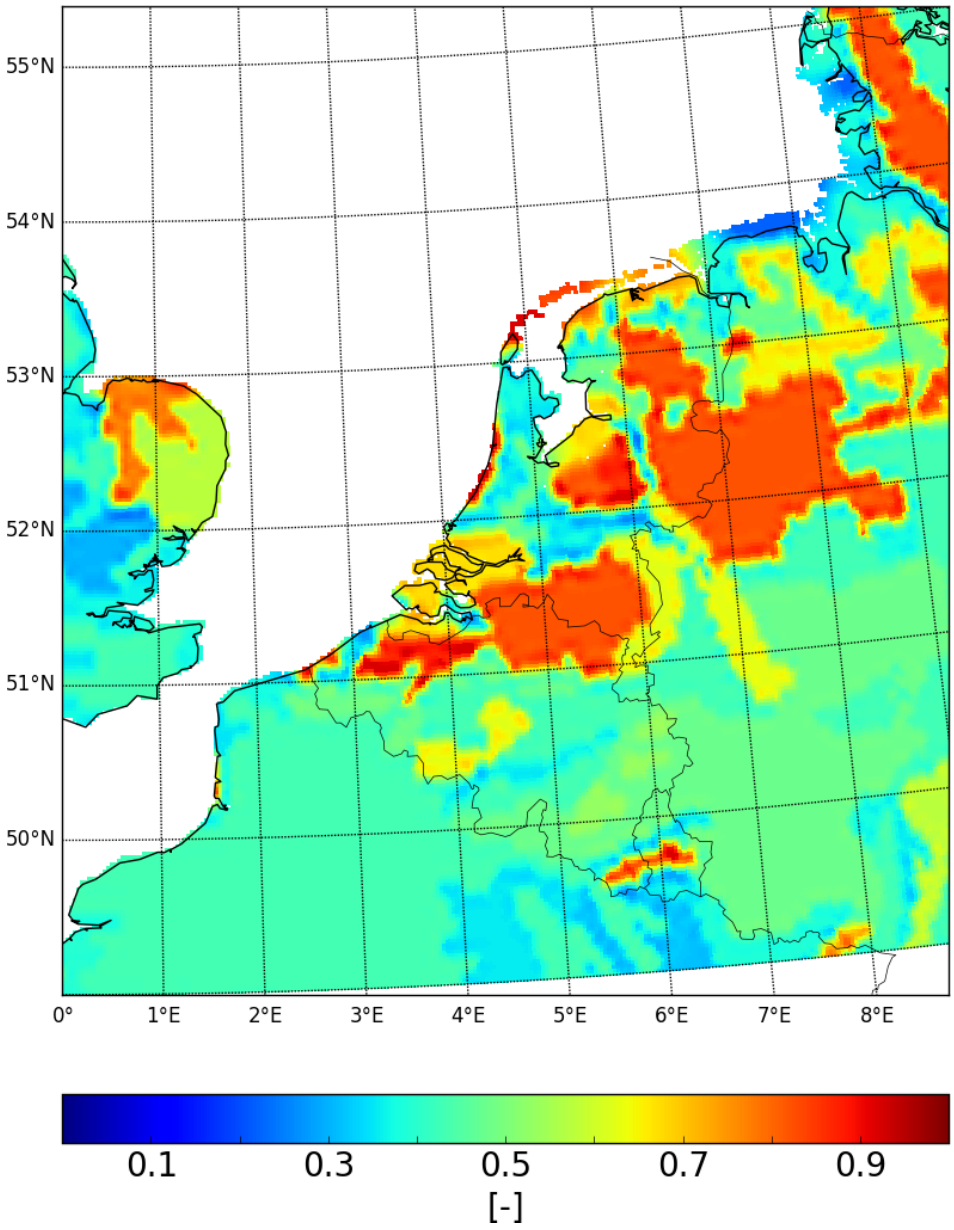


*Figure A.2: Spatial distribution of the fraction of sand for HARMONIE36.*

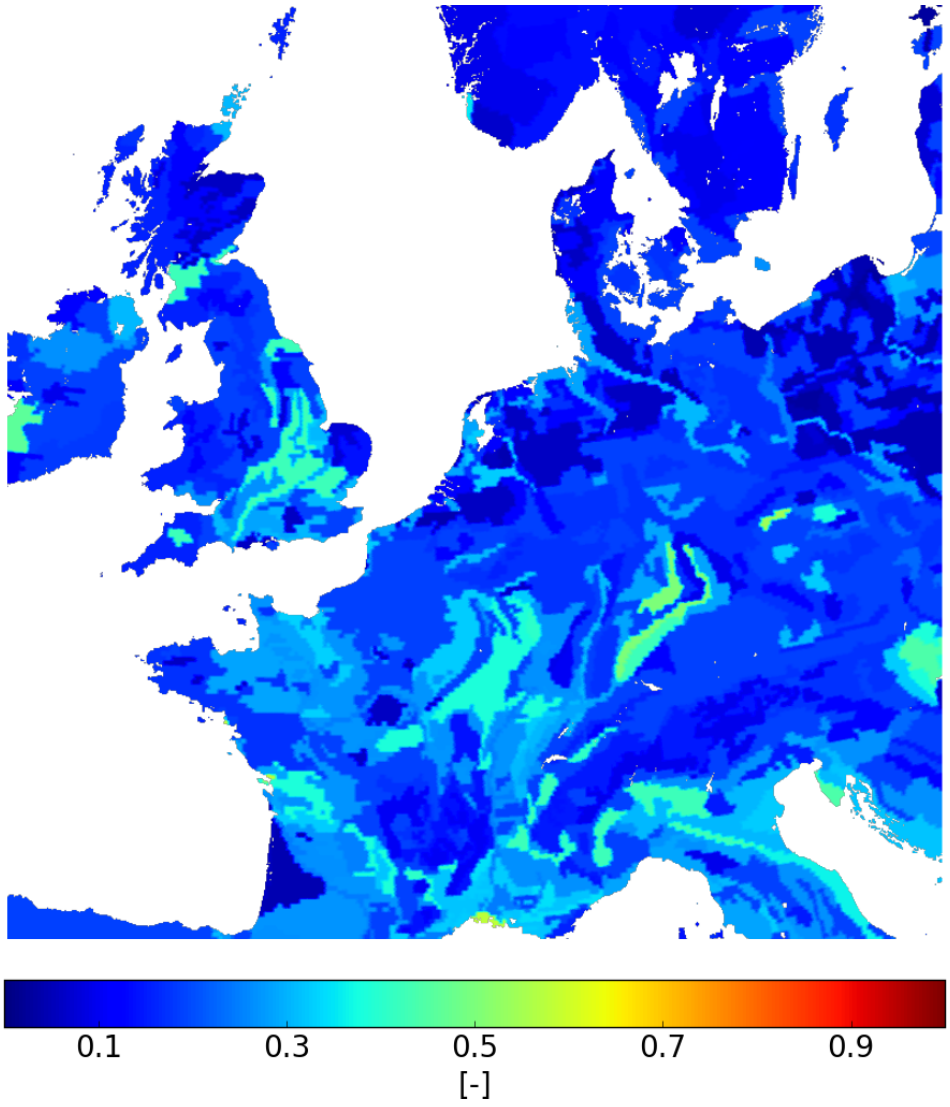


*Figure A.3: Spatial distribution of the fraction of clay for HARMONIE38.*

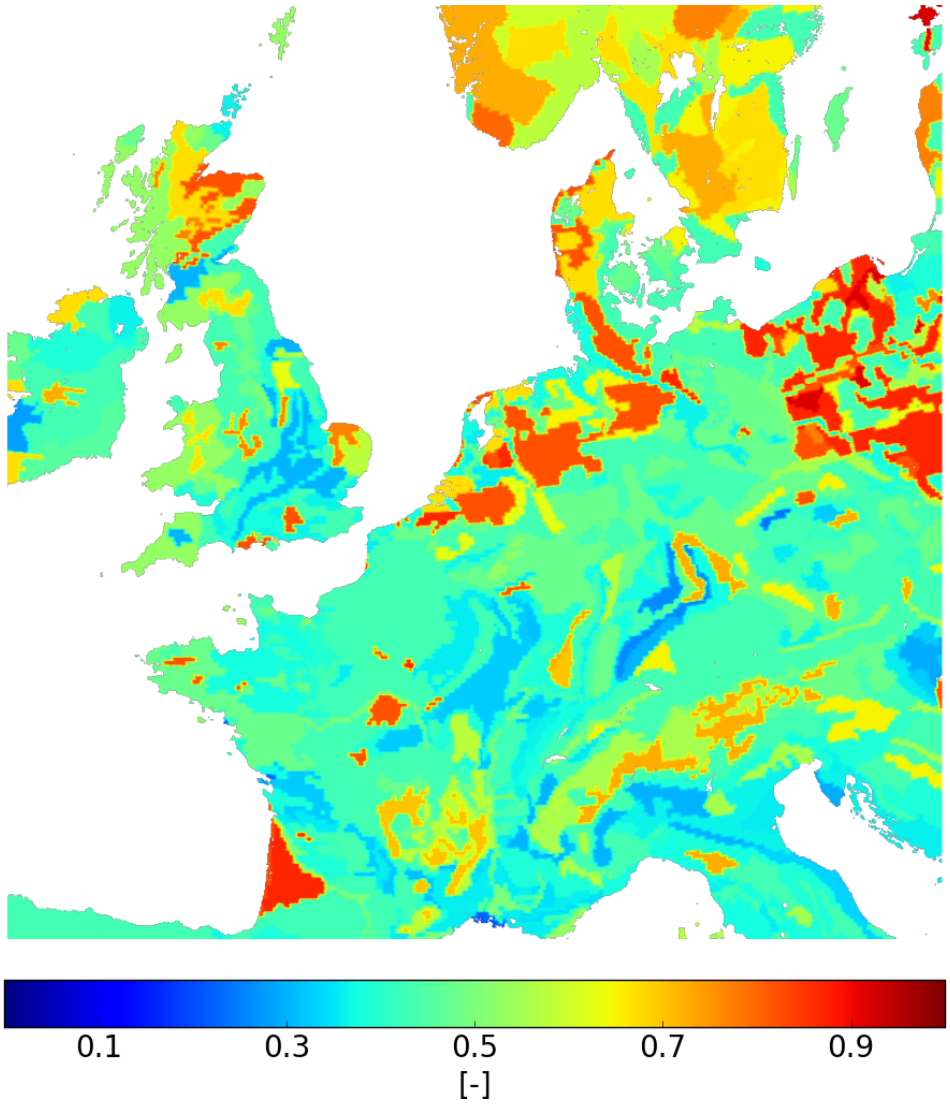


*Figure A.4: Spatial distirbution of the fraction of sand for HARMONIE38.*

## A.2 Available water profiles in HARMONIE38

Figures A.6 - A.9 represent the available water time series for the 19 vegetation types for HARMONIE38.

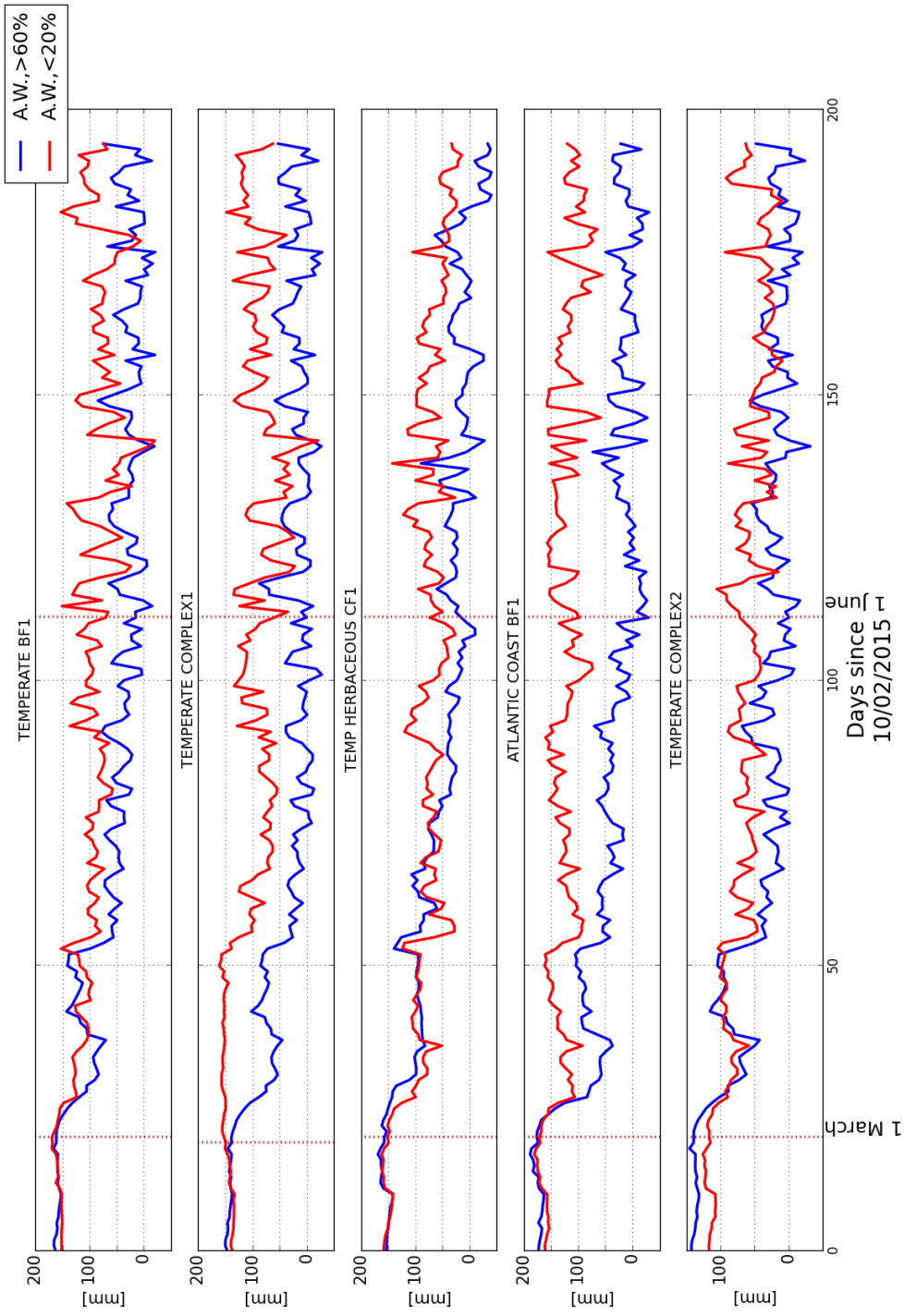


*Figure A.6: Available water (in mm, as defined in equation 8) for vegetation types 'Temperate BF1', 'Temperate complex1', 'Temperate herbaceus CF1', 'Atlantic coast BF1' and 'Temperate complex2'. The time interval is 10 February - 31 August 2015. The red line corresponds with the time profile of the location where less than 20% of the days, the Bowen ratio is high (B20). The blue line represents the time profile of the location where more than 60% of the days, the Bowen ratio is high (B60).*

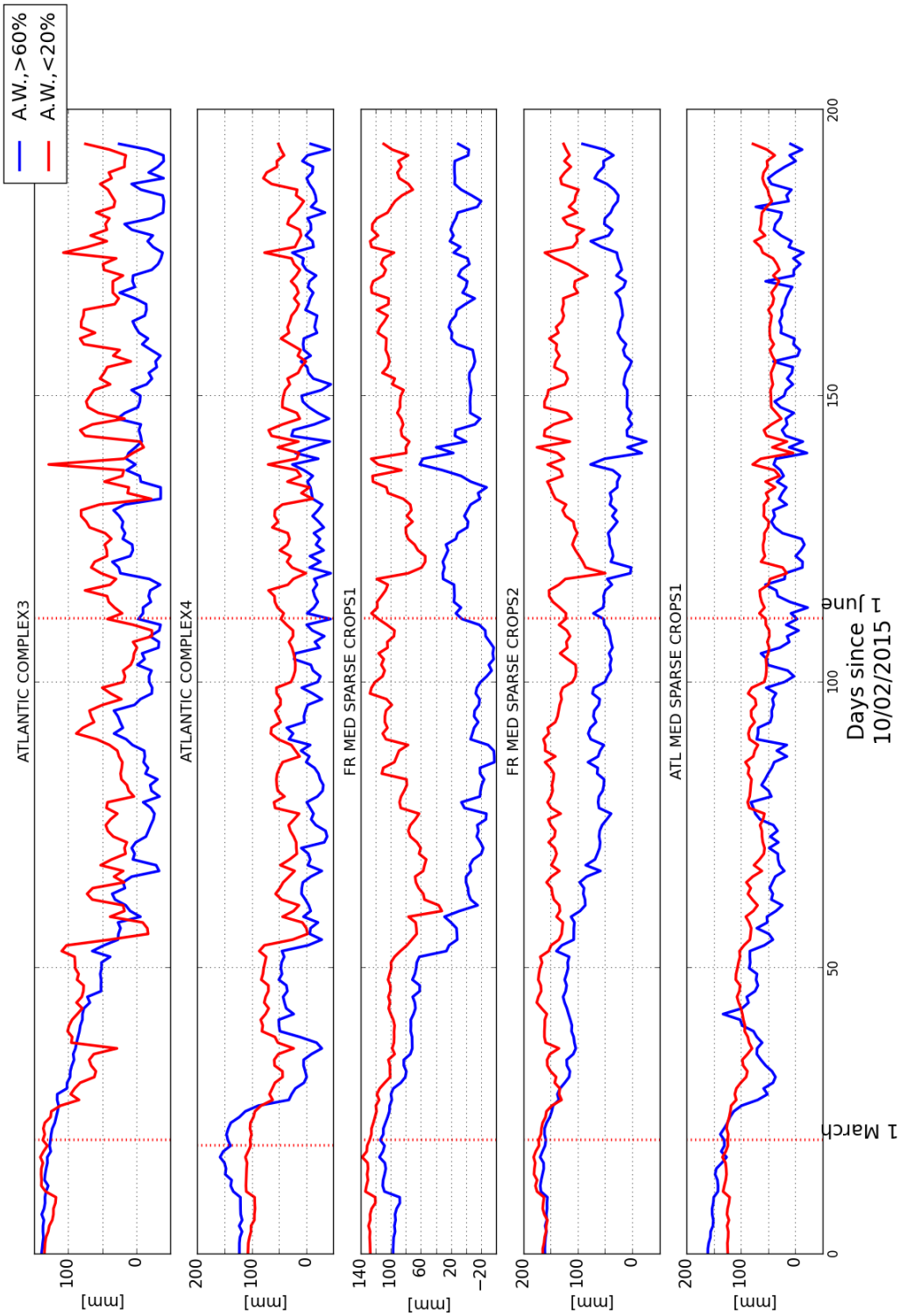


*Figure A.7: Available water (in mm, as defined in equation 8) for vegetation types 'Atlantic complex3', 'Atlantic complex4', 'Fr med sparse crops1', 'Fr med sparse crops2' and 'Atl med sparse crops1'. The time interval is 10 February - 31 August 2015. The red line corresponds with the time profile of the location where less than 20% of the days, the Bowen ratio is high (B20). The blue line represents the time profile of the location where more than 60% of the days, the Bowen ratio is high (B60).*

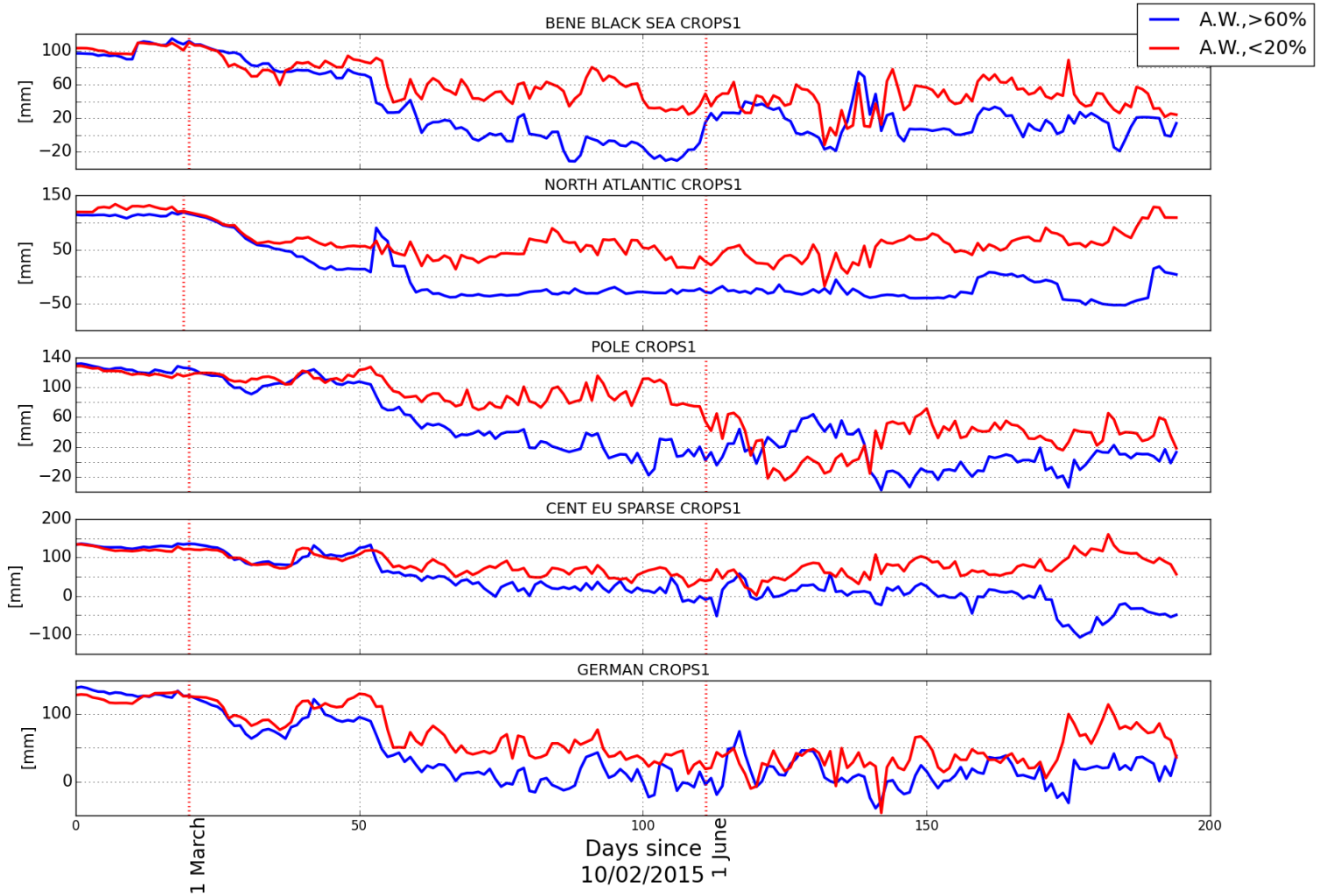


*Figure A.8: Available water (in mm, as defined in equation 8) for vegetation types 'Bene black sea crops1', 'North Atlantic crops1', 'Pole crops1', 'Cent EU sparse crops1' and 'German crops1'. The time interval is 10 February - 31 August 2015. The red line corresponds with the time profile of the location where less than 20% of the days, the Bowen ratio is high (B20). The blue line represents the time profile of the location where more than 60% of the days, the Bowen ratio is high (B60).*

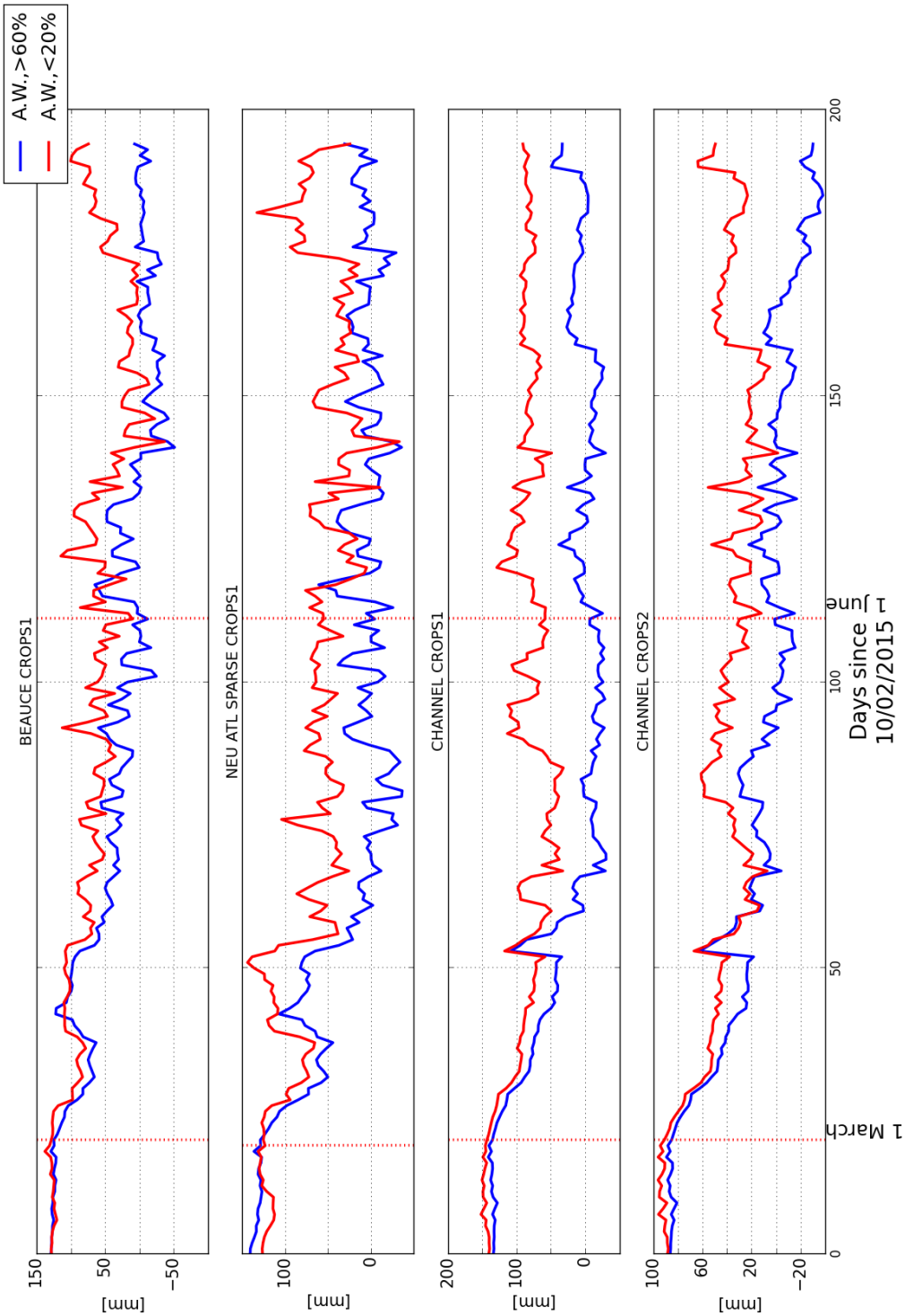


*Figure A.9: Available water (in mm, as defined in equation 8) for vegetation types 'Beauce crops1', 'Neu Atl sparse crops1', 'Channel crops1' and 'Channel crops2'. The time interval is 10 February - 31 August 2015. The red line corresponds with the time profile of the location where less than 20% of the days, the Bowen ratio is high (B20). The blue line represents the time profile of the location where more than 60% of the days, the Bowen ratio is high (B60).*

## A.3 Time series and data assimilation increments

### A.3.1 HARMONIE36

In figures A.10-A.16, the 3h-time series and average absolute difference for the time intervals in March and July for the 7 vegetation types in HARMONIE36 are plotted. The red line corresponds with the time profile of the location where less than 20% of the days, the Bowen ratio is high (B20). The blue line represents the time profile of the location where more than 60% of the days, the Bowen ratio is high (B60).

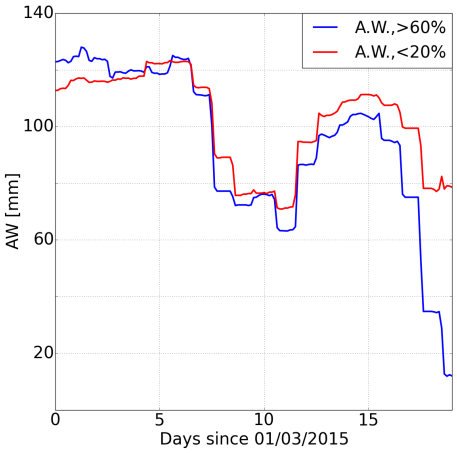


*(a) 3h-run profile, March*

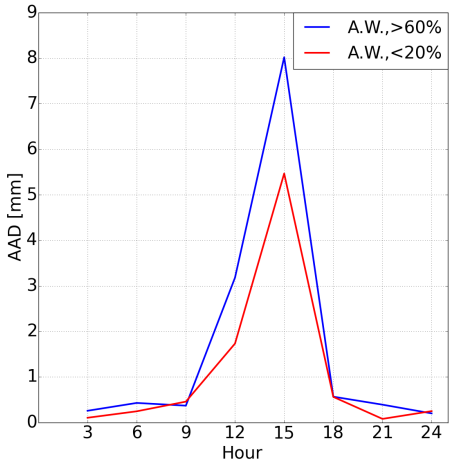


*(b) Data assimilation increments, March*

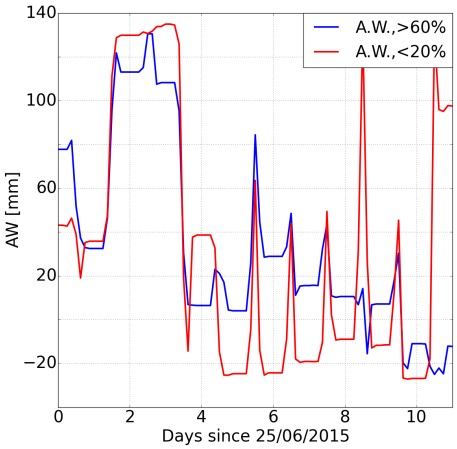


*(c) 3h-run profile, July*

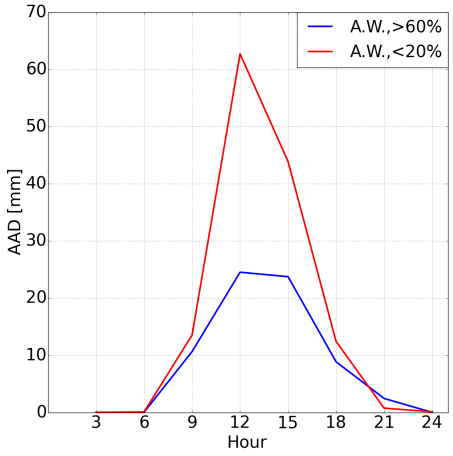


*(d) Data assimilation increments, July*

*Figure A.10: Crops (Temperate)*

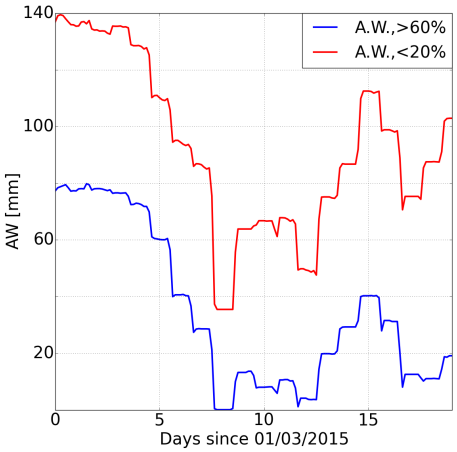


*(a) 3h-run profile, March*

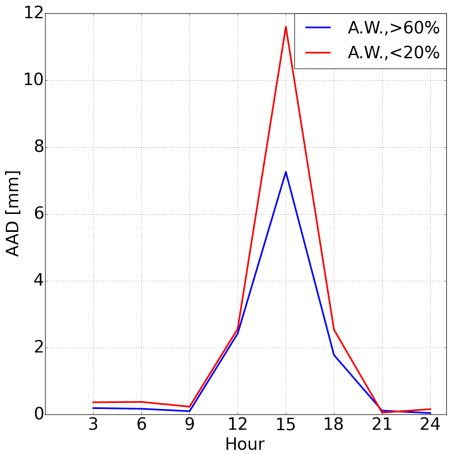


*(b) Data assimilation increments, March*

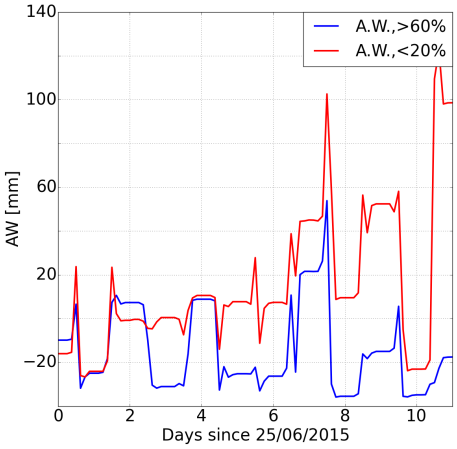


*(c) 3h-run profile, July*

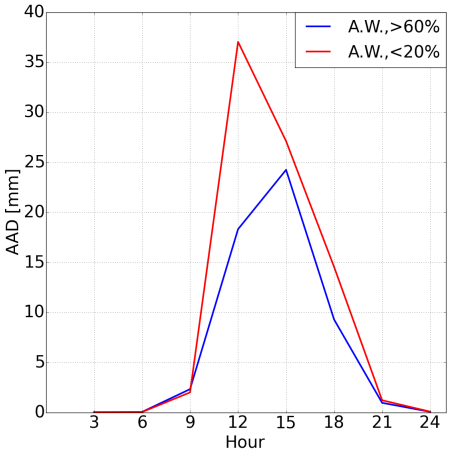


*(d) Data assimilation increments, July*

*Figure A.11: Crops (Warm temperate)*

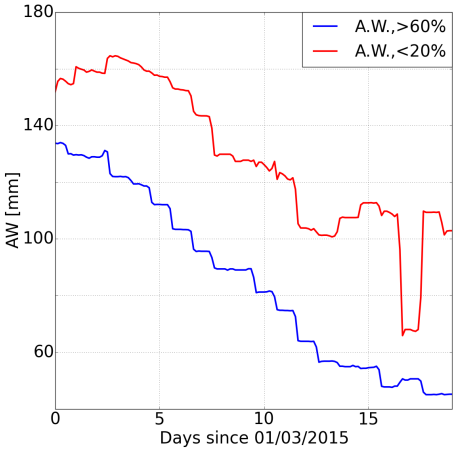


*(a) 3h-run profile, March*

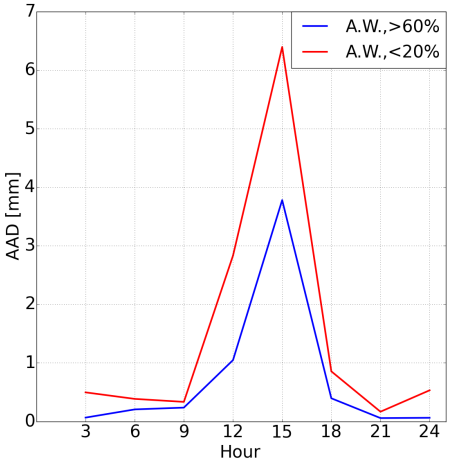


*(b) Data assimilation increments, March*

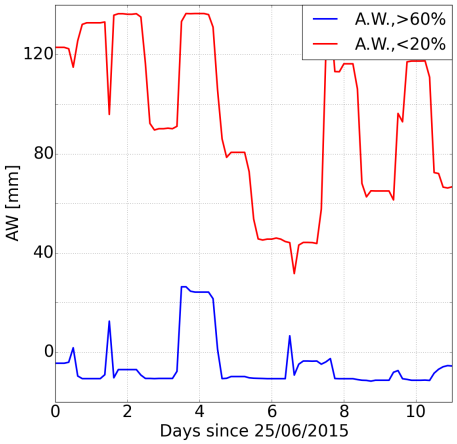


*(c) 3h-run profile, July*

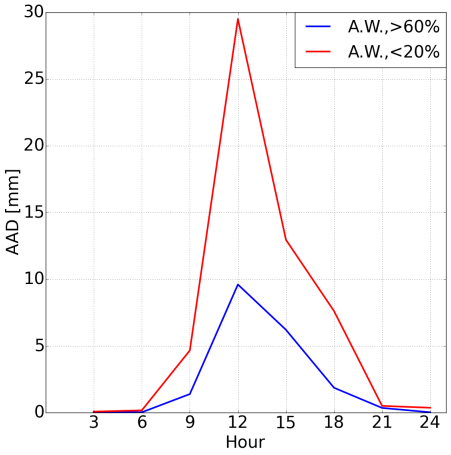


*(d) Data assimilation increments, July*

*Figure A.12: Pastures (Temperate)*

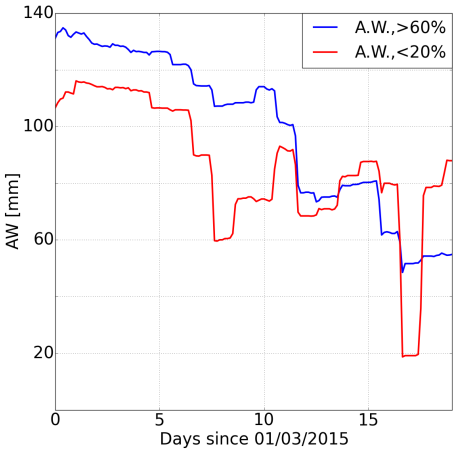


*(a) 3h-run profile, March*

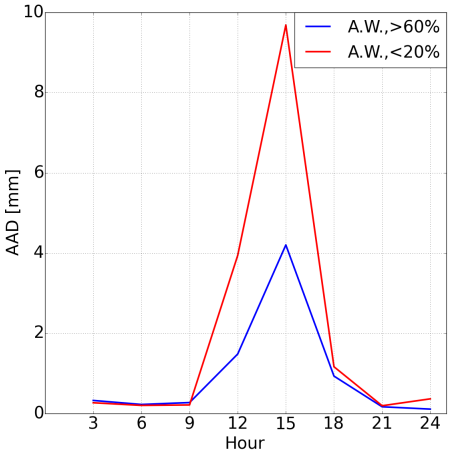


*(b) Data assimilation increments, March*

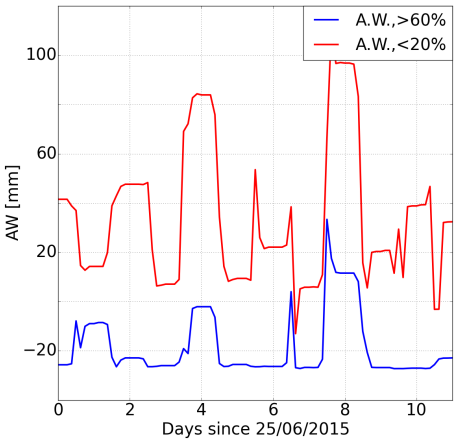


*(c) 3h-run profile, July*

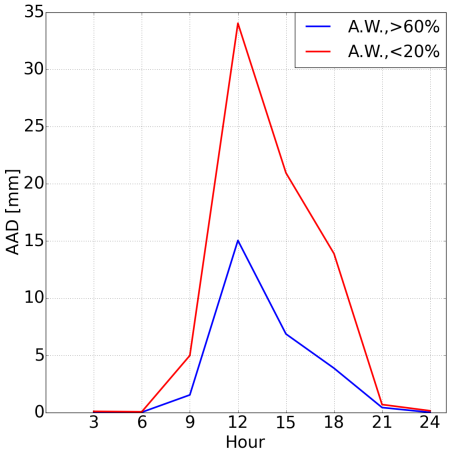


*(d) Data assimilation increments, July*

*Figure A.13: Complex cultivation pattern (Temperate)*

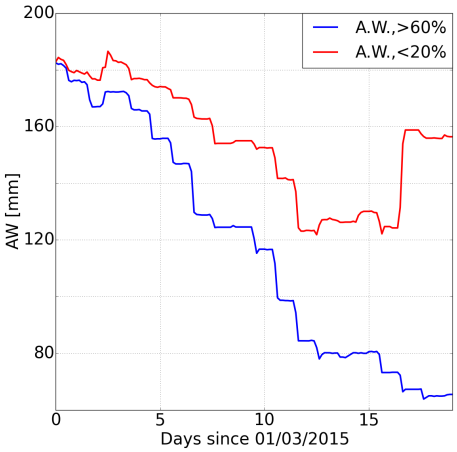


*(a) 3h-run profile, March*

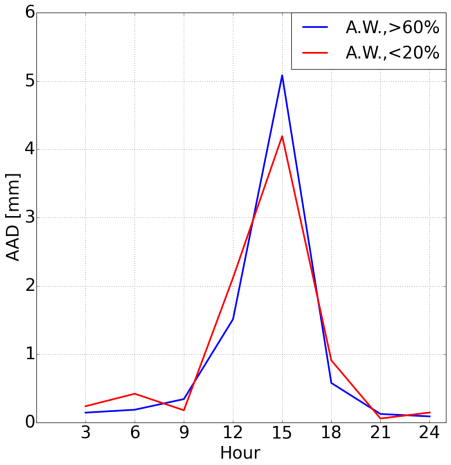


*(b) Data assimilation increments, March*

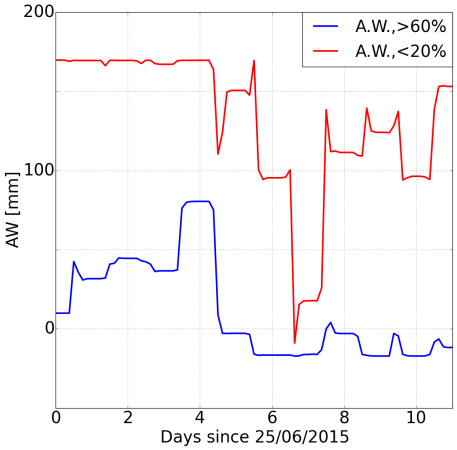


*(c) 3h-run profile, July*

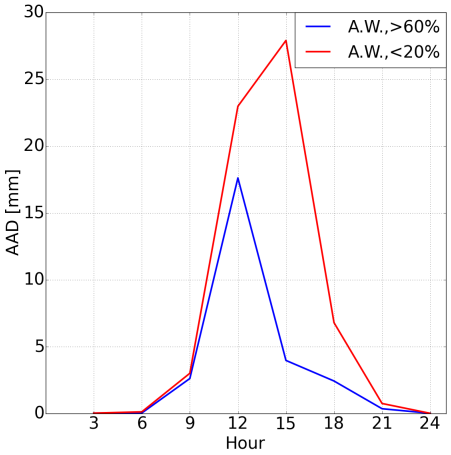


*(d) Data assimilation increments, July*

*Figure A.14: Broad-leaved forest (Temperate)*

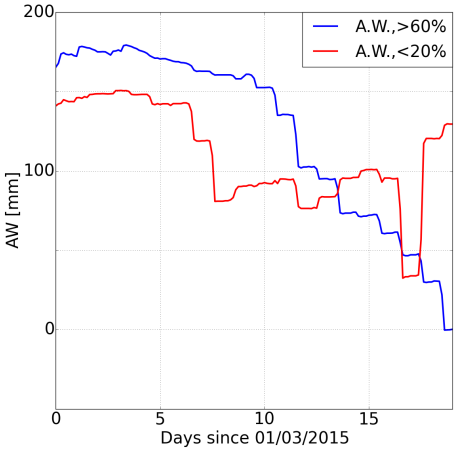


*(a) 3h-run profile, March*

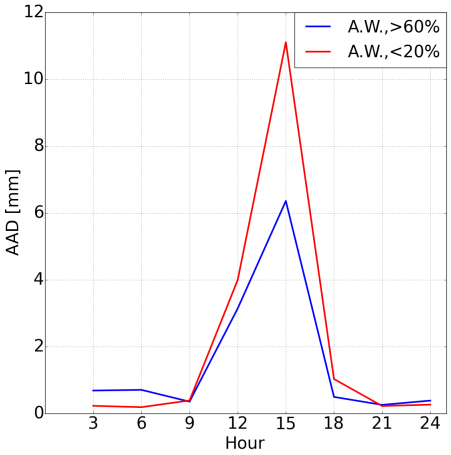


*(b) Data assimilation increments, March*

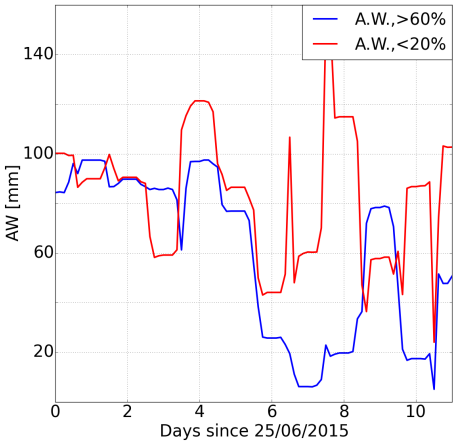


*(c) 3h-run profile, July*

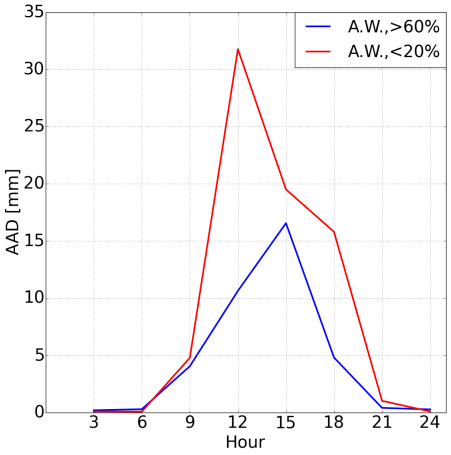


*(d) Data assimilation increments, July*

*Figure A.15: Coniferous forest (Temperate)*

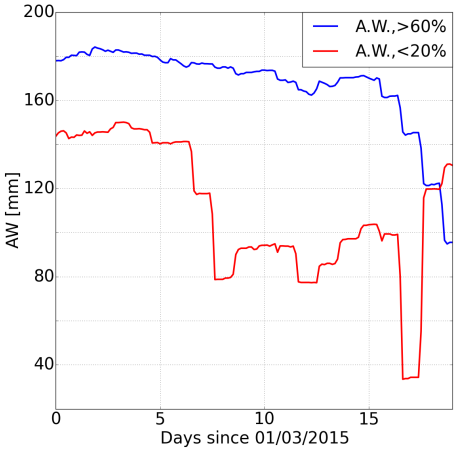


*(a) 3h-run profile, March*

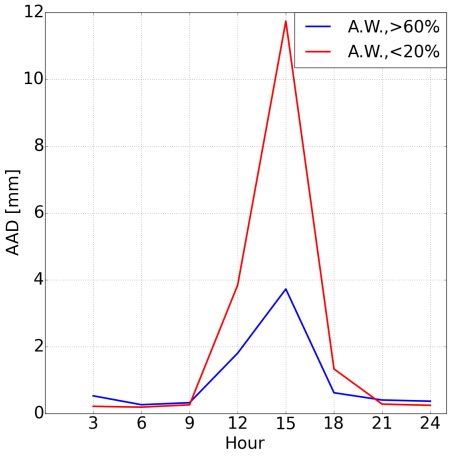


*(b) Data assimilation increments, March*

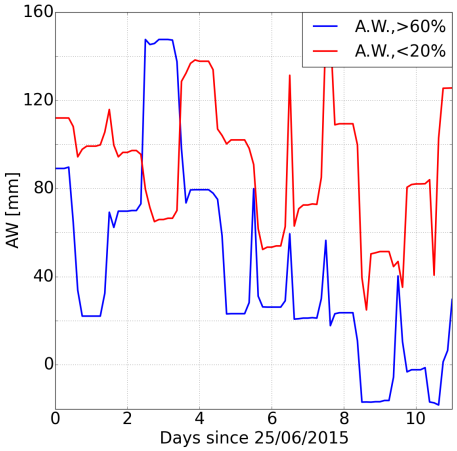


*(c) 3h-run profile, July*

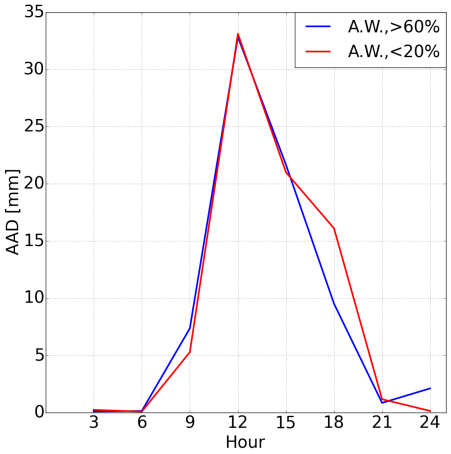


*(d) Data assimilation increments, July*

*Figure A.16: Mixed forest (Moutain)*

### A.3.2 HARMONIE38

In figures A.17-A.35, the 3h-time series and average absolute difference for the time intervals in March and July for the 19 vegetation types in HARMONIE38 are plotted. The red line corresponds with the time profile of the location where less than 20% of the days, the Bowen ratio is high (B20). The blue line represents the time profile of the location where more than 60% of the days, the Bowen ratio is high (B60).

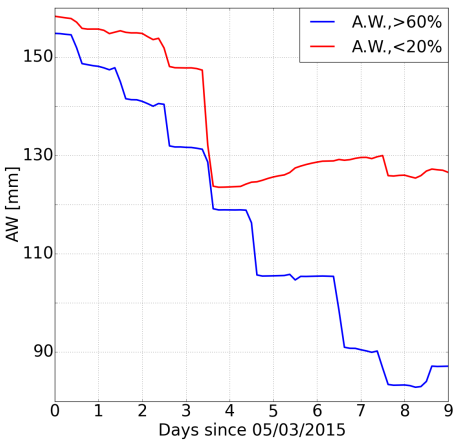


*(a) 3h-run profile, March*

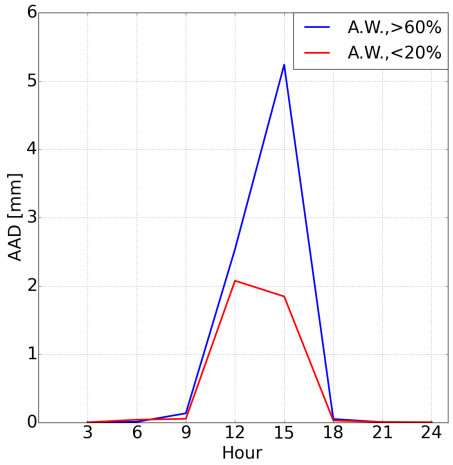


*(b) Data assimilation increments, March*

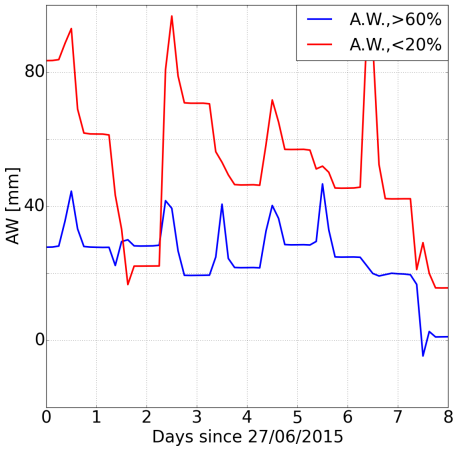


*(c) 3h-run profile, July*

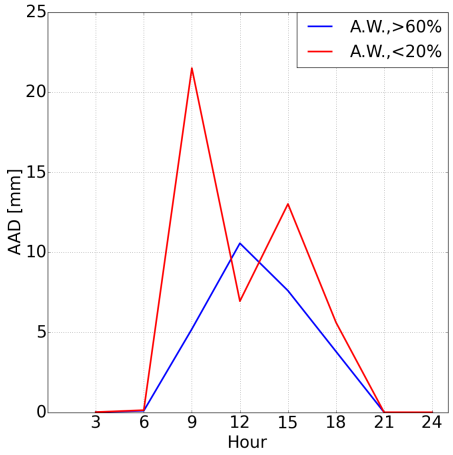


*(d) Data assimilation increments, July*

*Figure A.17: Temperate BF1*

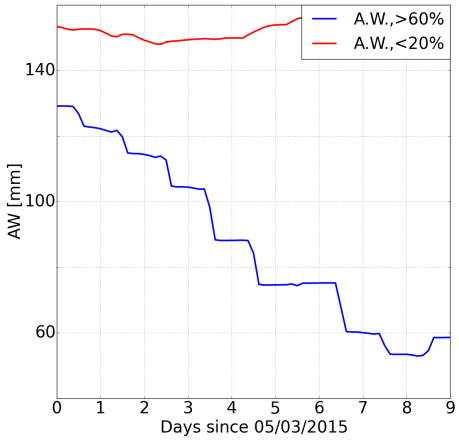


*(a) 3h-run profile, March*

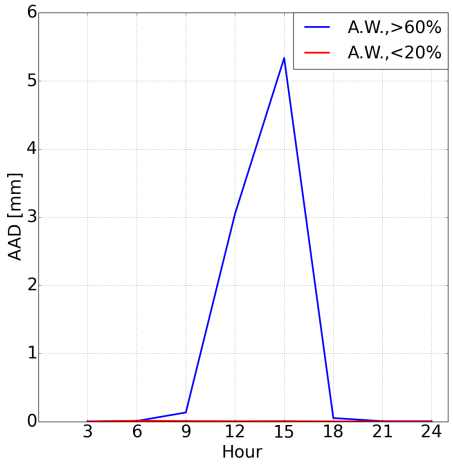


*(b) Data assimilation increments, March*

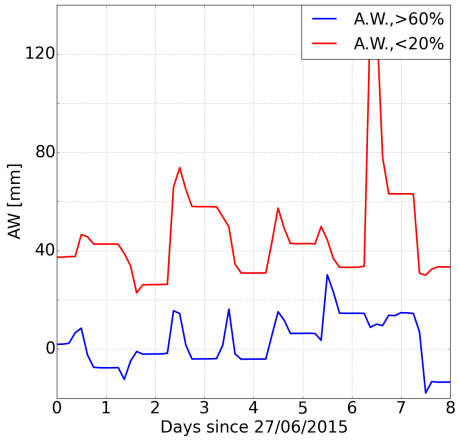


*(c) 3h-run profile, July*

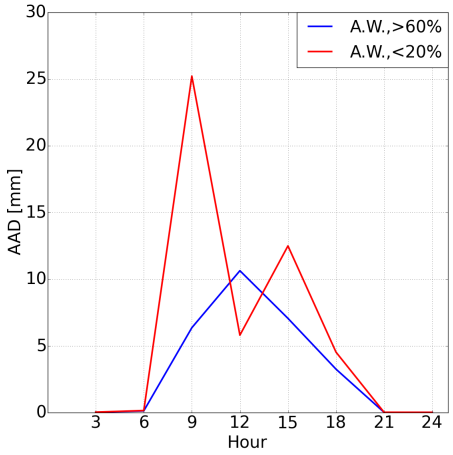


*(d) Data assimilation increments, July*

*Figure A.18: Temperate complex1*

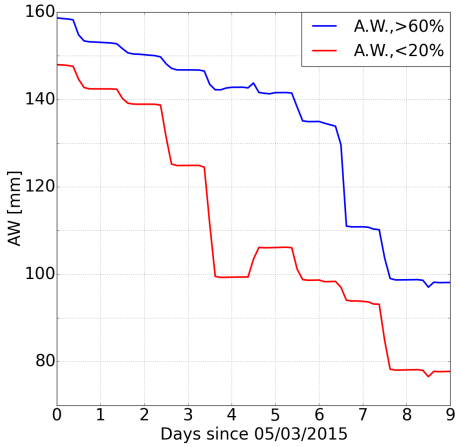


*(a) 3h-run profile, March*

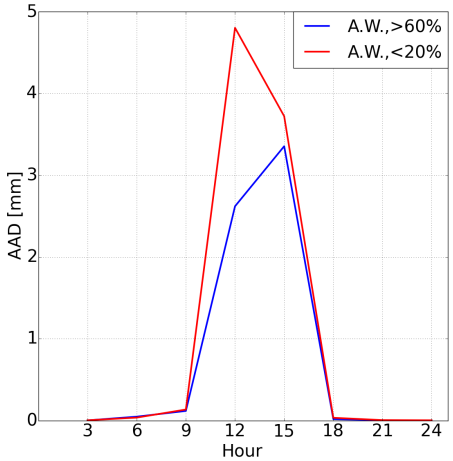


*(b) Data assimilation increments, March*

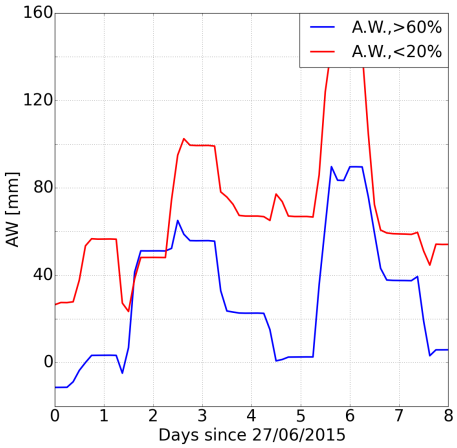


*(c) 3h-run profile, July*

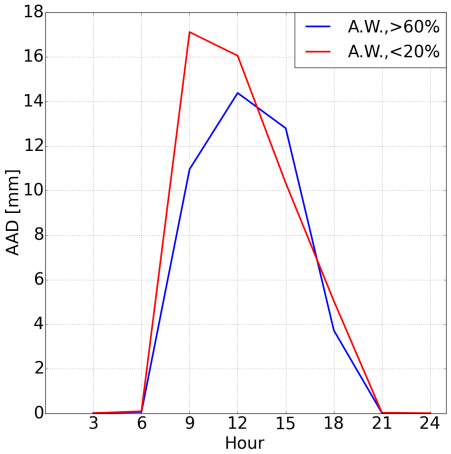


*(d) Data assimilation increments, July*

*Figure A.19: Temperate herbaceous CF1*

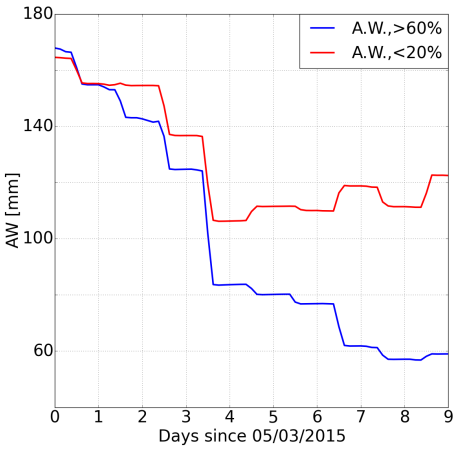


*(a) 3h-run profile, March*

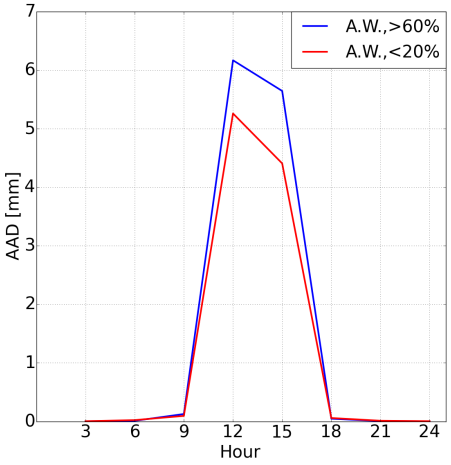


*(b) Data assimilation increments, March*

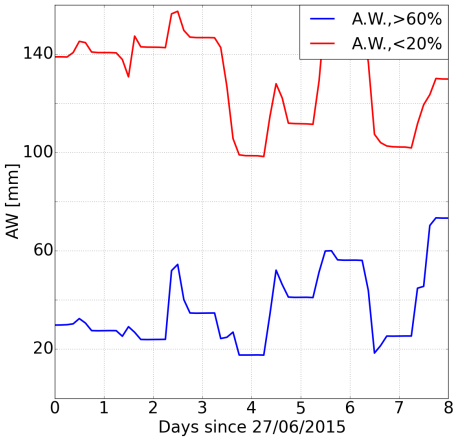


*(c) 3h-run profile, July*

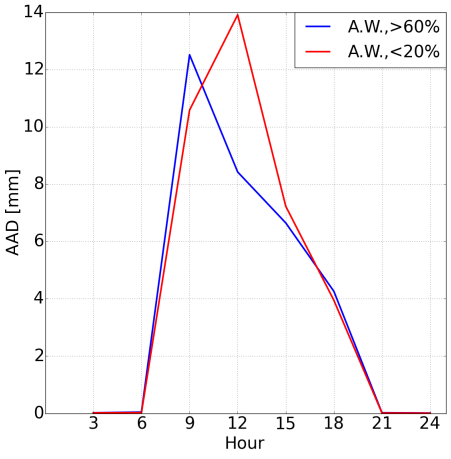


*(d) Data assimilation increments, July*

*Figure A.20: Atlantic coast BF1*

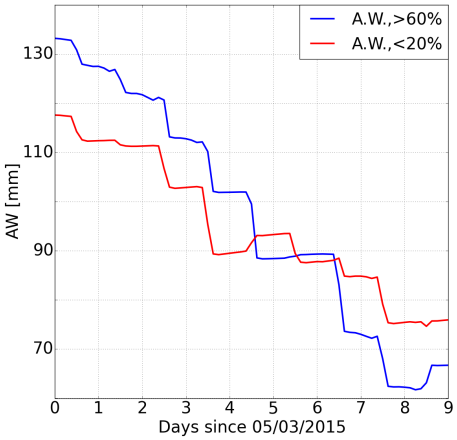


*(a) 3h-run profile, March*

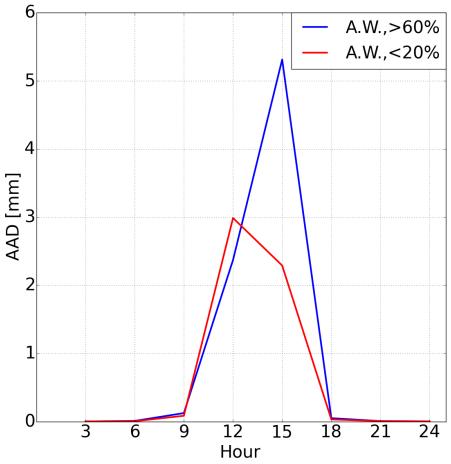


*(b) Data assimilation increments, March*

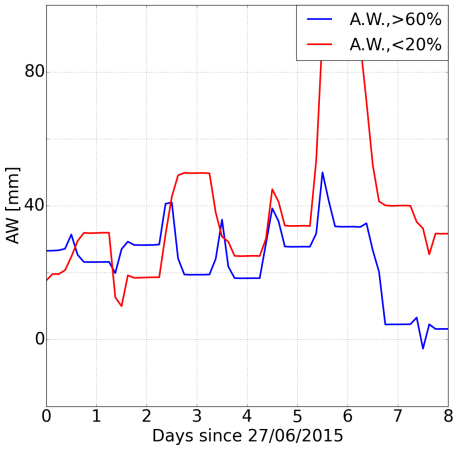


*(c) 3h-run profile, July*

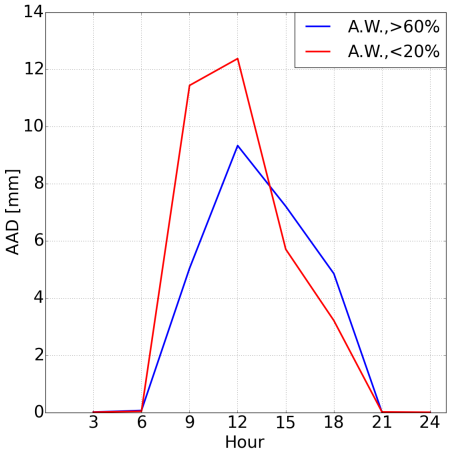


*(d) Data assimilation increments, July*

*Figure A.21: Temperate complex2*

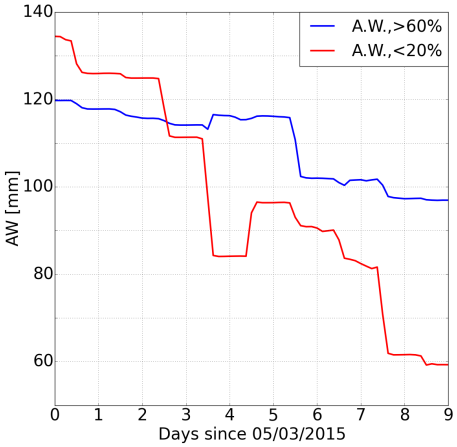


*(a) 3h-run profile, March*

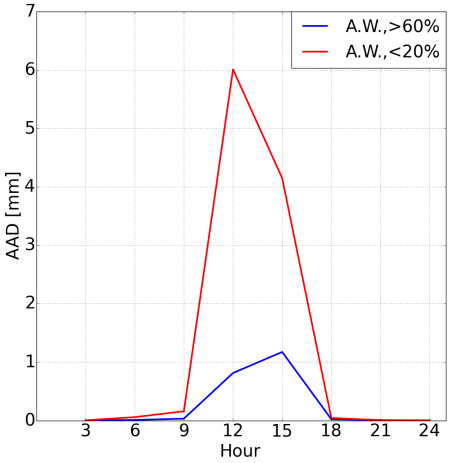


*(b) Data assimilation increments, March*

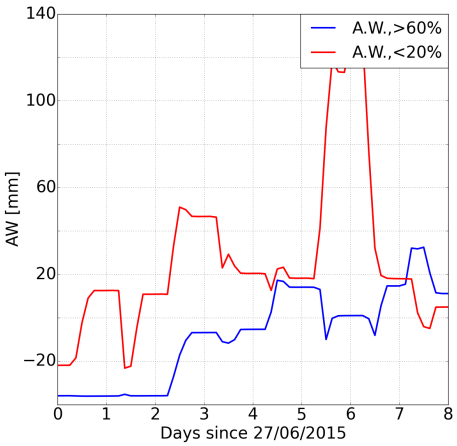


*(c) 3h-run profile, July*

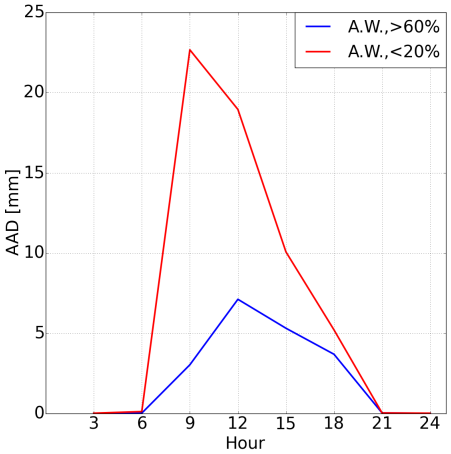


*(d) Data assimilation increments, July*

*Figure A.22: Atlantic complex3*

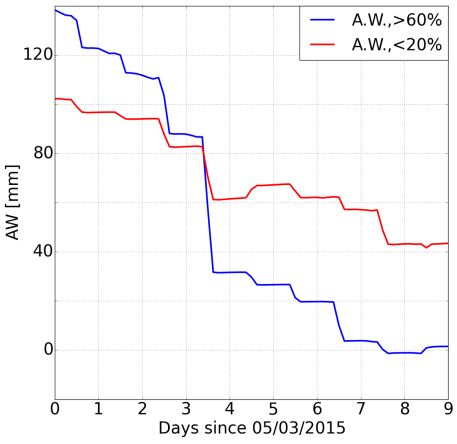


*(a) 3h-run profile, March*

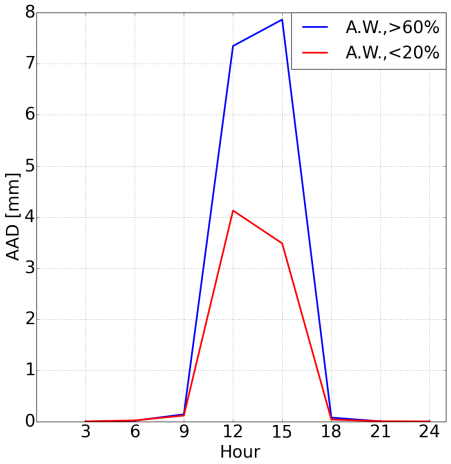


*(b) Data assimilation increments, March*

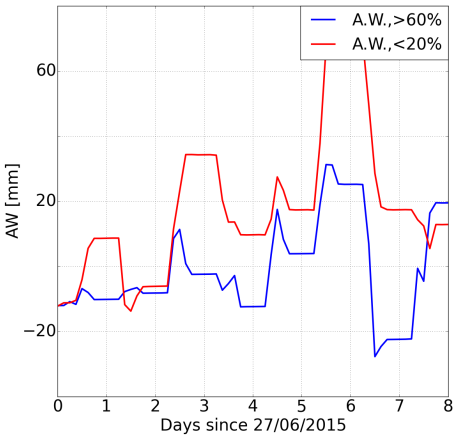


*(c) 3h-run profile, July*

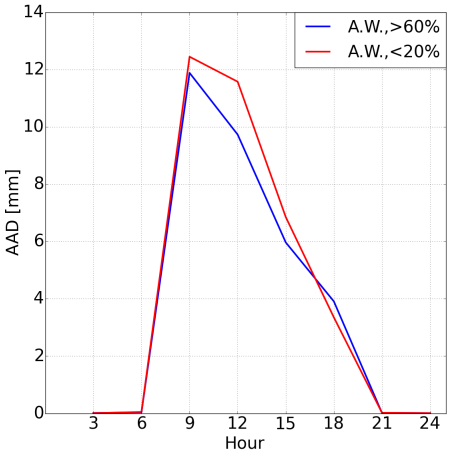


*(d) Data assimilation increments, July*

*Figure A.23: Atlantic complex4*

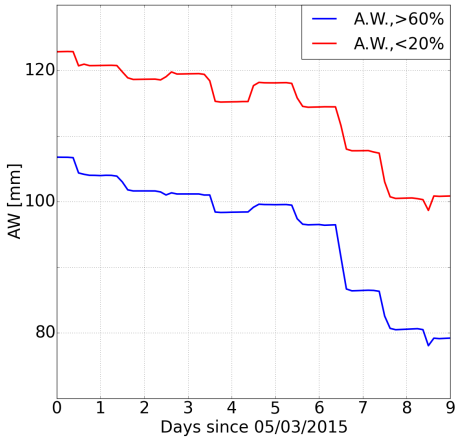


*(a) 3h-run profile, March*

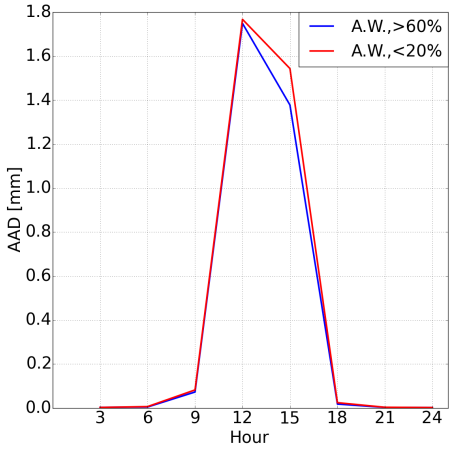


*(b) Data assimilation increments, March*

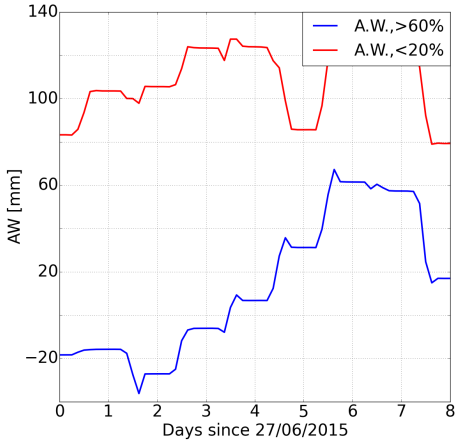


*(c) 3h-run profile, July*

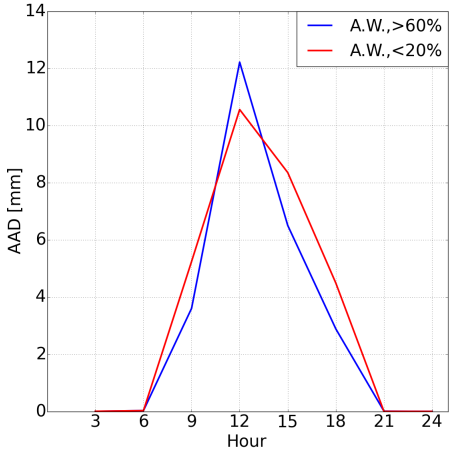


*(d) Data assimilation increments, July*

*Figure A.24: Fr med sparse crops1*

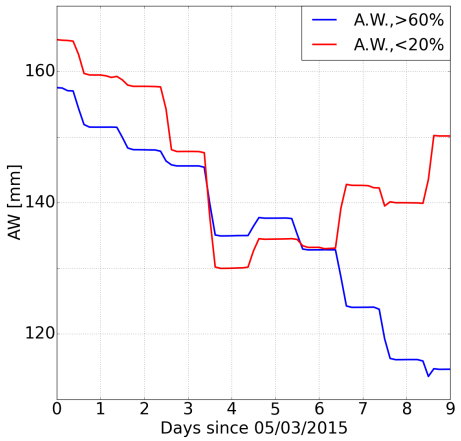


*(a) 3h-run profile, March*

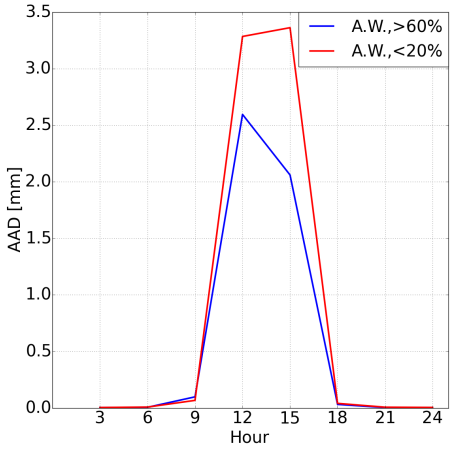


*(b) Data assimilation increments, March*

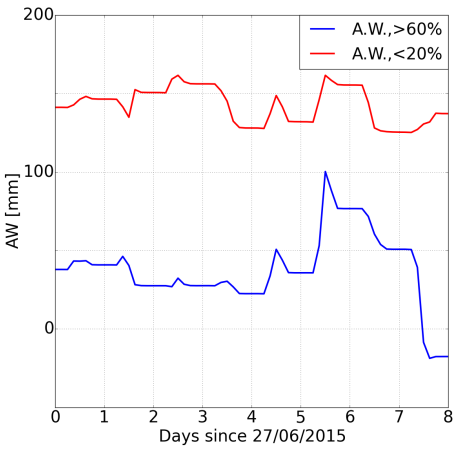


*(c) 3h-run profile, July*

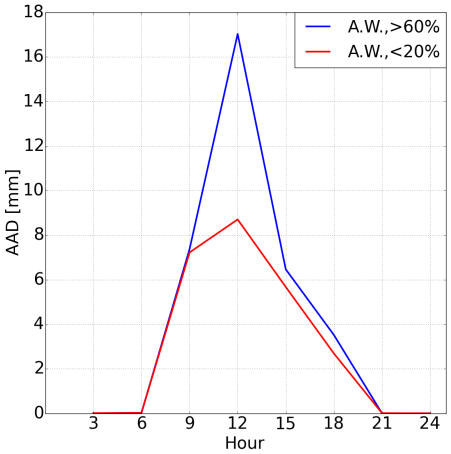


*(d) Data assimilation increments, July*

*Figure A.25: Fr med sparse crops2*

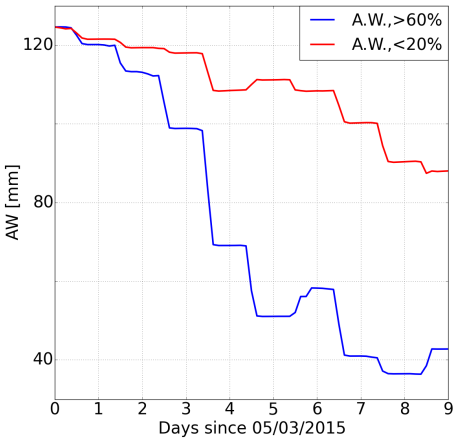


*(a) 3h-run profile, March*

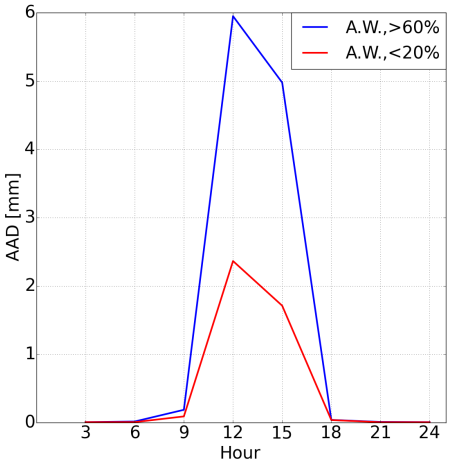


*(b) Data assimilation increments, March*

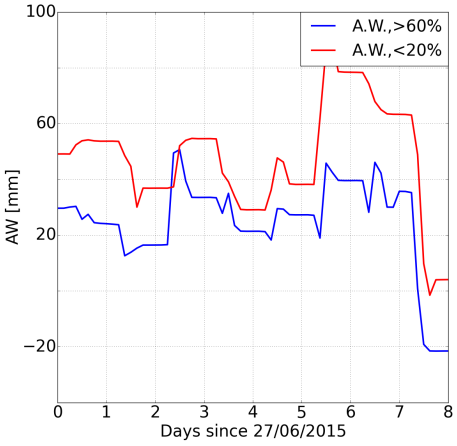


*(c) 3h-run profile, July*

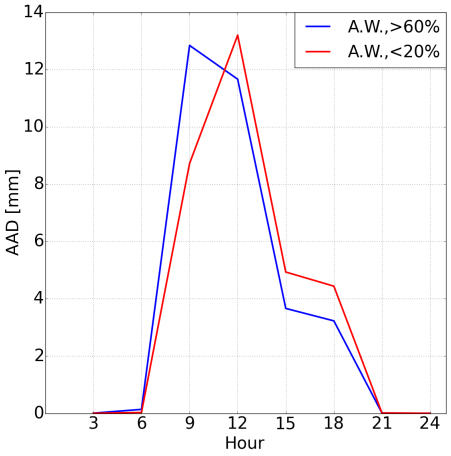


*(d) Data assimilation increments, July*

*Figure A.26: Atl med sparse crops1*

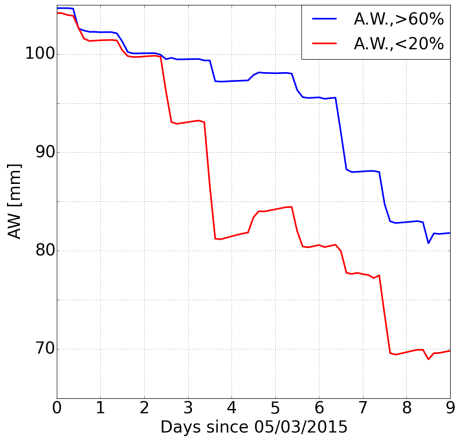


*(a) 3h-run profile, March*

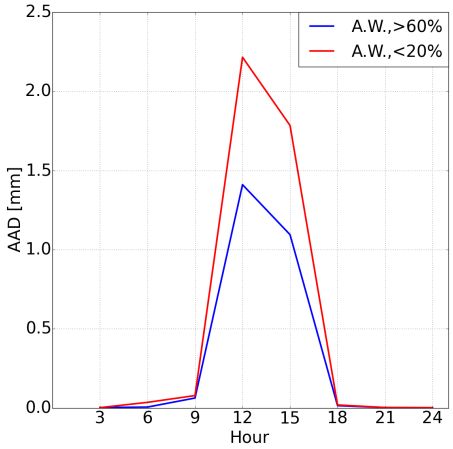


*(b) Data assimilation increments, March*

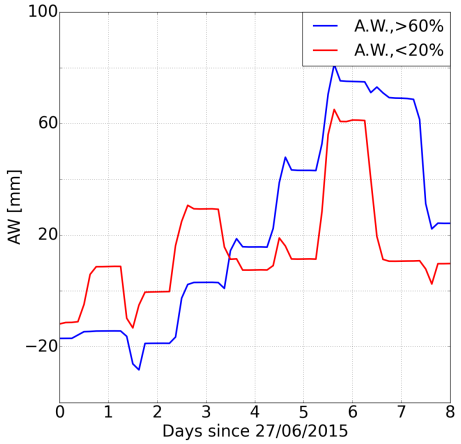


*(c) 3h-run profile, July*

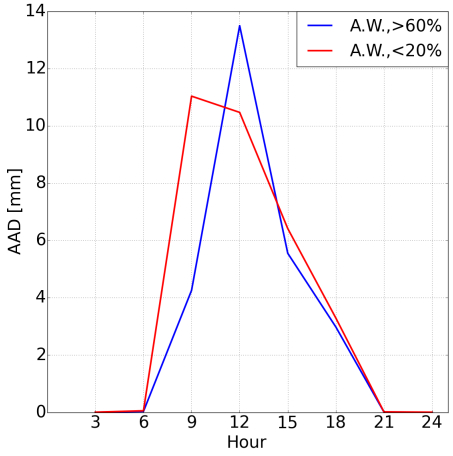


*(d) Data assimilation increments, July*

*Figure A.27: Bene black sea crops1*

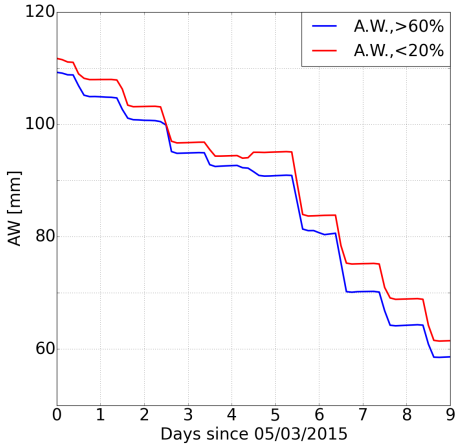


*(a) 3h-run profile, March*

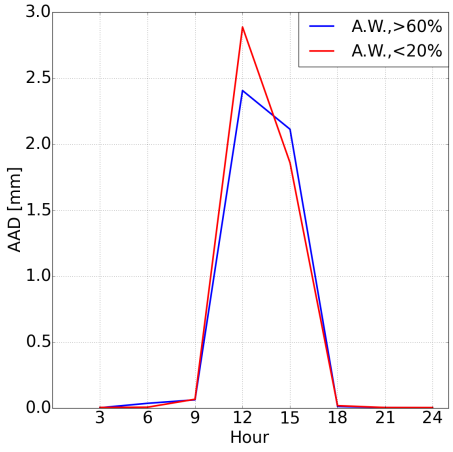


*(b) Data assimilation increments, March*

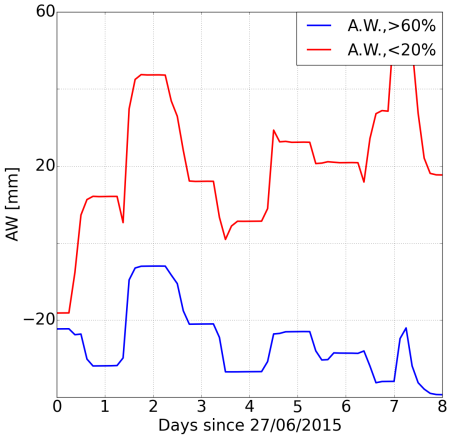


*(c) 3h-run profile, July*

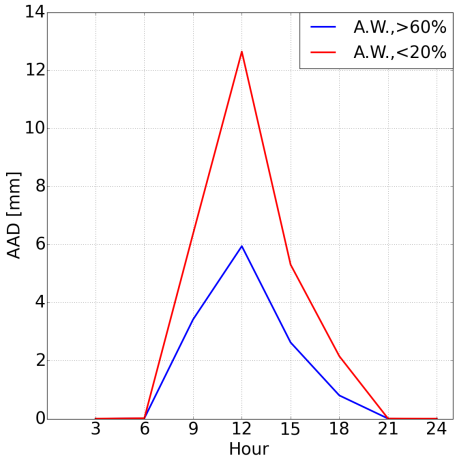


*(d) Data assimilation increments, July*

*Figure A.28: North Atlantic crops1*

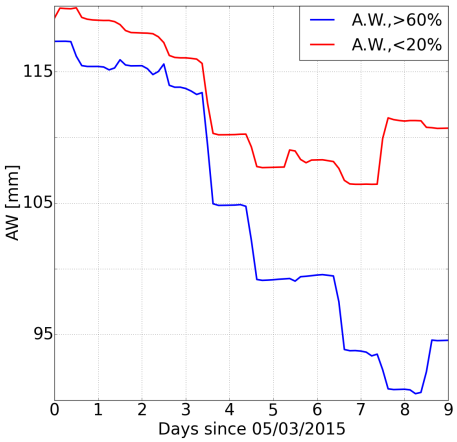


*(a) 3h-run profile, March*

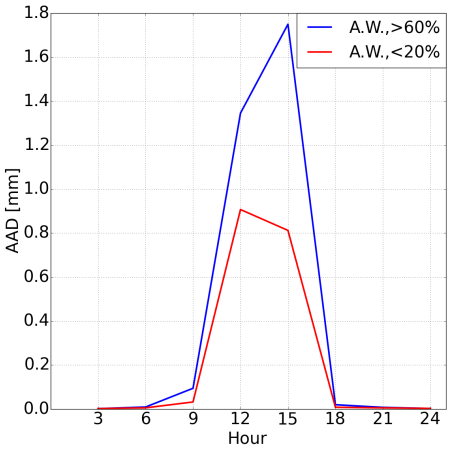


*(b) Data assimilation increments, March*

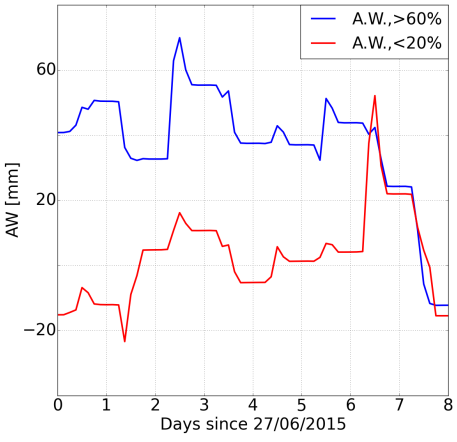


*(c) 3h-run profile, July*

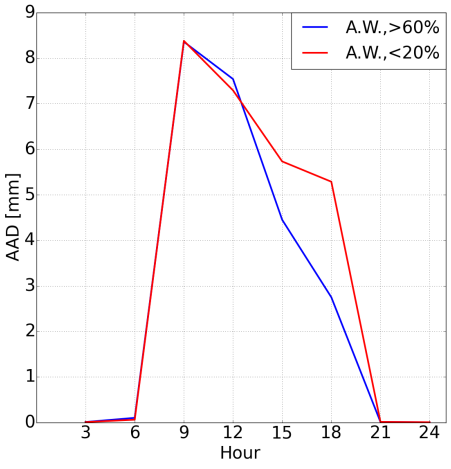


*(d) Data assimilation increments, July*

*Figure A.29: Pole crops1*

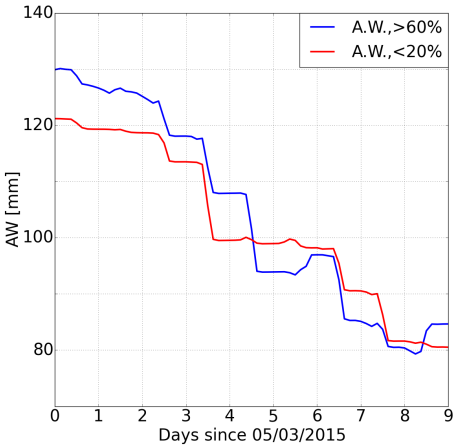


*(a) 3h-run profile, March*

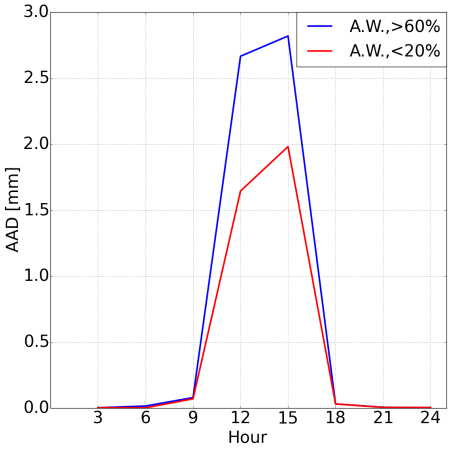


*(b) Data assimilation increments, March*

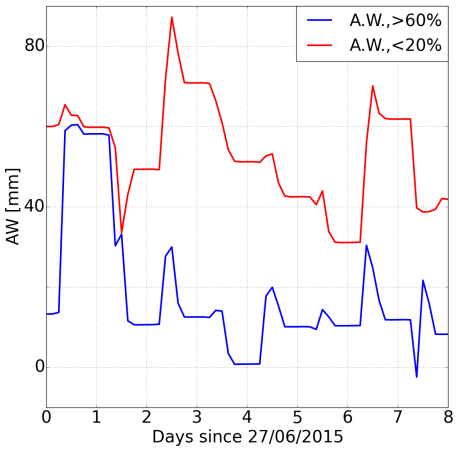


*(c) 3h-run profile, July*

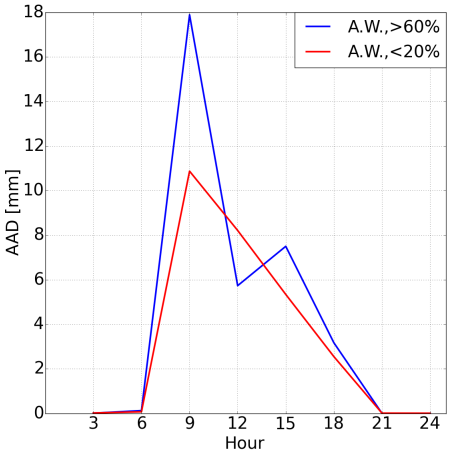


*(d) Data assimilation increments, July*

*Figure A.30: Cent EU sparse crops1*

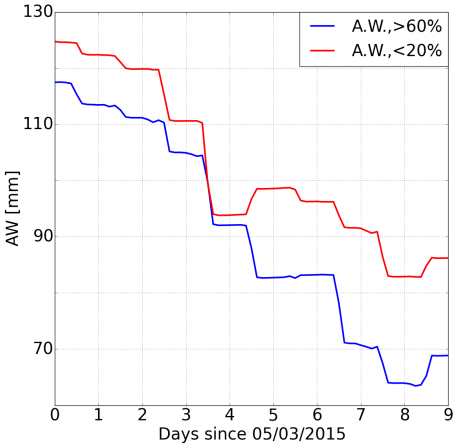


*(a) 3h-run profile, March*

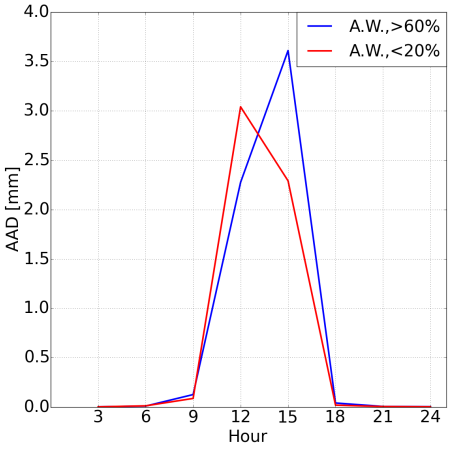


*(b) Data assimilation increments, March*

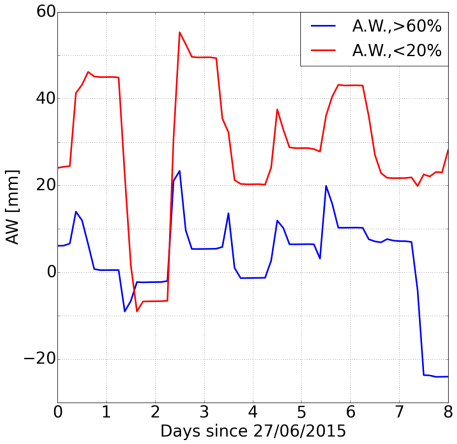


*(c) 3h-run profile, July*

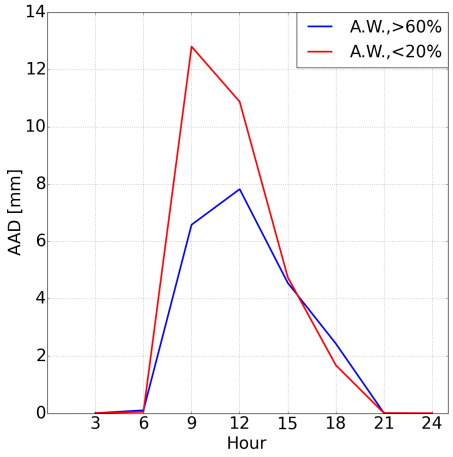


*(d) Data assimilation increments, July*

*Figure A.31: German crops1*

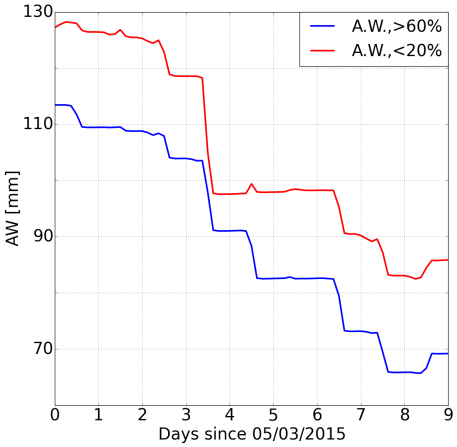


*(a) 3h-run profile, March*

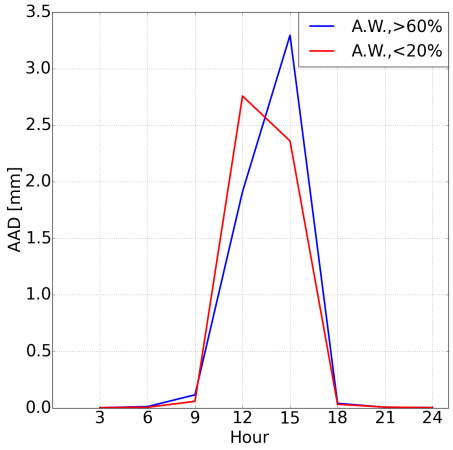


*(b) Data assimilation increments, March*

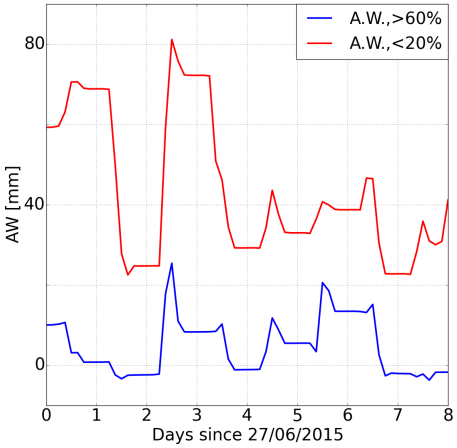


*(c) 3h-run profile, July*

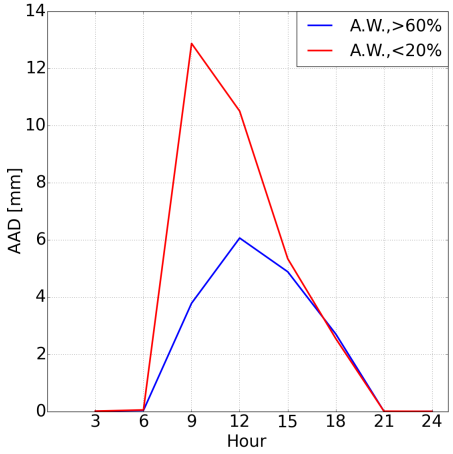


*(d) Data assimilation increments, July*

*Figure A.32: Beauce crops1*

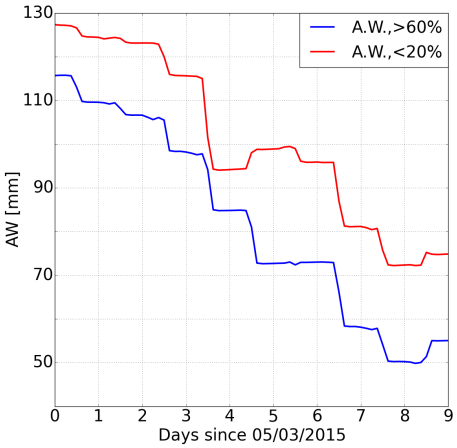


*(a) 3h-run profile, March*

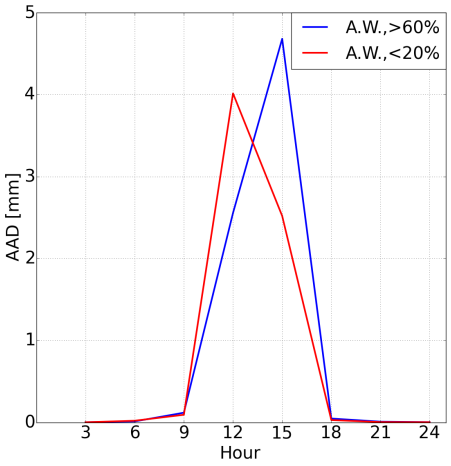


*(b) Data assimilation increments, March*

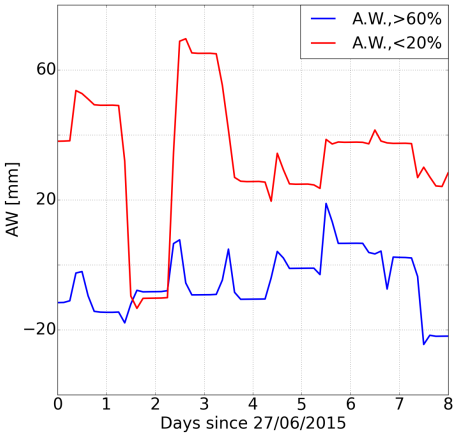


*(c) 3h-run profile, July*

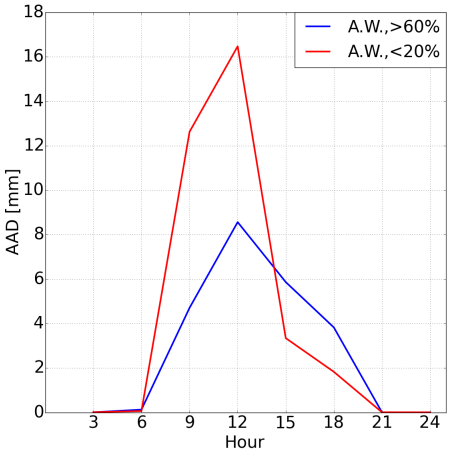


*(d) Data assimilation increments, July*

*Figure A.33: Neu Atl sparse crops1*

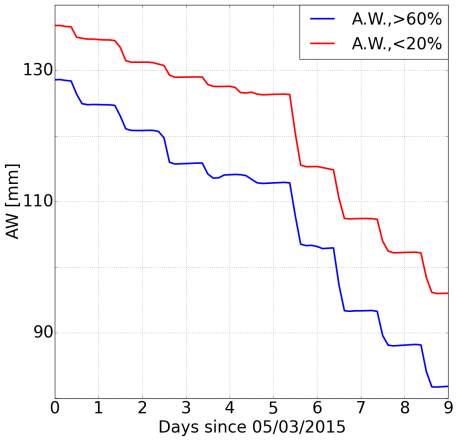


*(a) 3h-run profile, March*

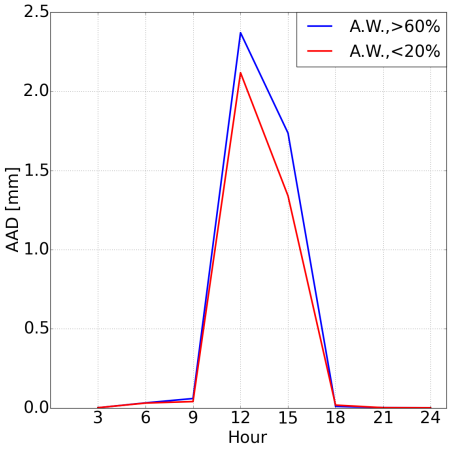


*(b) Data assimilation increments, March*

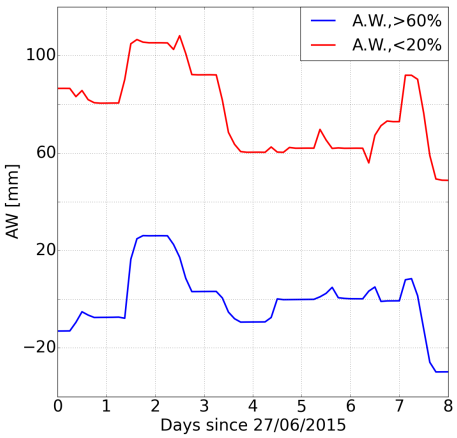


*(c) 3h-run profile, July*

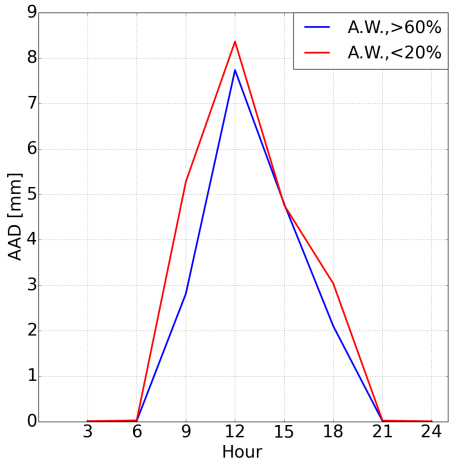


*(d) Data assimilation increments, July*

*Figure A.34: Channel crops1*

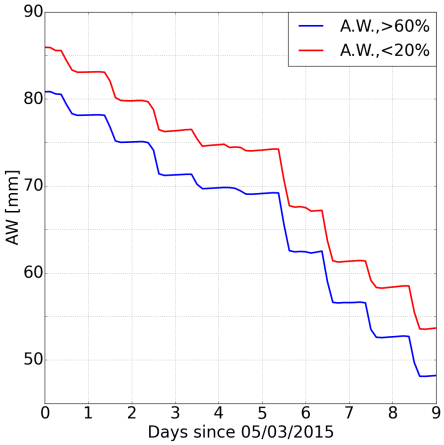


*(a) 3h-run profile, March*

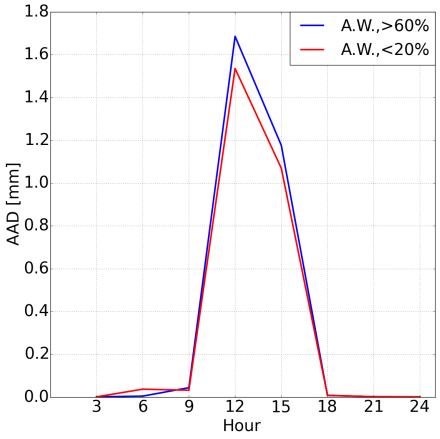


*(b) Data assimilation increments, March*

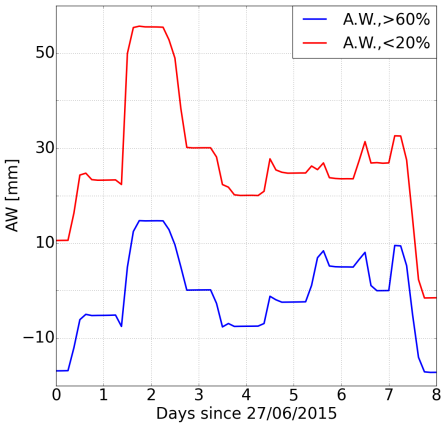


*(c) 3h-run profile, July*

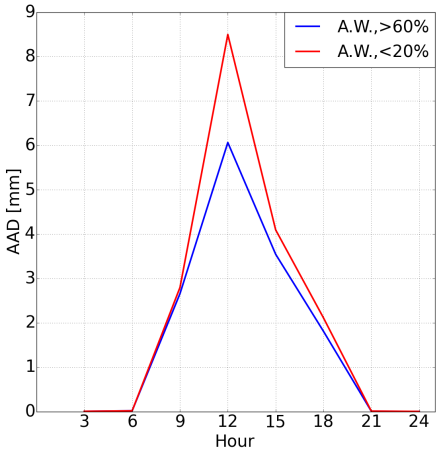


*(d) Data assimilation increments, July*

*Figure A.35: Channel crops2*

## A.4 Experiments in HARMONIE38

### A.4.1 Evapotranspiration rates

Figure A.36 shows the average evapotranspiration rate per day per grid point for all experiments in March and July. These evapotranspiration rates are calculated as

$$AER(t) = \frac{\sum_n \sum_m \left(AW^{+0h}(t-1)_n(m) - AW^{+3h}(t-1)_n(m)\right)}{n \cdot m} \tag{22}$$

With $n$ the number of days and $m$ the number of land grid points. Note that in large parts of the domain, average evapotranspiration rates will be higher than portrayed in figure A.36. This is due to the fact that the average is taken over the whole domain, whilst there are regions where (too) little evapotranspiration is taking place: these areas are indicated in blue in figures 18, A.41, 21 and 28. Soil moisture losses during the night are due to drainage and/or possible refreezing of soil moisture.

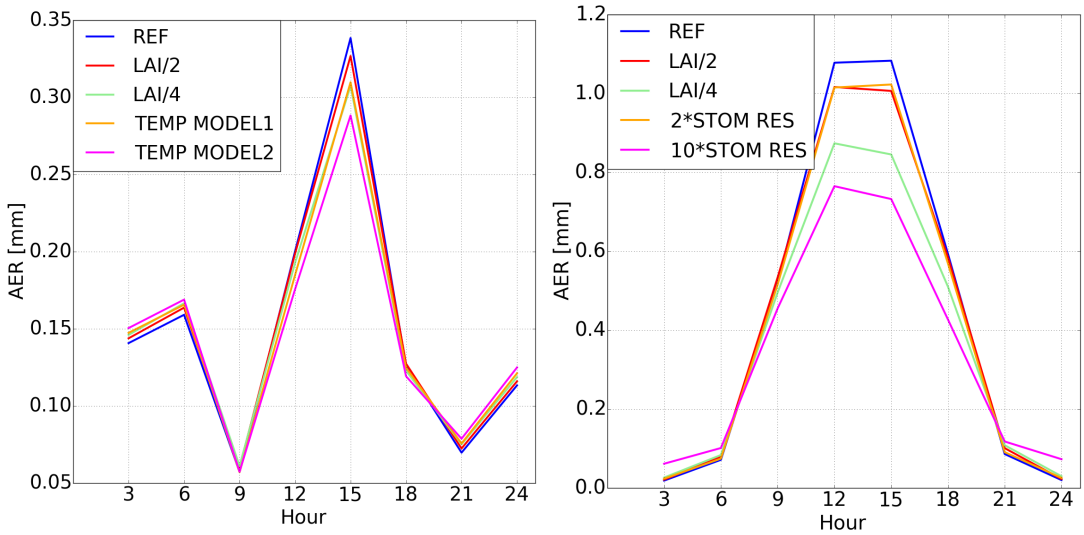


*(a) March* *(b) July*

*Figure A.36: Average evapotranspiration rates (AER) per grid point per day for all experiments conducted in the March and July time series. Evapotranspiration rates are calculated as in equation 22.*

### A.4.2 Mean and standard deviations

Figures A.37 - A.40 show the mean and standard deviation for every experiment discussed in section 4. For every experiment, the time period is 5 March 00:00 UTC - 13 March 2015 21:00 UTC.

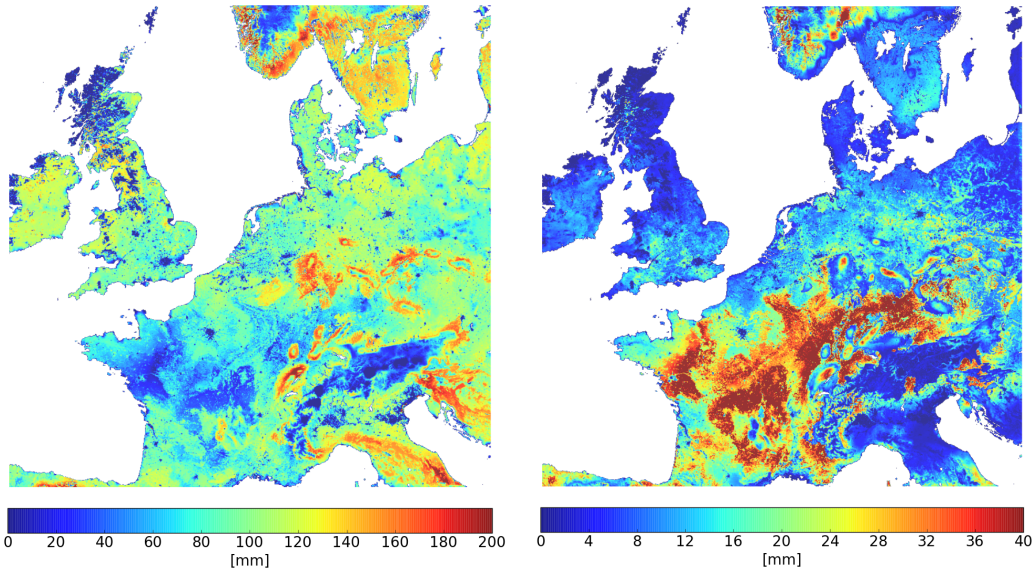


*(a) Mean* *(b) Standard deviation*

*Figure A.37: Reference run*

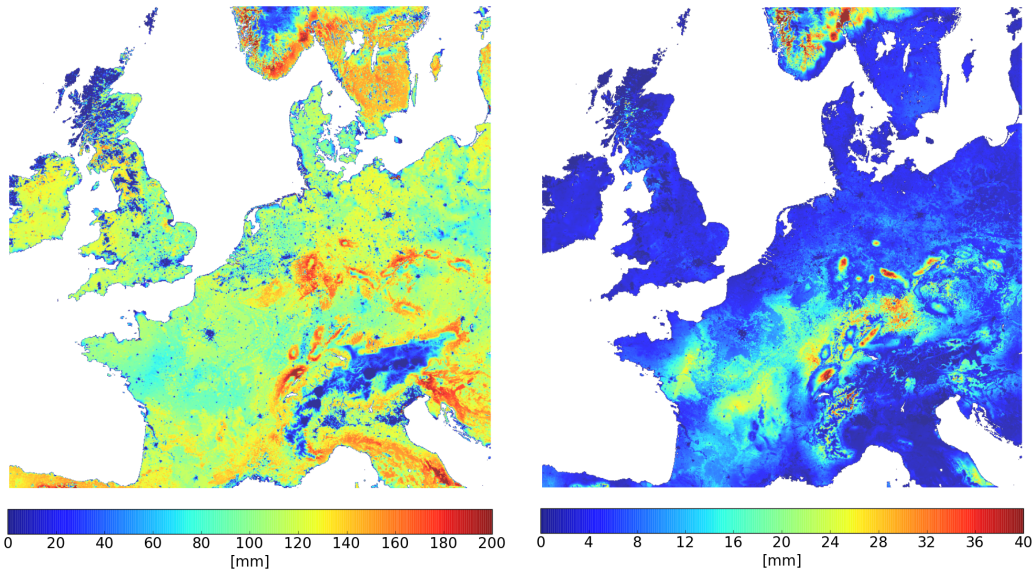


*(a) Mean* *(b) Standard deviation*

*Figure A.38: Experiment 2 - LAI/4*

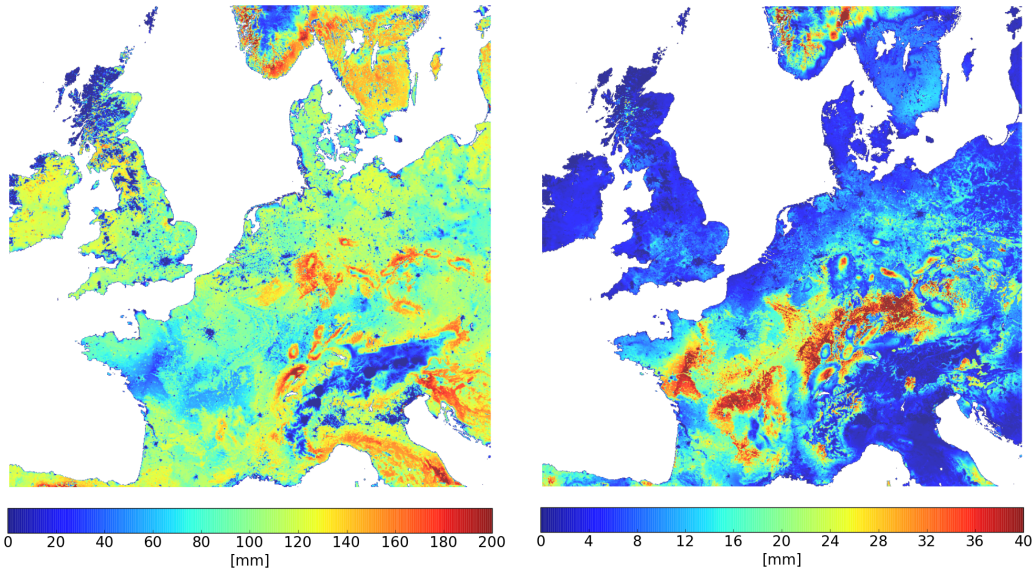


*(a) Mean* *(b) Standard deviation*

*Figure A.39: Temperature model 1*

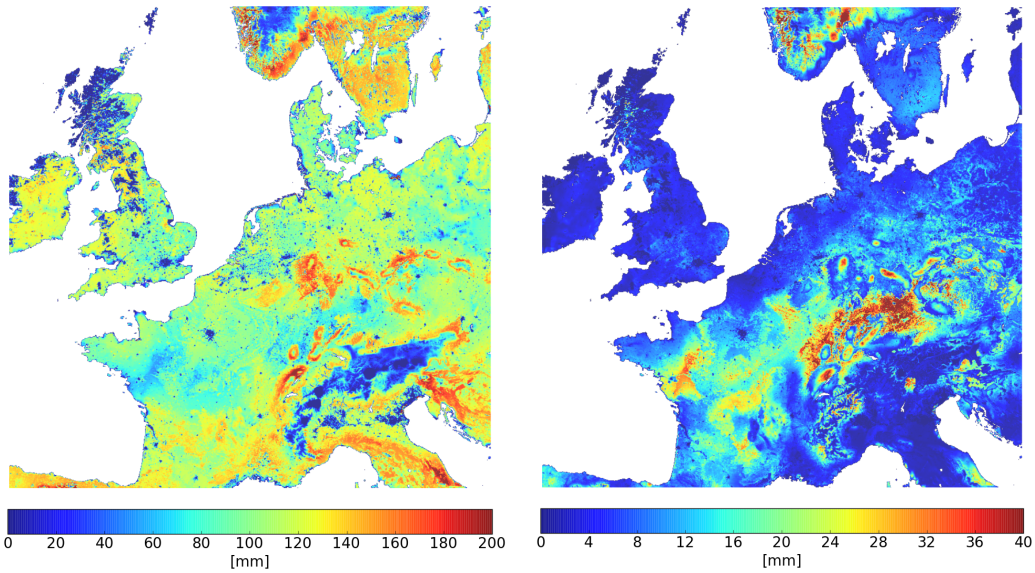


*(a) Mean* *(b) Standard deviation*

*Figure A.40: Temperature model 2.*

## A.5 Results for experiment 2 - LAI/2

Figures A.41 - A.43 represent the difference in available water in March and the mean and standard deviations in March and July for experiment 1 - LAI/2.

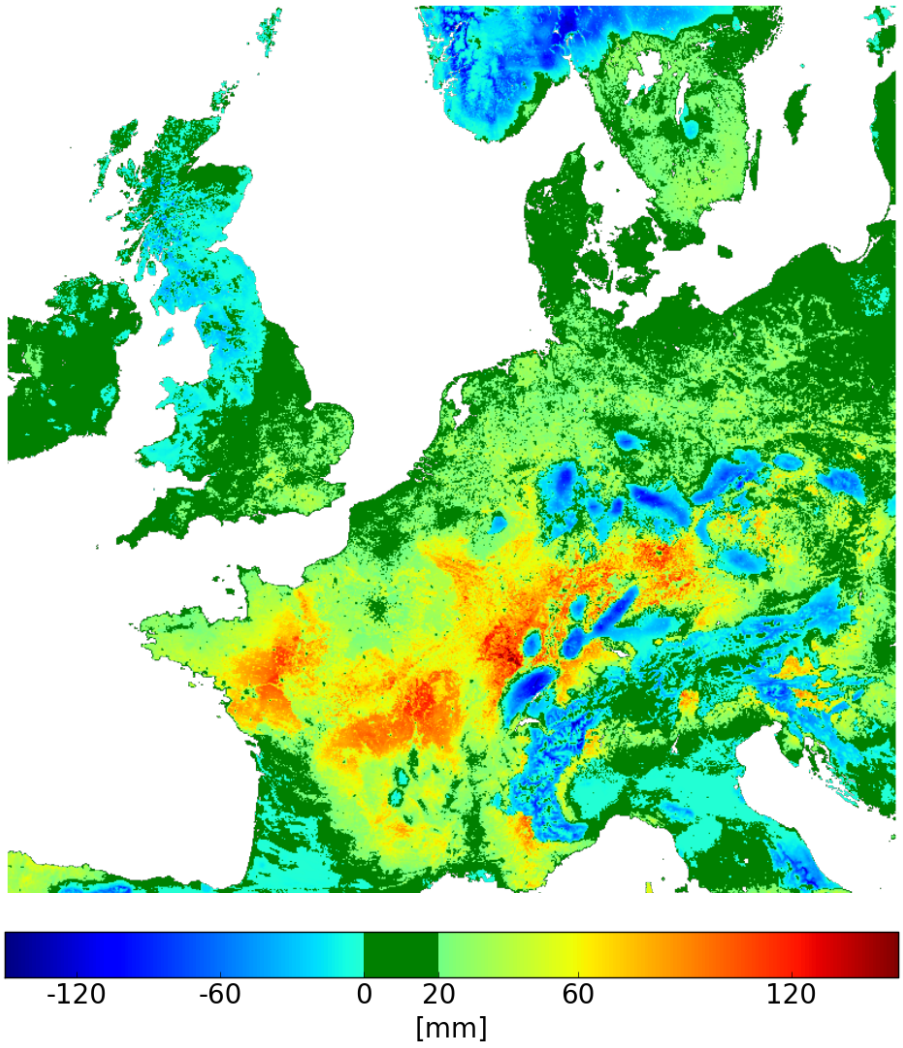


*Figure A.41: Difference in available water between 5 March 00:00 UTC and 13 March 2015 21:00 UTC*

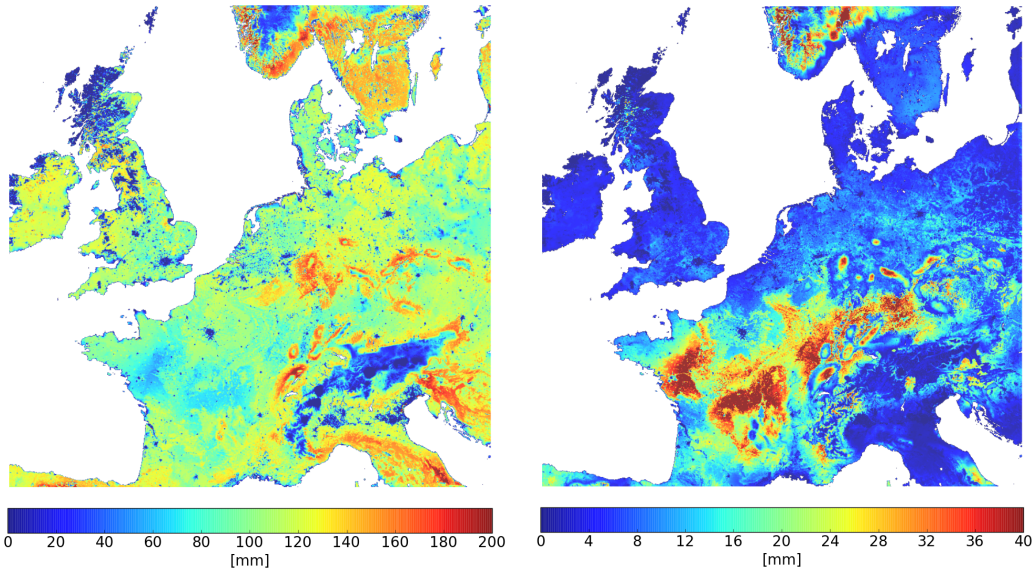


*(a) Mean* *(b) Standard deviation*

*Figure A.42: Mean available water and standard deviation in March.*

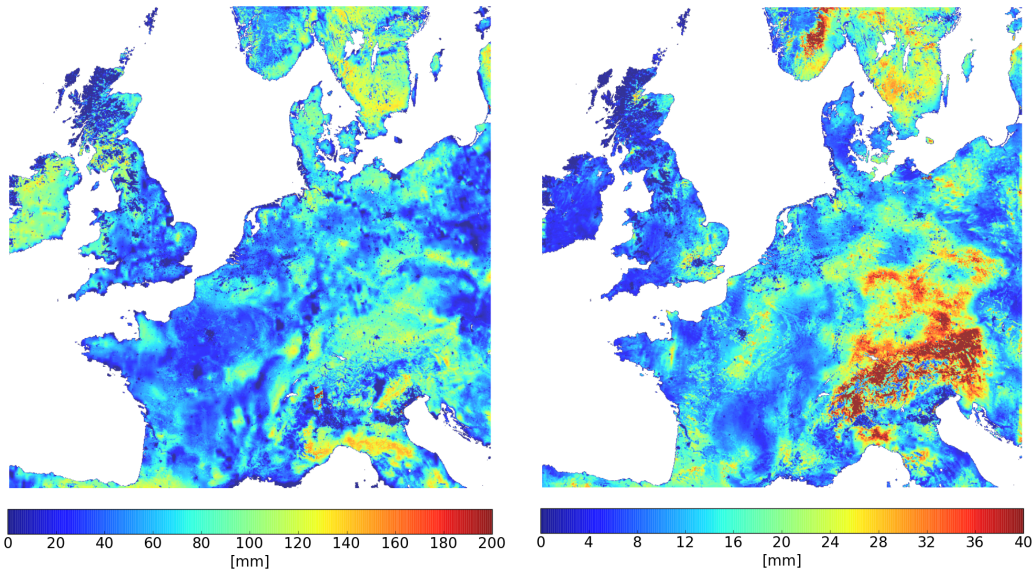


*(a) Mean available water* *(b) Standard deviation*

*Figure A.43: Mean available water and standard deviation in July.*

## A.6 $f_{LAI}$ values in both temperature models

Figures A.44 and A.45 represent the $f_{LAI}$ values at 12:00 UTC in the time interval 5 March - 13 March 2015 of Temperature model 1 and 2, respectively.

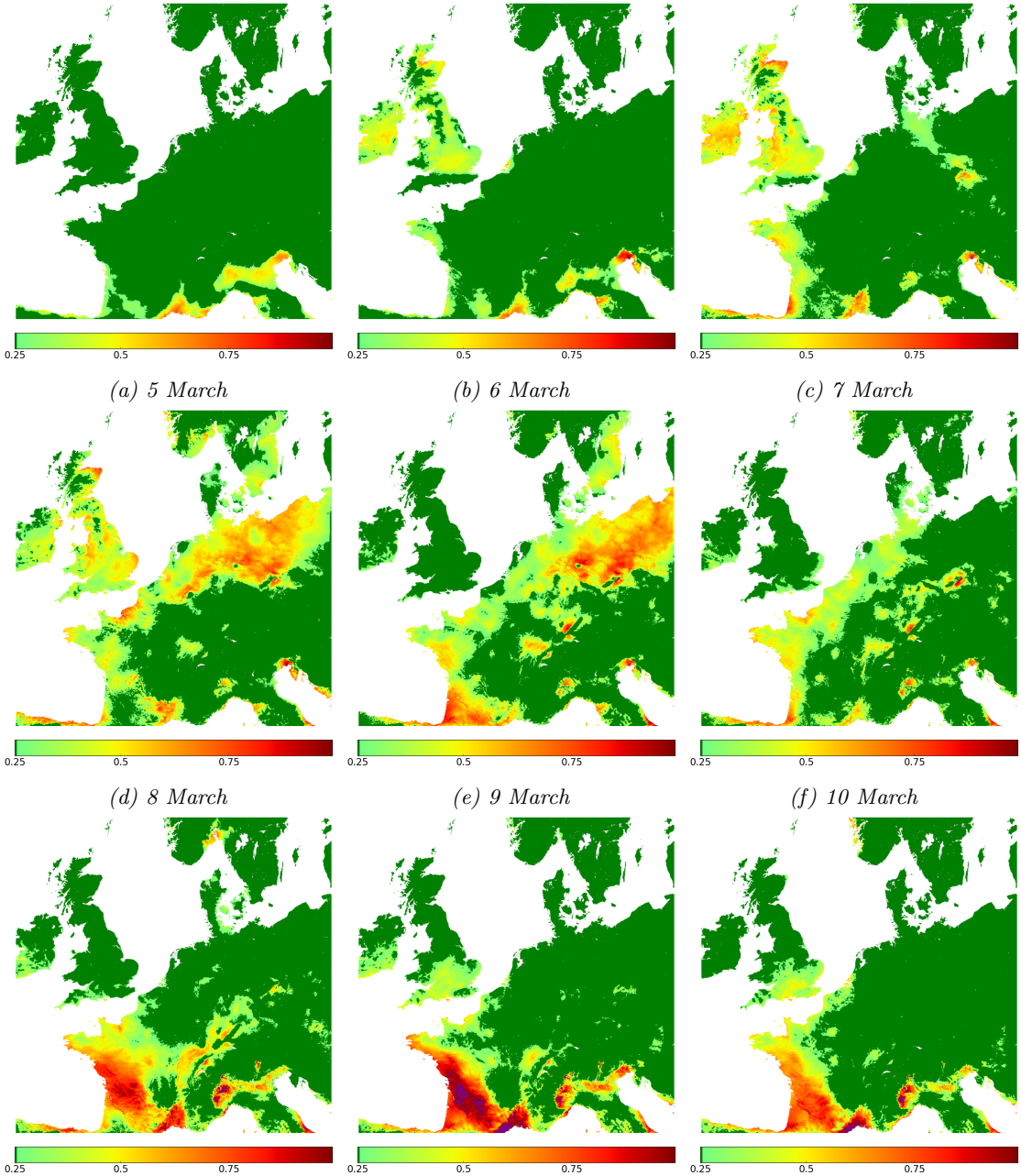


*(a) 5 March* *(b) 6 March* *(c) 7 March*

*(d) 8 March* *(e) 9 March* *(f) 10 March*

*(g) 11 March* *(h) 12 March* *(i) 13 March*

*Figure A.44: $f_{LAI}$ values at 12:00 UTC for Temperature model 1. Solid green areas indicate $f_{LAI}$ values of 0.25, purple areas $f_{LAI}$ values of 1.*

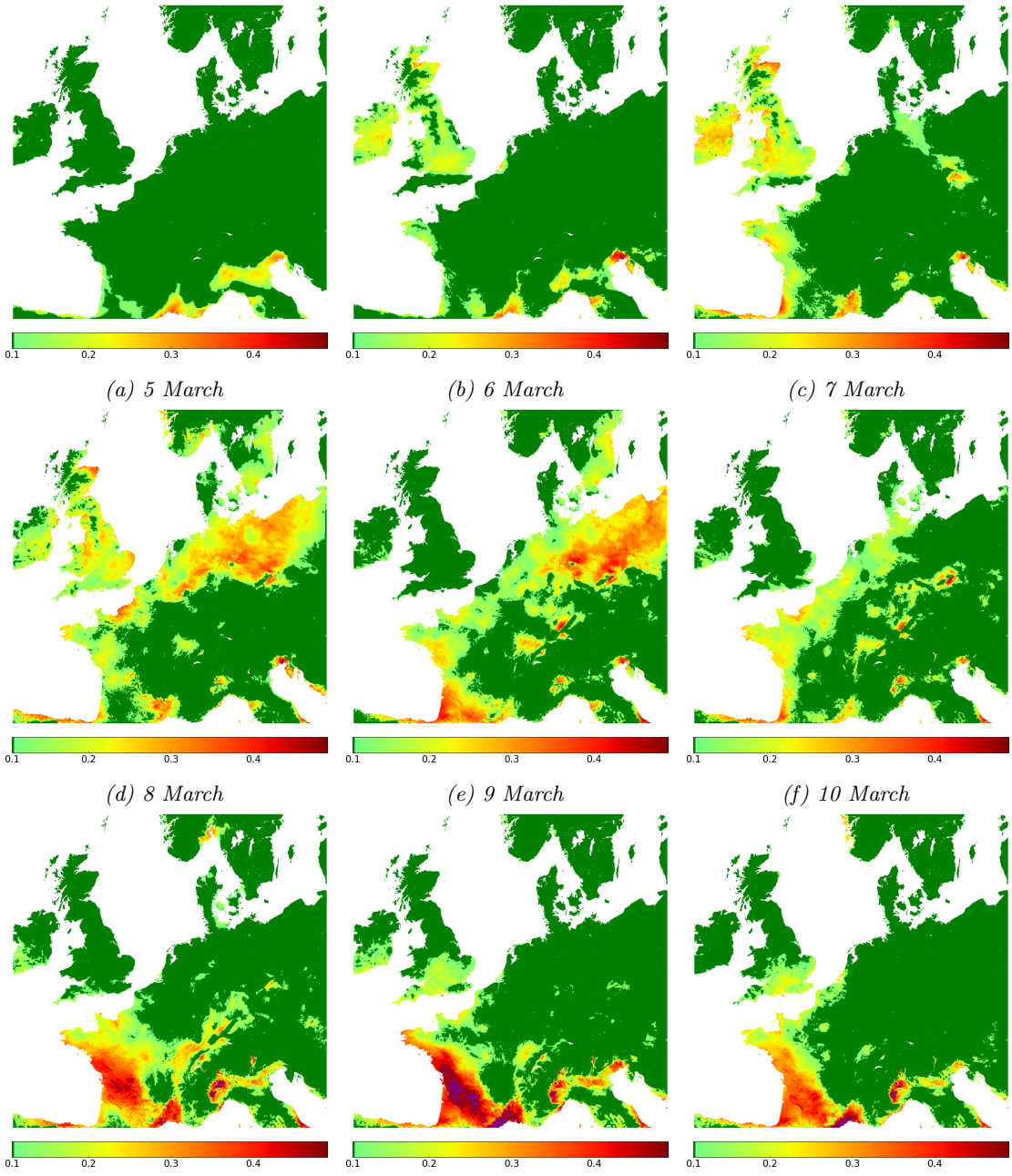


*(a) 5 March* *(b) 6 March* *(c) 7 March*

*(d) 8 March* *(e) 9 March* *(f) 10 March*

*(g) 11 March* *(h) 12 March* *(i) 13 March*

*Figure A.45: $f_{LAI}$ values at 12:00 UTC for Temperature model 2. Solid green areas indicate $f_{LAI}$ values of 0.1, purple areas $f_{LAI}$ values of 0.5.*

# References


Bhumralkar, C. (1975). Numerical experiments on the computation of ground surface temperature in an atmospheric general circulation model. *Journal of Applied Meteorology*, *14*(7), 1246–1258.

Blackadar, A. (1976). Modeling the nocturnal boundary layer. *Third Symposium on Atmospheric Turbulence, Diffusion and Air Quality*, 46–49.

Boone, A., Calvet, J., & Noilhan, J. (1999). Inclusion of a third soil layer in a land surface scheme using the force-restore method. *Journal of Applied Meteorology*, *38*(11), 1611–1630.

Butt, N., Bebber, D., Riutta, T., Crockatt, M., Morecroft, M., & Malhi, Y. (2014). Relationships between tree growth and weather extremes: Spatial and interspecific comparisons in a temperate broadleaf forest. *Forest Ecology and Management*, *334*, 209–216.

Centre Nationale de Recherches Météorologiques (2014). `http://www.cnrm-game-meteo.fr/?lang=fr`.

Centre Nationale de Recherches Météorologiques (2015). `https://opensource.cnrm-game-meteo.fr/projects/ecoclimap/wiki`.

Chapin III, F., Matson, P., & Vitousek, P. (2011). *Principles of terrestrial ecosystem ecology*. Springer.

Cornell University (2006). `http://www.gardening.cornell.edu/homegardening/scene7de0.html`.

Deardorff, J. (1997). A parameterization of ground-surface moisture content for use in atmospheric prediction models. *Journal of Applied Meteorology*, *16*(11), 1182–1185.

Eugster, W., Rouse, W., Pielke Sr., R., McFadden, J., Baldocchi, D., Kittel, T., Chapin III, F., Liston, G., Vidale, P., Vaganov, E., & Chambers, S. (2000). Land-atmosphere energy exchange in Arctic tundra and boreal forest: available data and feedbacks to climate. *Global Change Biology*, *6*, 84–115.

Faroux, S., Kaptué Tchuenté, A., Roujean, J.-L., Masson, V., Martin, E., & Le Moigne, P. (2014). ECOCLIMAPII/Europe: a twofold database of ecosystems and surface parameters at 1 km resolution based on satellite information for use in land surface, meteorological and climate models. *Geoscientific Model Development*, (6), 563–582.

Garrigues, S., Lacaze, R., Baret, F., Morisette, J., Weiss, M., Nickeson, J., Fernandes, R., Plummer, S., Shabanov, N., Myneni, R., Knyazikhin, Y., & Yang, W. (2008). Validation and intercomparison of global leaf area index products derived from remote sensing data. *Journal of Geophysical Research*, *113*.

Hänninen, H. (2016). *Boreal and Temperate Trees in a Changing Climate: Modelling the Ecophysiology of Seasonality*. Springer.

Hatfield, J., Boote, K., Fay, P., Hahn, L., Izaurralde, C., Kimball, B., Mader, T., Morgan, J., Ort, D., Polley, W., Thomson, A., & Wolfe, D. (2008). Agriculture. *The effects of climate change on agriculture, land resources, water resources, and biodiversity in the United States*.

Hatfield, J. & Prueger, H. (2015). Temperature extremes: Effect on plant growth and development. *Weather and Climate Extremes*, *10*, 4–10.

Hollinger, D., Kelliher, F., J.N.Byers, J.E.Hunt, T.M.McSeveny, & P.L.Weir (1994). Carbon dioxide exchange between an undisturbed old-growth temperate forest and the atmosphere. *Ecology*, *75*(1), 134–150.

Jacquemin, B. & Noilhan, J. (1990). Validation of a land surface parameterization using the hapex-mobilhy data set. *Boundary-Layer Meteorology*, *52*, 93–134.

Jarvis, P. (1976). The interpretation of the variations in leaf water potential and stomatal conducance found in canopies in the field. *Philosophical Transactions of the Royal Society of London, Series B, Biological Sciences*, *273*(927), 593–610.

Jarvis, P. & Linder, S. (2000). Botany: Constraints to growth of boreal forests. *Nature*, *405*, 904–905.

Krug, H. (1997). Environmental influences on development, growth and yield. *The Physiology of Vegetable Crops*.

Le Moigne, P., Boone, A., Belamari, S., Brun, E., Calvet, J.-C., Decharme, B., Faroux, S., Gibelin, A.-L., Giordani, H., Lafont, S., Lebeaupin, C., Mahfouf, J.-F., Martin, E., Masson, V., Mironov, D., Morin, S., Noilhan, J., Tulet, P., Van Den Hurk, B., & Vionnet, V. (2012). SURFEX scientific documentation. (2).

Masson, V., Champeaux, J.-L., Chauvin, F., Meriguet, C., & Lacaze, R. (2003). A global database of land surface parameters at 1-km resolution in meteorological and climate models. *Journal of Climate*, *16*(9), 1261–1282.

National Aeronautics and Space Administration (2016). `http://earthobservatory.nasa.gov/Experiments/Biome/bioconiferous.php`.

National Oceanic and Atmospheric Administration (2009). `http://w1.weather.gov/glossary/`.

Oke, T. (1987). *Boundary layer climates*. Routledge.

Rubatzky, V. & Yamaguchi, M. (1997). *World Vegetables, 2nd edition*. Chapman and Hall.

Sluijter, R. (2003). `https://www.knmi.nl/nederland-nu/klimatologie/maand-en-seizoensoverzichten/2003/zomer`.

Sluijter, R. (2006). `https://www.knmi.nl/nederland-nu/klimatologie/maand-en-seizoensoverzichten/2006/zomer`.

Sluijter, R. (2015). `https://www.knmi.nl/nederland-nu/klimatologie/maand-en-seizoensoverzichten/2015/zomer`.

Sykes, M. & Colin Prentice, I. (1996). Climate change, tree species distributions and forest dynamics: A case study in the mixed conifer/northern hardwoods zone of northern europe. *Climatic Change*, *34*(2), 161–177.

Tanja, S., Berninger, F., Vesala, T., Markkanen, T., Hari, P., Mäkelä, A., Ilvesniem, H., Hänninen, H., Nikinmaa, E., Huttula, T., Laurila, T., Aurela, M., Grelle, A., Lindroth, A., Arneth, A., Shibistova, O., & Lloyd, J. (2003). Air temperature triggers the recovery of evergreen boreal forest photosynthesis in spring. *Global Change Biology*, *9*, 1410–1426.

the Food and Agriculture Organization of the United Nations (2015). `http://www.fao.org/nr/water/cropinfo_potato.html`.

Williams, A. (1992). *Clarification and Interpretation of the 1987 Manual*.